

Aus dem
Helmholtz-Zentrum München
Institut für Epidemiologie (EPI)



**Modeling temporal and spatial variations of meteorological parameters
for epidemiological application
in German cohorts**

Dissertation
zum Erwerb des Doctor of Philosophy (Ph.D.) an der Medizinischen Fakultät der
Ludwig-Maximilians-Universität München

vorgelegt von
Nikolaos Nikolaou

aus
Athen / Griechenland

Jahr
2024

Mit Genehmigung der Medizinischen Fakultät der
Ludwig-Maximilians-Universität München

Erstes Gutachten: Prof. Dr. Annette Peters
Zweites Gutachten: Prof. Dr. Dennis Nowak
Drittes Gutachten: Priv. Doz. Dr. Ursula Berger
Viertes Gutachten: Prof. Dr. Eva Grill

Dekan: Prof. Dr. med. Thomas Gudermann

Tag der mündlichen Prüfung: 17.12.2024

Στην αδερφή μου, Σίσσυ...

To the memory of my sister, Sissy...



LUDWIG-
MAXIMILIANS-
UNIVERSITÄT
MÜNCHEN

Dekanat Medizinische Fakultät
Promotionsbüro



Affidavit

Nikolaou, Nikolaos

Surname, first name

I hereby declare, that the submitted thesis entitled

Modeling temporal and spatial variations of meteorological parameters for epidemiological application in German cohorts

is my own work. I have only used the sources indicated and have not made unauthorised use of services of a third party. Where the work of others has been quoted or reproduced, the source is always given.

I further declare that the dissertation presented here has not been submitted in the same or similar form to any other institution for the purpose of obtaining an academic degree.

Neuherberg, 19.12.2024

Place, Date

Nikolaos Nikolaou

Signature doctoral candidate



Dean's Office Medical Faculty
Doctoral Office



Confirmation of congruency between printed and electronic version of the doctoral thesis

Nikolaou, Nikolaos

Surname, first name

I hereby declare that the electronic version of the submitted thesis, entitled

Modeling temporal and spatial variations of meteorological parameters for epidemiological application in German cohorts

is congruent with the printed version both in content and format.

Neuherberg, 19.12.2024

Place, Date

Nikolaos Nikolaou

Signature doctoral candidate

Table of content

Affidavit	4
Confirmation of congruency	5
List of abbreviations	8
List of publications	10
1. Contribution to the publications.....	11
1.1 Contribution to paper I.....	11
1.2 Contribution to paper II.....	12
2. Introductory summary	13
2.1 Background.....	13
2.1.1 Problem statement.....	14
2.1.2 Previous modeling techniques	15
2.1.3 Additional gaps and challenges identified	16
2.2 Objectives	17
2.3 Methods	18
2.3.1 Study area.....	18
2.3.2 Material	19
2.3.3 Modeling	20
2.3.4 Model performance	22
2.3.5 Uncovering spatiotemporal patterns	23
2.3.6 Case studies	23
2.3.7 Code for the statistical analyses	23
2.4 Results.....	24
2.4.1 Air temperature models.....	24
2.4.2 Relative humidity model.....	25
2.5 Discussion.....	26
2.5.1 Summary of key findings.....	26
2.5.2 Further important insights	27
2.5.3 Link between publications	28
2.5.4 Contributions to environmental epidemiology	29
2.5.5 Novelties	31
2.5.6 Strengths and limitations.....	32
2.5.7 Computational challenges.....	33
2.6 Conclusion and outlook.....	33
2.6.1 Data dissemination	34

2.6.2 Data impact.....	35
2.6.3 Future research.....	36
3. Paper I.....	38
3.1 Supplementary material for Paper I	52
4. Paper II.....	81
4.1 Supplementary material for Paper II.....	91
References.....	110
Appendix.....	123
Further projects	123
PhD experience - further insights	124
Acknowledgements	126
List of scientific publications to date	128

List of abbreviations

AI	Artificial Intelligence
CV	Cross Validation
DEM	Digital Elevation Model
DGEpi	German Society for Epidemiology
DTR	Diurnal Air Temperature Range
DWD	German Meteorological Service
EGU	European Geosciences Union
EnRi	Research Group Environmental Risks
EPI-HMGU	Institute of Epidemiology, Helmholtz Munich
EQ	Equation
GERICS	Climate Service Center Germany
Helmholtz AI	Helmholtz Artificial Intelligence Cooperation Unit
HI-CAM	Helmholtz Initiative Climate Adaptation and Mitigation
IBE	Institute for Medical Information Processing, Biometry, and Epidemiology
ISEE	International Society for Environmental Epidemiology
KORA	Cooperative Health Research in the Region of Augsburg
LMU	Ludwig Maximilian University of Munich
LST	Land Surface Temperature
MAPE	Mean Absolute Percentage Error
ML	Machine Learning
MPE	Mean Percentage Error
MRC	Medical Research Council
NAKO	German National Cohort
NDVI	Normalized Difference Vegetation Index
PhD-EPH	PhD Program - Medical Research in Epidemiology and Public Health
RF	Random Forest

RH	Relative Humidity
RKI	Robert Koch Institute
RMSE	Root Mean Square Error
SES	Socio-economic Status
TAC	Thesis Advisory Committee
T_{air}	Air Temperature
T_{max}	Maximum Air Temperature
T_{mean}	Mean Air Temperature
T_{min}	Minimum Air Temperature
TPS	Thin Plate Spline
UHI	Urban Heat Island
USGS	United States Geological Survey
WS	Wind Speed
ZKI-PH	Centre for Artificial Intelligence in Public Health Research

List of publications

This PhD Thesis consists of the following two publications:

- I. **Nikolaou, N.**, Dallavalle, M., Stafoggia, M., Bouwer, L.M., Peters, A., Chen, K., Wolf, K., Schneider, A., 2023. High-resolution spatiotemporal modeling of daily near-surface air temperature in Germany over the period 2000–2020. Environmental Research, 219, p.115062. <https://doi.org/10.1016/j.envres.2022.115062>

- II. **Nikolaou, N.**, Bouwer, L.M., Dallavalle, M., Valizadeh, M., Stafoggia, M., Peters, A., Wolf, K., Schneider, A., 2023. Improved daily estimates of relative humidity at high resolution across Germany: A random forest approach. Environmental Research, 238, p.117173. <https://doi.org/10.1016/j.envres.2023.117173>

1. Contribution to the publications

This PhD Thesis comprises two publications that have been published in Environmental Research, an internationally peer-reviewed scientific journal. It is noteworthy that Environmental Research has an Impact Factor of 8.3 and holds a place in the top 12 % of Environmental Sciences Journals and top 8 % in Public, Environmental & Occupational Health Journals, as indicated by the Journal Citations Reports[®] 2022 of Clarivate.

I, Nikolaos Nikolaou, am the first author of both publications incorporated in this PhD Thesis. In addition to the specific contributions outlined below based on the CRediT author statement (1.1 Contribution to paper I and 1.2 Contribution to paper II), I presented the findings in regular Thesis Advisory Committee (TAC) meetings, the Work-In-Progress seminars of the Research Group Environmental Risks (EnRI), the Monday seminars of the Institute of Epidemiology, Helmholtz Munich (EPI-HMGU), the PhD Journal Clubs of the Institute for Medical Information Processing, Biometry, and Epidemiology (IBE), Ludwig Maximilian University of Munich (LMU), and the seminars of the Helmholtz Initiative Climate Adaptation and Mitigation (HI-CAM) project as well as in multiple conferences such as the International Society for Environmental Epidemiology (ISEE) 2022 and the Helmholtz Artificial Intelligence Cooperation Unit (Helmholtz AI) 2022, among other forums. I also presented the generated datasets from the publications during an invited talk at the Medical Research Council (MRC) Health Collaborations Workshop 2024. I incorporated into the manuscripts the feedback from the TAC members and the multi-disciplinary audiences of these talks. I additionally drafted both manuscripts, facilitated communication among co-authors, incorporated co-authors' comments, and made decisions regarding journal submissions. Being the first and corresponding author, I managed the submission and publication processes for both papers. This involved incorporating feedback from the peer-review, revising the manuscripts accordingly, and overseeing proofreading and post-production responsibilities.

1.1 Contribution to paper I

In the first publication, entitled “High-resolution spatiotemporal modeling of daily near-surface air temperature in Germany over the period 2000-2020”, a multi-stage modeling approach was developed to enhance the spatiotemporal coverage of near-surface air temperature (T_{air}) data in

Germany after 2000, addressing limitations of data from conventional weather stations. The study successfully demonstrated the models' strong performance in estimating countrywide daily T_{air} at 1×1 km resolution, revealing high T_{air} spatial variability, and consistent warming trends post-2016, providing a critical tool for temperature-based epidemiological studies and broader research applications. I contributed to the conceptualization, data curation, methodology, formal analysis, visualization, writing - original draft, writing - review & editing of this publication.

1.2 Contribution to paper II

In the second publication, entitled "Improved daily estimates of relative humidity at high resolution across Germany: A random forest approach", the challenge of estimating near-surface relative humidity (RH) in high resolution across Germany was addressed, given the limited available methods and the incapacity of weather stations to capture the spatiotemporal RH variability adequately, for the first time, by developing a machine learning (ML) modeling scheme. Through the implementation of a random forest (RF) model that incorporated various environmental features, the study successfully predicted countrywide daily mean RH at 1×1 km resolution after 2000. The findings highlighted the substantial spatial variability in RH and suggest the dataset's suitability for environmental and epidemiological research. I contributed to the conceptualization, data curation, methodology, analysis, visualization, writing - original draft, writing - review & editing of this publication.

2. Introductory summary

2.1 Background

Climate change stands as one of the paramount global challenges confronting humanity and the entirety of its living environment in the 21st century and beyond. In this context, meteorological exposures undergo transformation, altering patterns and intensities, thereby necessitating their thorough examination, which is vital for preparing and adapting to this new era. Among the crucial meteorological exposures, air temperature (T_{air}) and relative humidity (RH) stand out.

Near-surface T_{air} , measured 2 m above the ground, serves as a critical meteorological parameter and it is the foremost indicator of climate change. T_{air} is steadily rising globally, especially after the millennium, with 2023 to be the warmest year on record¹ and projections suggesting further increases by the century's end². This applies to Germany as well, where the trend toward higher T_{air} persists³ and there have been greater increases compared to the global averages. In the period 2013-2022, Germany experienced a rise of 2.1°C in average T_{air} compared to the first recorded 30-year period 1881-1910, surpassing the global increase of merely 1.1°C during the same intervals, and being the hottest 10-year term in record for the country⁴.

Non-optimal T_{air} (high and low ambient temperatures) has a significant impact on human health⁵, including morbidity⁶ and mortality⁷, especially affecting the cardiovascular⁸ and respiratory health⁹. Heat exacerbates adverse pregnancy outcomes¹⁰, mental health decline¹¹, reduced physical capacity¹² while both heat and cold are linked with impaired cognitive function¹³. Vulnerable populations, including the elderly¹⁴, people with chronic conditions¹⁵, and children¹⁶, are particularly susceptible to heat-related illnesses. Human health can be negatively impacted by T_{air} , whether over short-¹⁷ or long-term exposure¹⁸. The T_{air} -health association is projected to deteriorate in the coming decades due to climate change and population aging¹⁹. The research focus mainly lies on extreme T_{air} values and prolonged periods of very high T_{air} , i.e., heatwaves, but also variations within moderate T_{air} ranges pose significant threats to public health²⁰⁻²², necessitating high resolution T_{air} exposure datasets for improved epidemiological assessments.

Near-surface RH, also measured 2 m above the ground and assessing the degree of atmospheric saturation, is a key meteorological and climatological factor and holds significance across various

research fields. From agriculture²³ and atmospheric science^{24,25} to hydrology and climatology²⁶. RH is also vital for plant growth and animal life²⁷. Germany, a country with notably high RH levels but also high spatial variability due to its unique landscape, offers a captivating setting for its detailed assessment and subsequent research projects.

RH-health literature is still scarce but there are studies indicating RH impact on human health²⁸.²⁹. RH has been linked to elevated cause-specific mortality, especially cardiovascular, diabetes and chronic obstructive pulmonary disease mortality³⁰ along with its morbidity effects^{31, 32}, while elderly³³ and children^{34, 35} are particularly vulnerable to its exposure. Additionally, RH influences the transmission of droplet-³⁶ and vector-borne³⁷ diseases, potentially also promoting the spread of COVID-19³⁸. RH also plays an important role in heat-related health impacts³⁹. Moreover, RH can contribute to health disorders through its connection with synoptic weather patterns^{40, 41}. High-pressure systems typically bring clear skies and dry conditions, lowering RH, while low-pressure ones are associated with rising air and cloud formation, leading to increased RH. Understanding these dynamics is crucial for public health planning, particularly in the context of climate change, which is expected to alter synoptic weather patterns⁴² and their associated RH levels.

2.1.1 Problem statement

In environmental epidemiology, T_{air} and RH data are typically assigned to health studies' participants based on the proximity of weather stations according to the stations' availability within the study area. For instance, if only one station is available in a cohort's study area, all participants usually get assigned the data from that single station, resulting in the loss of spatial variation information. Even if multiple stations are present in the greater area, the assignment to participants may be based on proximity, averaging, or other criteria, yet spatial variability remains a challenge. Additionally, temporal variation poses a significant issue as weather stations may not consistently measure data over time, leading to gaps or discontinuity in the dataset. Despite the ideal scenario of multiple stations with continuous measurements, the limited number of weather monitors, along with their uneven distribution, particularly in rural areas, coupled with their frequent placement in park-like settings or at airports, hampers their ability to accurately capture the spatiotemporal fluctuations of T_{air} and RH in complex geo-climatic urban and rural landscapes as of Germany.

This deficiency potentially introduces errors in the exposure assessment of health studies' participants. There are two primary types of exposure measurement error⁴³: classical and Berkson, which often also act simultaneously⁴⁴ in the context of T_{air} and RH, compounding the challenges of accurately assessing exposure levels. These errors in most cases lead to health effect estimates biased towards the null hypothesis of no association⁴⁵ or imprecise estimates and, therefore, lead to an underestimation of risks or misinterpretation of effects. The extent of bias in exposure-response relationships is directly influenced by the volume of the measurement error, which can vary due to several factors including spatial differences, such as the proximity of a study participant's residential address to the exposure source⁴⁶ or the magnitude of the variability of an environmental exposure in space.

Numerous studies reporting null effects may be subject to these limitations, potentially masking significant associations between environmental factors like T_{air} and RH and health outcomes. This suggests a pressing need to re-evaluate and prioritize research efforts aimed at gaining a deeper understanding of the true impact of these exposures on human health. One primary and essential solution entails adopting high resolution modeling techniques to capture and analyze these exposures more accurately, and thus substantially reducing exposure measurement error.

2.1.2 Previous modeling techniques

In recent years, significant progress has been made in modeling meteorological variables and compiling spatiotemporal maps of these variables in gridded sets. However, there is still considerable room for improvement. Interpolation methods like inverse distance weighting, regression-kriging, and thin plate spline (TPS) among others, are commonly used for countrywide mapping⁴⁷⁻⁵⁰ but encounter challenges such as sensitivity to station locations and difficulty capturing between-station variability, as well as struggles with neighboring effects, obstructing accurate representation of intra-city variability and mostly of urban heat island (UHI). Linear regression, generalized additive models, mixed models, and ML techniques such as XGBoost and RF, along with other methods, as well as ensemble models, are increasingly employed⁵¹⁻⁵³ to address these issues, often in conjunction with multi-stage approaches⁵⁴ to improve accuracy and coverage. Each method has its own strengths and limitations, necessitating adjustments based on country-specific settings and data availability. Notably, remote sensing data are gaining

prominence due to their widespread availability, accessibility without costs, high quality, and real-time updates, playing an increasingly important role in meteorological estimations⁵⁵⁻⁵⁷.

2.1.3 Additional gaps and challenges identified

While mean air temperature (T_{mean}) is one of the most commonly used metrics in environmental epidemiology, emphasis to minimum and maximum air temperature (T_{min} and T_{max}) is critical but currently lacking focus. Climate change impacts T_{min} and T_{max} unequally, with T_{min} , particularly in urban areas, showing a greater increase⁵⁸, exacerbating nocturnal heat stress⁵⁹. Modeling T_{min} and T_{max} aids in estimating the diurnal air temperature range (DTR), which also affects human health⁶⁰ and is still underrepresented in the literature. The limited availability of high resolution daily T_{min} , T_{max} and DTR data constraints in-depth epidemiological investigations, especially at the national scale, necessary for informing future policies.

To date, there exists an evident gap in research investigating the direct impact of RH exposure on human health, as well as the underlying mechanisms involved because RH is mostly used as a confounder, effect modifier or as an index component in studies focusing in T_{air} effects^{39, 61, 62}. Detailed research in this area is needed, emphasizing the critical necessity for epidemiologists to have access to reliable RH datasets of high resolution.

Moreover, while there are plenty of T_{air} modeling techniques, with their limitations and space for improvement, there is a clear methodological gap in RH modeling frameworks, particularly concerning the limited input data sources used, the prediction of high spatiotemporally-resolved RH, the accuracy of the past models and the timeframes spanning single seasons or years only.

Satellite-based data present a viable alternative owing to its accessibility, high resolution and quality, and near real-time availability. However, relying solely on satellite-based data, such as land surface temperature (LST), is inadequate for comprehensive environmental health analyses. In the temperature-health studies, the focus is the 2 m above the ground T_{air} , while spectroradiometers in satellites provide surface temperature values, which may not fully represent T_{air} despite their high correlation, necessitating sophisticated calibration. Additionally, satellite datasets often encounter severe measurement gaps in their time series due to cloud cover. Lastly, it is noteworthy that there exists no suitable satellite-derived metric to serve as a proxy for RH.

Finally, it is important to note that there has been limited research conducted in Germany regarding the modeling of meteorological parameters. The existing weather data and maps primarily serve weather monitoring and forecasting or analyzing climate trends within the field of meteorology rather than being oriented to the needs of health research. Consequently, they often do not fit epidemiological analyses, either exhibiting limited spatial variability with coarse resolution or failing to cover the large temporal periods relevant to German health studies. This presents a significant gap in obtaining highly resolved meteorological data, particularly T_{air} and RH, which are crucial for the exposure assessment in German cohorts or other (nationwide) datasets for environmental health analyses (e.g., registries, administrative or insurance data). Addressing these issues and exploring German analyses are imperative. This PhD Thesis fills this gap by introducing the first study using an extensive input database for estimating T_{air} , employing a sophisticated multi-stage statistical scheme, and extending the temporal scope to also match the German National Cohort (NAKO) study, which lacks comparable data. Furthermore, this PhD Thesis presents a pioneering analysis estimating RH directly, rather than calculating it from other modeled data, and also extends the temporal scope to encompass multiple health studies. These novel methodologies can be adapted for use in other spatial settings as well.

2.2 Objectives

In light of the inadequacies associated with traditionally used weather station observations in capturing the intricate spatiotemporal variations of meteorological parameters like T_{air} and RH and resulting in exposure misclassification and challenges in assessing local health impacts, there is a critical need for high resolution environmental exposure datasets. This PhD Thesis aimed to address these limitations not only to meet the current demands of environmental epidemiology but also to extend its applicability to various research domains beyond the field. This PhD Thesis aimed to improve substantially the spatiotemporal coverage of T_{air} and RH data in Germany's complex topographic landscape from 2000 on, specifically tailored for epidemiological research, such as the local Cooperative Health Research in the Region of Augsburg (KORA) cohort⁶³ and the countrywide NAKO study⁶⁴, which involves over 200,000 participants. In the same context, one of the additional requirements was the T_{air} and RH models to be readily extendable to future

years, effectively fitting to new cohorts or the follow-up periods of existing ones as well as updated registries, administrative databases and insurance records. Another main objective of this PhD Thesis was to provide insights into the variability of T_{air} and RH over Germany for the past two decades amid a rapidly changing climate.

The specific objectives (SOs) of this PhD Thesis are outlined as follows:

(SO1) Enhance T_{air} data coverage in Germany through remote sensing and regression-based modeling. This involved generating a complete T_{air} dataset including daily 1×1 km German-wide maps of T_{min} , T_{mean} , T_{max} , and DTR.

(SO2) Introduce a novel modeling scheme to enhance the spatiotemporal representation of RH data in 1×1 km resolution across Germany. This involved leveraging T_{air} data, alongside other observation, remote sensing, and modeled data, and employing a RF approach. The overarching aim was to not only contribute to the existing literature but also to offer a method that can be generalized for the creation of highly resolved RH datasets in other spatial settings/ countries with similar data availability.

(SO3) Offer insights into T_{air} and RH variability and spatial distribution across Germany over the past two decades. Identify regions with higher temperatures or altered humidity patterns and analyze their trends in recent years.

(SO4) Investigate and emphasize the improvement of exposure assessment on German health studies by spatiotemporal modeling, aiming for better capturing the high T_{air} and RH variability in space and time.

2.3 Methods

2.3.1 Study area

Germany is located in central Europe, spans 357,595 km² and is home to a population of 84.6 million people⁶⁵. The country showcases a heterogeneous topography, ranging from the southern mountain range of Alps to the North and Baltic Seas coastlines in the north, featuring major cities, mountainous areas, inland water bodies, forested areas, and a big proportion of arable land. With elevations varying from 3.54 m below sea to 2,962 m, Germany experiences a temperate to

continental climate⁶⁶. For the statistical analysis of this PhD Thesis, the mainland of Germany was divided into 366,536 grid cells of 1 × 1 km using the European INSPIRE standard and Lambert Azimuthal Equal-Area projection (EPSG: 3035) (©GeoBasis-DE/BKG (2021)).

2.3.2 Material

A large amount of publicly available data was collected and integrated into the T_{air} and RH modeling frameworks, including meteorological observations by networks of weather stations, remote sensing information by satellites, and spatiotemporally resolved modeled data from various sources. Table 1 summarizes the data used for the T_{air} models, the RH model, or both, along with their key technical characteristics. Details can be found in the corresponding sections *2.2 Materials* and *2.2 Input data* from the publications I and II of this PhD Thesis, respectively.

	Variable	Unit	Abbreviation	Resolution		Source	For model(s)		
				Temporal	Spatial		T_{air}	RH	
Weather station observations	Air temperature (minimum, mean & maximum)	°C	T_{air} (T_{min} , T_{mean} , T_{max})	Daily	-	DWD ⁶⁷	✓		
	Relative humidity (mean)	%	RH	Daily	-	DWD ⁶⁷		✓	
	Wind speed (mean)	m/s	WS	Daily	-	DWD ⁶⁷		✓	
Remote sensing information	Normalized difference vegetation index	-	NDVI	Monthly	1 × 1 km	USGS ⁶⁸	✓	✓	
	Land surface temperature (day- & night-time)	K	LST	Daily	1 × 1 km	USGS ⁶⁹	✓		
	Digital elevation model	m	DEM	-	30-arc-second	USGS ⁷⁰	✓	✓	
	CORINE land cover	Urban fabric	%	-	'12 & '18	100 m	Copernicus ^{71, 72}	✓	
		Arable land	%	-	'12 & '18	100 m	Copernicus ^{71, 72}	✓	

True color band composite	Pastures	%	-	'12 & '18	100 m	Copernicus ^{71, 72}	✓
	Forests	%	-	'12 & '18	100 m	Copernicus ^{71, 72}	✓
	Inland waters	%	-	'12 & '18	100 m	Copernicus ^{71, 72}	✓
	Red band	-	-	Daily	500 m	USGS ⁷³	✓
	Green band	-	-	Daily	500 m	USGS ⁷³	✓
	Blue band	-	-	Daily	500 m	USGS ⁷³	✓
Modeled data	Air temperature (mean)	°C	T _{mean}	Daily	1 × 1 km	EPI-HMGU ⁷⁴	✓
	Precipitation	mm	-	Daily	1 × 1 km	DWD ⁷⁵	✓

DWD = German meteorological service; USGS = United States geological survey; EPI-HMGU = Institute of Epidemiology, Helmholtz Munich, '12 = 2012, '18 = 2018.

Data were collected at spatial and temporal resolutions optimized for the modeling objectives. Following data collection, homogenization procedures were implemented as required. The land cover and true color band composite data were aggregated to a resolution of 1 × 1 km and LST measurements were converted to Celsius degrees for instance.

2.3.3 Modeling

Multi-stage regression-based models were applied for estimating the three T_{air} metrics, namely T_{min} , T_{mean} and T_{max} , while a ML algorithm was employed for estimating RH.

2.3.3.1 Air temperature models

The T_{air} modeling process was divided in three stages. In the first stage, the focus was on the grid cells with available T_{air} observations from German Meteorological Service (DWD) weather stations and satellite-derived LST values to calibrate their established strong and positive relationship, tailoring the model to account for the distinctive spatial and geo-climate characteristics of Germany. Specifically, the country's surface and altitude variations were addressed by adjusting the model for elevation. Information on greenness, urbanization, water, forests, pastures and arable land was included as well. The model incorporated a daily random slope for LST to accommodate daily fluctuations in the relationship between T_{air} and LST (EQ1).

In the second stage, T_{air} was predicted for grid cell-day combinations lacking T_{air} observations but having LST data available. This was achieved by using the regression coefficients obtained from (EQ1). In the third stage, T_{air} was estimated for grid cells and days lacking both T_{air} observations and LST data. A linear mixed model was employed, regressing second stage T_{air} predictions against daily 1×1 km interpolated T_{air} values through TPS, utilizing random grid-cell-specific intercepts and slopes (EQ2). For each T_{air} measure, i.e., T_{min} , T_{mean} and T_{max} , a separate regression was applied. Nighttime LST was utilized for T_{min} and T_{mean} models, whereas daytime LST for the T_{max} model. All models were developed on an annual basis. DTR was then calculated by subtracting T_{min} from T_{max} .

$$(EQ1) \quad T_{airij} = b_0 + u_j + (b_1 + v_j) \cdot LST_{ij} + b_2 \cdot DEM_i + b_3 \cdot NDVI_{ij} + b_4 \cdot UrbanFabric_i + b_5 \cdot ArableLand_i + b_6 \cdot Pastures_i + b_7 \cdot Forests_i + b_8 \cdot InlandWaters_i + \epsilon_{ij}$$

where,

- i stands for grid cell; j stands for day.
- b_0 and u_j stand for the fixed and the random intercepts, respectively.
- b_1 and v_j stand for the fixed and the random slopes, respectively.
- ϵ_{ij} is the error term at grid cell i on day j .

$$(EQ2) \quad \text{Second stage } T_{airij} = a_i + b_i \cdot \text{int}T_{airij} + \epsilon_{ij}$$

where,

- i stands for grid cell; j stands for day.
- a_i and b_i stand for the i grid-cell-specific intercepts and slopes.
- $\text{int}T_{airij}$ stands for the TPS interpolated T_{air} values at the grid cell i on day j .
- ϵ_{ij} is the error term at grid cell i on day j .

2.3.3.2 Relative humidity model

RH was predicted by using a RF model consisting of 500 trees and 8 randomly sampled variables as candidates at every split, trained per year to capture annual variations. Due to the inherent robustness of RF, extensive hyperparameter tuning was unnecessary. Instead of employing complex methods, the analysis was opted for trial and error, deviating from the default settings, and observed no significant differences in model performance across various hyperparameter

sets. Daily mean RH was modeled predicting measurements at DWD station locations, with predictors including T_{mean} , the true color band composite (bands 1 = red, 3 = blue and 4 = green), precipitation, wind speed (WS), elevation and NDVI. The geographical coordinates, i.e., longitude and latitude, and the day of the year were also incorporated into the model for capturing spatial and daily variations in the response-predictor relationship. The formula was the following:

$$\text{RH}_{ij} \sim T_{\text{mean}_{ij}} + \text{RedBand}_{ij} + \text{GreenBand}_{ij} + \text{BlueBand}_{ij} + \text{Precipitation}_{ij} + \text{WS}_{ij} + \text{DEM}_i + \\ + \text{NDVI}_{ij} + \text{Longitude}_i + \text{Latitude}_i + \text{DayofYear}_j$$

where i stands for monitor location and j stands for day.

In the prediction step, the RF model was applied to all grid cells and days without available RH measurements from DWD weather stations, generating a complete RH dataset all across Germany. Similar to T_{air} , models were developed year wise to enable easy extension to future years.

2.3.4 Model performance

Extensive performance testing of the T_{air} and RH models was conducted, both on local and countrywide scales. Additional validation using data from external, independent sources was performed. Various sensitivity analyses supplemented and strengthened the validation process, including comparisons by season, extreme values, and comparing urban and rural areas.

2.3.4.1 Air temperature models

The models' performances [R^2 , root mean square error (RMSE) and mean signed error] were assessed separately for the first and third stages through a ten-fold cross validation (CV). Temporal and spatial metrics were also computed for the first stage. In the third stage, validation involved a subset of DWD weather stations for days in grid cells where LST data were missing and had not yet been integrated into the modeling pipeline.

Additionally, two validations were conducted with data from external sources: a small-scale validation using a dense and independent monitoring network in the region of Augsburg in South Germany⁷⁶, and a large-scale validation using the DWD TRY project's dataset⁷⁷ in a countrywide setting. The small-scale validation involved 4-minute T_{air} measurements from 82 devices during

2013-2018, aggregated to daily T_{\min} , T_{mean} , and T_{\max} values. For the large-scale validation, the T_{mean} model predictions generated in this PhD Thesis were also compared with the DWD TRY project's openly available daily T_{mean} predictions, for the overlapping period 2001-2012.

2.3.4.2 Relative humidity model

The model's performance [R^2 , RMSE, mean absolute percentage error (MAPE) and mean percentage error (MPE)] was evaluated through a ten-fold CV.

RH predictions also underwent validation using the monitoring network featuring 82 devices with 4-minute temporal resolution located in Augsburg city and adjacent counties from 2015 to 2019. 4-minute RH values were aggregated to daily means and 7-day averages.

2.3.5 Uncovering spatiotemporal patterns

The spatiotemporal T_{air} and RH patterns over the last two decades were investigated through extensive descriptive analysis (statistics and visualization included), considering both overall trends and seasonal variations. For T_{air} , variations were also studied in the NAKO study centers, strategically located to represent diverse areas, including rural and urban settings. The focus was on study regions with over 2000 inhabitants/ km².

2.3.6 Case studies

Augsburg, a study center of both KORA and NAKO cohorts, and Regensburg, a study center of the NAKO cohort, were selected as case studies to analyze the spatiotemporal variability and distribution of modeled T_{air} and RH compared to the observed values at the available DWD sites and to quantify and illustrate the enhancements in exposure assessment of cohort studies participants by high resolution data.

2.3.7 Code for the statistical analyses

The analysis code was developed in R, versions 4.0.2⁷⁸ and 4.2.2⁷⁹ for the T_{air} models and the RH model, respectively. The "LM4" package⁸⁰ was used for the linear mixed models in T_{air} modeling and the "ranger" package⁸¹ for the RF model in RH modeling. Parallel computing techniques were employed. QGIS, version 3.10.5-A Coruna⁸² was also used for analysis and visualization purposes.

2.4 Results

The overarching aim of this PhD Thesis was to improve the available meteorological database for German health studies (SO4) and suggest novel and reliable modeling schemes for other countries and spatial settings with similar data availability (SO1 and SO2). In addition, a significant goal of this PhD Thesis was to assess the spatiotemporal patterns and trends of T_{air} and RH in Germany after 2000 (SO3). Here, the key findings are summarized for each publication.

2.4.1 Air temperature models

Key finding 1: All T_{air} models, i.e., T_{min} , T_{mean} and T_{max} , demonstrated very high accuracy ($0.91 \leq R^2 \leq 0.98$) and low errors ($1.03^\circ\text{C} \leq \text{RMSE} \leq 2.02^\circ\text{C}$) (Paper I - Tables 1, S1 and S2) while maintaining missing values close to 1% countrywide (Paper I - Table S5). External data validation confirmed the models' excellent performance in the local setting of Augsburg, South Germany ($0.74 \leq R^2 \leq 0.99$, $0.87^\circ\text{C} \leq \text{RMSE} \leq 2.05^\circ\text{C}$) (Paper I - Tables 2, S6 - S8, Fig. 2 and Figure S4). The T_{mean} model countrywide comparisons against DWD TRY T_{mean} model, demonstrated a high level of correspondence ($0.71 \leq R^2 \leq 0.99$, $0.79^\circ\text{C} \leq \text{RMSE} \leq 1.19^\circ\text{C}$) (Paper I - Tables 3, S9 - S13 and Fig. 3). Nonetheless, the T_{mean} model predictions generated for this PhD Thesis successfully captured a broader T_{mean} distribution and better portrayed the spatial variations in a small-scale setting (Paper I - Figure S5).

Key finding 2: Annual T_{mean} averages ranged from 8.56°C to 10.42°C , with post-2016 years consistently hotter than the 21-year average (Paper I - Fig. 7, plot 2), a finding that was particularly evident in the most densely populated NAKO study centers (Paper I - Figure S8). The German-wide spatial variability of T_{air} exceeded even 15°C annually on average, influenced by features like mountains, rivers, coastlines and urbanization (Paper I - Fig. 7, plot 1). The Alps and the Harz area exhibited the lowest countrywide T_{air} values. In contrast, densely populated urban regions (e.g., from Stuttgart to Frankfurt) and major metropolitan areas (e.g., of Hamburg) recorded considerably higher temperatures, particularly for T_{min} and T_{mean} , compared to the neighboring rural settings (Paper I - Fig. 7, plot 1). Eastern Germany, especially the North-Eastern region, witnessed greater variations in DTR, whereas cities, mountains, and large water bodies exhibited smaller DTR values (Paper I - Figure S7).

Key finding 3: High resolution spatiotemporal modeling enhanced the representation of T_{air} variability and reduced exposure misclassification for KORA cohort participants in Augsburg, South Germany. In long term, the city center was approximately 2°C warmer than the neighboring rural areas, and within these rural regions, there was also significant variation even among adjacent tiles (Paper I - Fig. 4). The two DWD weather stations in Augsburg region were found to provide values below the mean, and in some cases, even below the first quartile of the T_{mean} model's distribution (Paper I - Fig. 5 and 6), given that the residences of KORA participants averaged a distance of 10 km from the DWD closest station, and in some instances extended up to 20 km (Paper I - Figure S6).

2.4.2 Relative humidity model

Key finding 4: The RH model attained strong performance (R^2 of 0.83, RMSE of 5.07%, MAPE of 5.19% , MPE of - 0.53%) (Paper II - Table 1). The model performed best in fall and in the upper 10% of the dataset (Paper II - Fig. 1 and Figures S8 and S9). Comparing the RH predictions with measurements from Augsburg's dense monitoring network confirmed their accuracy and reliability ($R^2 \geq 0.86$, $\text{RMSE} \leq 5.45\%$, $\text{MAPE} \leq 5.59\%$, $\text{MPE} \leq 3.11\%$) (Paper II - Table 2 and Figure S10).

Key finding 5: Germany was characterized by high RH values, i.e., 22y-average of 79% and significant spatial variability, exceeding 12% on annual averages (Paper II - Fig. 4). RH spatial patterns and high heterogeneity were influenced by factors like urbanization, mountains, rivers, forests, and coastlines. Metropolitan areas, including Berlin, Hamburg, and Munich, showed significantly lower RH values than neighboring rural settings (Paper II - Fig. 4, plot 1). Winter and fall were the most humid seasons (Paper II - Figure S14). Despite yearly fluctuations, no clear increasing or decreasing trend was observed for RH over the past two decades. The most humid year was found to be 2001 (81.30%) while the most arid was 2003 (75.31%). It is noteworthy that three consecutive years out of the last five were considerably dry (2018: 75.52%, 2019: 76.83% and 2020: 75.53%) (Paper II - Fig. 4, plot 2).

Key finding 6: In the case study of Regensburg, the city center exhibited 4.5% lower RH values than the surrounding rural county (Paper II - Fig. 2). Daily RH variability, crucial for epidemiological analysis, reaching up to 9% on specific days (Paper II - Figure S11). Even neighboring tiles in the rural region displayed variations. The average RH in Regensburg, as measured by the only DWD

weather station available, was notably lower than the first quartile of the RH predictions distribution from the RF model (Paper II - Fig. 3).

2.5 Discussion

2.5.1 Summary of key findings

In this PhD Thesis, highly resolved (daily, 1 × 1 km) spatiotemporal datasets for T_{air} (T_{min} , T_{mean} , T_{max} , DTR) and RH (mean) were developed for Germany. Both traditional statistical methodologies and state-of-the-art ML algorithms were employed, and novel modeling schemes were introduced. Specifically, a three-stage approach encompassing two linear mixed models, and a RF model were integrated to model T_{air} and RH, respectively. These approaches went beyond the conventional interpolation of weather station data incorporating additional information from sources including ground monitoring networks and satellites. A variety of meteorological, remote sensing, geographical and land cover predictors were incorporated to the models. Consistently high explained variances (T_{air} : $0.91 \leq R^2 \leq 0.98$, RH: $R^2 = 0.83$) and low errors (T_{air} : $1.03^\circ\text{C} \leq \text{RMSE} \leq 2.02^\circ\text{C}$, RH: $\text{RMSE} = 5.07\%$) were observed. Extensive sensitivity analyses, e.g., seasonal comparisons or comparisons to extremes and the detailed external validation, both at small and large scales, further confirmed the robustness of the T_{air} and RH modeling frameworks.

Annual T_{mean} averages ranged from 8.56°C to 10.42°C , with post-2016 years to be consistently hotter. Germany exhibited high RH values (22-year average of 79%) but without specific temporal trends over the last two decades, yet notably experiencing three of its driest years (2018-2020) within the last five. Spatial variability across the country was found to be very high for both T_{air} and RH, exceeding 15°C for T_{air} and 12% for RH on yearly averages, largely influenced by features such as water bodies, mountains and urbanization.

The high importance of the spatiotemporal T_{air} and RH modeling for exposure assessment in local and countrywide epidemiological studies was clearly demonstrated, exemplified by two case studies, in Augsburg and Regensburg. The models effectively captured a broad range of spatial T_{air} and RH variability, surpassing the reliance solely on meteorological observations. While the DWD station values could not adequately reflect the high T_{air} values of the Augsburg city's center

or the high RH values of Regensburg outskirts, partly due to the considerable distance of participants' residences from these stations, the methodologies used in the PhD Thesis exhibited significant added value. By incorporating additional data sources alongside meteorological observations, the T_{air} and RH prediction accuracy were substantially improved. This enhanced capability to capture T_{air} and RH spatial variability is crucial for assessing differences in individual human exposure in epidemiological studies.

Overall, the results endorsed the proposed models as suitable for high resolution spatiotemporal and countrywide T_{air} and RH estimations for epidemiological use.

2.5.2 Further important insights

This PhD Thesis revealed significant increasing trends in T_{air} in Germany by the beginning of this century. Since 2014, the four hottest years of the last two decades have occurred, with the last three years consecutively being the warmest overall. This trend was more pronounced in large German cities. Additionally, the T_{air} models' outputs can be leveraged for calculating various temperature metrics, including heat or cold days, as well as heat nights. Given the high-resolution of the T_{air} models, important temperature exposure insights that cannot be captured by crude countrywide T_{air} averages were detected, highlighting the impact on both local and countrywide levels over a short time frame. For example, in 2015, despite having a lower T_{air} average across Germany compared to 2014, a significant increase in heat days was observed, particularly in the southern and eastern parts of the country (Figure 1). These findings are crucial for guiding climate change adaptation strategies, initiating targeted research efforts, addressing potential masking effects resulting from hidden discrepancies highlighted in Figure 1, and informing risk reduction policies for German authorities.

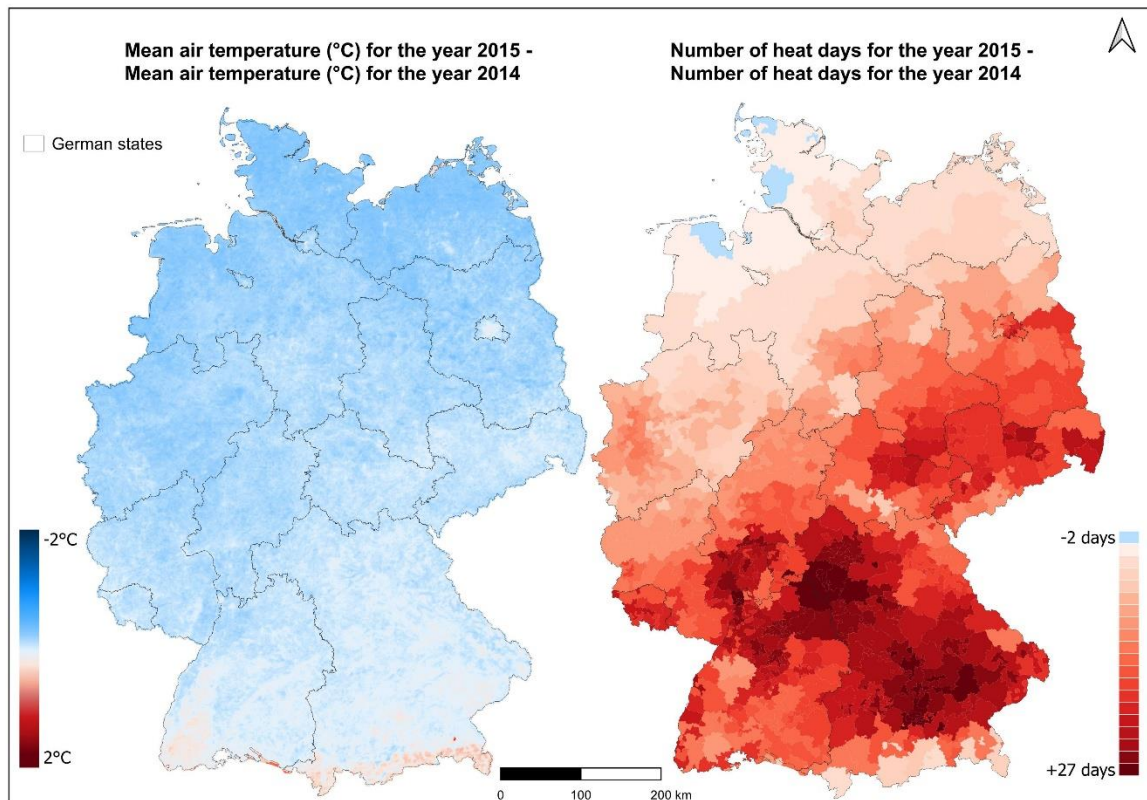


Figure 1. Left plot: Difference between the T_{mean} of 2015 and 2014 (T_{mean} of 2015 minus T_{mean} of 2014) across Germany in a gridded dataset of 1×1 km resolution. Right plot: Difference between the number of heat days ($T_{\text{max}} > 30^{\circ}\text{C}$) of 2015 and 2014 (number of heat days in 2015 minus number of heat days in 2014) across Germany in 3-digit zip code.

2.5.3 Link between publications

In this PhD thesis, T_{air} modeling predominantly relied on LST data due to their strong correlation, with additional predictors serving a complementary role. The robust linear association between T_{air} and LST facilitated the use of linear mixed models to calibrate their relationship effectively. However, modeling RH proved challenging due to the lack of a suitable proxy, contributing to the scarcity of literature in RH modeling and the limited success of previous efforts. Consequently, the T_{mean} dataset, developed for this PhD Thesis, played a pivotal role in RH modeling as a primary predictor, complemented by additional variables. Indeed, T_{mean} emerged as one of the most significant predictors for RH (Paper II - Figure S6).

2.5.4 Contributions to environmental epidemiology

In environmental epidemiology, particularly in studies concerning the health effects of T_{air} and RH or their use as a confounder or effect modifier, it exists a clear need of valid exposure assessment. The case studies conducted in Augsburg and Regensburg for this PhD Thesis, underscore the significant relevance of highly resolved meteorological datasets for the exposure assessment of cohort participants. Current practices in studying T_{air} and RH health effects often rely on data from sparse ground-based monitoring networks, which are distributed unevenly throughout the country and inadequate for capturing their spatial variations, especially in areas of high urbanization. Typically, cohort and other health studies' participants would be assigned T_{air} and RH observations from the nearest weather station or a weighted average of available stations that often have a long distance from the participants' residences, as shown in the KORA case study of this PhD Thesis, leading to exposure values that may not well represent their actual location. This discrepancy can result in exposure errors and biased health effect estimates. This PhD Thesis, however, accounted for T_{air} and RH variability and trends, reducing exposure misclassification and providing a more accurate representation of T_{air} and RH exposure for epidemiological studies in Germany.

Furthermore, particular attention was paid to capturing local disparities of T_{air} and RH. The modeling schemes employed in this PhD Thesis depicted more sufficiently the exposures of cohort participants after going beyond the use of location or city averages, or basic spatial interpolation. The importance of capturing local variations was particularly evident in the NAKO study locations, where the trends of increasing T_{air} over the years were more profound compared to the German averages. Such insights are vital not only for large-scale health studies but also for countrywide planning, enabling the identification of hotspots and informed decision-making.

In addition, there are many studies of environmental epidemiology which require coarser spatial extents, depending on the health data they analyze. For instance, datasets of hospital admissions and mortality from the German Research Data Center (FDZ) necessitate aggregation at broader administrative levels rather than individual processing. Leveraging the datasets' high resolution and comprehensive spatial coverage, it is ensured that the aggregated data remain highly representative and effectively capture variations, even at coarser administrative levels, as illustrated in Figure 2 for RH.

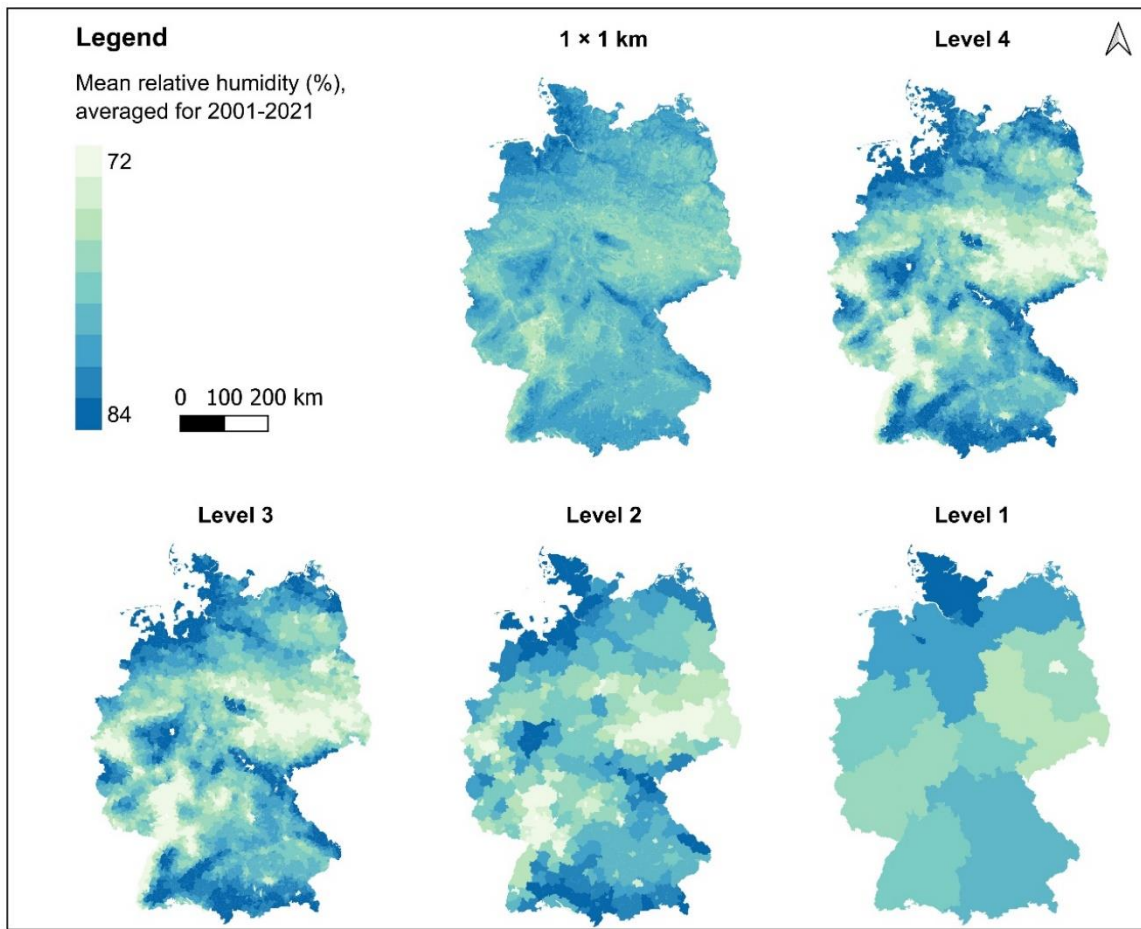


Figure 2. Spatial pattern of the averaged RH in Germany during 2001-2021 in 1×1 km gridded set (original resolution of the RH dataset) and in 4 different German administrative levels as defined by the Database of Global Administrative Areas (GADM)⁸³. Level 1 = States, Level 2 = Districts, Level 3 = Municipalities, Level 4 = Towns.

The contribution of this PhD Thesis to the field of environmental epidemiology is also evidenced through the active utilization and analysis of the generated T_{air} and RH datasets. In particular, the usage of the T_{air} data, which were generated earlier and thus became available sooner, has revealed compelling findings, including lower short- and medium-term T_{air} to be associated with increases in biomarkers of subclinical inflammation⁸⁴, a correlation between higher daily T_{air} and shorter leukocyte telomere length⁸⁵, and the first evidence indicating that medium- and long-term exposures to high T_{air} contribute to increases in epigenetic age acceleration⁸⁶. Additionally, in a German-specific analysis as part of a European study, heat was found to be linked with cardiovascular disease mortality with stronger effects among women and greater vulnerability in highly urbanized, densely populated areas with sparse green spaces, and elevated levels of

particulate matter⁸⁷. Also, T_{air} was studied as one of the environmental exposures which collectively increase the risk of Distal Sensorimotor Polyneuropathy in the elderly, particularly individuals with obesity. Lower T_{air} in the warm season was identified as a contributing factor⁸⁸. Moreover, temperature was considered as one of the environmental exposures investigated for potential increase in the risk of incident type 2 diabetes, without strong associations to be found⁸⁹. Strengthened evidence for the adverse heat impact on respiratory mortality in Northern Europe, was discovered by using the T_{air} dataset⁹⁰, also highlighting vulnerable subpopulations and regions. In a study of multiple environmental exposures, it was found that T_{air} was positively associated with prevalent diabetes in men⁹¹. The produced T_{air} data have additionally been employed in a nationwide German analysis of cause-specific cardiopulmonary mortality, where heat-related increases were identified⁹². In an analysis on heat mortality in Germany, 48,000 heat-related deaths were estimated during 2014-2023, with most of the cases being attributable to heatwaves⁹³ while another study in five European countries revealed heat-related mortality risk increases in higher PM and ozone levels, especially in urban and low-greenness areas⁹⁴.

2.5.5 Novelties

To the best of our knowledge, this PhD Thesis represents the first comprehensive effort in Germany to provide highly resolved spatiotemporal datasets for both T_{air} and RH, spanning from 2000 on, a critical asset for recent German cohorts, registries, administrative records, and insurance data where other sources are lacking. By prioritizing regression-based modeling for T_{air} over spatial interpolation methods that were already used in the German-specific analyses, issues such as neighborhood effects were effectively tackled, thereby portraying better intra-city variability where the majority of cohort participants live. The validation procedures applied in this PhD Thesis, being introduced for the first time in German-specific datasets to this extent, incorporating sophisticated techniques and independent data sources, ensured the reliability of the generated products at both local and countrywide scales. The introduction of a ML scheme for RH modeling for the first time in Germany, not only lowered previously reported errors but also achieved higher R^2 values, thus amplifying precision and reliability. Moreover, this innovative approach constitutes a strong contribution to the literature, potentially serving as a blueprint for similar spatial settings having analogous data availability.

2.5.6 Strengths and limitations

A significant strength of this PhD thesis was that both generated datasets of T_{air} and RH underwent an extensive external validation. Local level validation through a ground-based network and countrywide validation with a different model approach for T_{mean} , showed strong performance and low errors. In addition, the datasets generated in this PhD Thesis boasted high spatial and temporal resolutions, covering Germany over 21 or 22 years at 1×1 km resolution, enabling detailed spatiotemporal analysis. Notably, the methods applied, and the structure of the code allow for the seamless update of both T_{air} and RH datasets, for every future year after downloading the needed data, and consequently the linkage to recent and follow-up health studies. This capability also allows the construction of extended time series in the future, such as of a 30-year period, enabling the calculation of a climate normal. This output is ideal for individual-level epidemiological studies without geographical limitations. Additionally, our T_{air} and RH mapping supports environmental epidemiology research, while our dataset serves as a valuable resource beyond health studies, aiding in the development of high resolution models for predicting T_{air} and RH.

This PhD Thesis was also subject to limitations. Potential resampling and interpolation errors may arise in satellite-derived and previously modeled data. However, all predictors included to the models underwent rigorous evaluation. The selected predictors are known for their high-quality standards and widespread use. Additionally, data gaps on these predictors resulted in missing T_{air} and RH values in the final products of this PhD Thesis. Nevertheless, these gaps were negligible, accounting for less than 1% of the T_{air} and RH datasets, and primarily occurred in areas adjacent to water with sparse to zero population densities, thus having minimal to no impact on missing participants' exposures in epidemiological studies. Another limitation pertains to the availability of meteorological data. The validation with data from independent sources, i.e., external, was limited to the Augsburg region due to the absence of other German-wide monitoring networks, apart from DWD. While this limits the representation of T_{air} and RH variability across Germany, the Augsburg area exhibited substantial spatial variability for all metrics, encompassing both rural and urban zones. In addition, broader validation was ensured by excluding a percentage of countrywide DWD T_{air} observations from the modeling pipeline to serve as independent validation data for the T_{air} metrics. Moreover, countrywide comparison of T_{mean} was

conducted against another DWD spatiotemporal model. Additionally, for the RH model, the ten-fold division was implemented by monitor location through Germany. Another limitation lies in the spatial resolution of 1×1 km, which may be deemed coarse for certain analyses. However, the highly resolved spatiotemporal models provide a significantly better representation of both T_{air} and RH variability compared to the commonly used weather stations, and they effectively captured spatial variations in the local regions of Augsburg and Regensburg, underscoring the sufficiency of their 1×1 km resolution. Finally, the 21- and 22-year timeframe used for analyzing the spatiotemporal T_{air} and RH patterns may be constrained for complete climate change investigations which typically use a 30-year period. This period was limited by the availability of the respective satellite data (most available after February 2000, e.g., LST), yet it provided valuable insights into climate trends in Germany for the first two decades of 21st century and can be extended over the coming years.

2.5.7 Computational challenges

Strong computational challenges are inherent in highly resolved environmental data modeling for a large country like Germany, particularly given the targeted spatial and temporal extents of this PhD Thesis. There was an emerging demand for high-end coding in order to mitigate associated costs. In this PhD Thesis, to streamline operations and decrease computational burdens, sophisticated code optimizations such as parallel processing (e.g., package “foreach”⁹⁵) were implemented. The processing time for T_{air} models was substantially reduced from the initial 47 days to 24 days for all models over the whole period, with further optimization enabling completion within a mere 1 day for each subsequent year. Similarly, the RH model underwent intricate optimization, resulting in a reduction to less than 1 day for annual runs. These optimizations were essential in managing the computational demands of handling vast datasets, ensuring efficient utilization of resources.

2.6 Conclusion and outlook

In this PhD Thesis, significant effort was devoted to tackling the crucial task of refining meteorological exposure assessment under a shifting climate. In this context, this PhD Thesis contributes substantially to mitigating exposure misclassification in epidemiological studies

exploring the impact of meteorological conditions in Germany. Specifically, this PhD Thesis achieved a more precise representation of T_{air} and RH variability, enhancing our understanding of their spatiotemporal patterns and evolution over recent decades across the country. Leveraging a multi-stage scheme of linear mixed models, daily T_{min} , T_{mean} and T_{max} were estimated and DTR was calculated across Germany from 2000 to 2020, providing a complete T_{air} dataset. Simultaneously, by integrating observation, modeled and remote sensing data under a RF modeling framework, RH was predicted across Germany from 2000 to 2021. The rigorous validation process, conducted at both local and nationwide levels for T_{air} and RH, provided compelling evidence for the high standards and reliability of these models. The datasets generated proved to be highly compatible with contemporary German health cohorts, ranging from local studies such as the KORA cohort to countrywide initiatives like NAKO study. The T_{air} and RH datasets not only serve as invaluable resources for environmental-epidemiological studies but also hold potential for other research applications. Last but not least, beyond its immediate context, this PhD thesis established a blueprint that can be applied to other countries and spatial settings sharing comparable data availability.

Amidst a rapidly changing climate, such models stand as indispensable tools for advancing both scientific understanding and public health protection. Over the course of this PhD Thesis, the generated T_{air} and RH datasets was requested, transferred, and employed by a multitude of scientific teams in Germany for various health analyses (2.6.2 Data impact). These collaborations hold the promise of significantly advancing the field of environmental epidemiology in Germany by simply integrating better data in our research field.

2.6.1 Data dissemination

During the progression of this PhD Thesis, I had the opportunity to present my ongoing and completed work on multiple occasions, including scientific meetings, conferences, symposia, as well as various seminars, webinars, and workshops. Notable presentations included the discussion of the T_{air} modeling process and data at the ISEE Young 2021 Virtual Conference⁹⁶, the PhD program - Medical Research in Epidemiology and Public Health (PhD-EPH) Annual Retreat 2021, and the RH modeling scheme and data at the European Geosciences Union (EGU) General Assembly 2022⁹⁷, the Helmholtz AI Conference 2022 and the 34th Annual Conference of

the ISEE⁹⁸. Furthermore, a joint presentation on T_{air} and RH models and data took place at the German Society for Epidemiology (DGEpi) workshop entitled “Challenges and opportunities regarding exposure assessment in environmental epidemiology”. Additionally, I shared insights on the T_{air} and RH models and data at the seminar series of the EPI-HMGU Institute and the HI-CAM project, the PhD-EPH journal clubs, as well as at the Robert Koch Institute (RKI) Symposium Artificial Intelligence in Public Health Research and the MRC Health Collaborations Workshop, where I was invited to speak. This engagement effectively contributed to the promotion of the T_{air} and RH datasets.

2.6.2 Data impact

The T_{air} and RH datasets produced in the context of this PhD Thesis have garnered significant interest and have been requested by scientific teams in Germany and abroad. We readily supplied our data to the inquiring scientists, who have since incorporated them into various German and European research projects or are presently employing them. For instance, the data have been transferred to scientists of EPI-HMGU, of the Climate Service Center Germany (GERICS), Hereon, of the Centre for Artificial Intelligence in Public Health Research (ZKI-PH), RKI, of the German Center for Neurodegenerative Diseases (DZNE), of the Federal Statistical Office of Germany (DESTATIS - Statistisches Bundesamt) and of the University of Eastern Finland. They are being used in multiple projects such as the HI-CAM⁹⁹, Noise2NAKO^{AI100}, EXHAUSTION¹⁰¹ and AIR-LOCK¹⁰² and have been linked with health and individual data from cohorts such as the KORA⁶³, NAKO⁶⁴ and Rhineland study¹⁰³. The data also align with insurance records and are being used in projects such as the DigiMed¹⁰⁴ and KlimGesVor¹⁰⁵, which utilize data from the AOK insurance company¹⁰⁶. Additionally, they have been linked with hospital admission and mortality data from FDZ¹⁰⁷.

There are several of noteworthy publications already, demonstrating the considerable impact this PhD Thesis has already made in the field of epidemiology, particularly in environmental epidemiology. These published works have been described in section 2.5.4 Contributions to environmental epidemiology.

Furthermore, there is a lot of ongoing research, many manuscripts under preparation, under review or to be submitted soon. For example, short-term exposure T_{air} impacts on self-rated health

status were investigated for participants in Augsburg, Germany, without strong evidence to be found¹⁰⁸. Moreover, the RH dataset has been already used in a complementary role, as a possible confounder of the effects of air pollution reductions on mortality changes during the COVID-19 lockdown period¹⁰⁹. Additionally, in a study I worked on during my PhD time, we built a ML pipeline to identify the driving environmental, socio-economic status (SES) and individual factors for cardiovascular health, employing both the T_{air} and RH datasets, and we identified non-optimal T_{air} as one of the main drivers for hypertension¹¹⁰ (Appendix - Further projects). EPI-HMGU presently investigates the relationship between short- and long-term heat exposure and cause-specific cardiopulmonary morbidity¹¹¹, also trying to identify vulnerability factors, and the short-term heat effects on cardiovascular¹¹² and respiratory¹¹³ morbidity and mortality in Germany. ZKI-PH, RKI aims to investigate outbreaks of Legion's disease in Germany linked with RH and DESTATIS targets to offer insights about the viability of Eurostat's suggested methodology for local climate regulation and explore improvements at the national level. GERICS aims to assess the utility of insurance data in evaluating morbidity impacts from heat extremes in Germany, beginning with highly detailed insurance data for the federal state of North Rhine-Westphalia.

2.6.3 Future research

Looking ahead and contemplating the near and distant future of the field, it is imperative for meteorological exposure assessment research to undergo significant advancements. The future of exposure assessment studies should target finer spatial resolutions, particularly on a city-specific scale, with a dedicated emphasis on the UHI effect which is very difficult to be precisely captured with the current available datasets and modeling standards. Applications already exist utilizing micrometeorological simulations¹¹⁴ (e.g., Palm4U model¹¹⁵), although they are not suitable for epidemiological analysis due to their limited temporal extent of one to few days. In addition, finer temporal resolution, such as hourly values crucial for epidemiological research, can be achieved from our modeling schemes through appropriate restructuring and modifications. Despite the considerable computational and storage costs associated with these refinements, they can be feasibly implemented through high-performance computing, a tool we intend to use in the imminent future. Moreover, to accomplish a more nuanced comprehension of environmental exposures, estimating additional meteorological features and indices in Germany

becomes essential. This includes incorporating parameters like absolute and specific humidity, or the compilation of maps of indices such as wet-bulb globe temperature, heat index, apparent temperature, and humidex.

3. Paper I

Title: High-resolution spatiotemporal modeling of daily near-surface air temperature in Germany over the period 2000–2020

Authors: Nikolaos Nikolaou, Marco Dallavalle, Massimo Stafoggia, Laurens M. Bouwer, Annette Peters, Kai Chen, Kathrin Wolf, Alexandra Schneider

Journal: Environmental Research

Year: 2023

Volume: 219

Pages: 115062

DOI: <https://doi.org/10.1016/j.envres.2022.115062>

Supplements: <https://www.sciencedirect.com/science/article/pii/S0013935122023891?via%3Dihub#appsec1>

Impact factor: 8.3 (Journal Citations Reports® 2022)

Rank: 32/275 in category Environmental Sciences and
16/207 in category Public, Environmental & Occupational Health
(Journal Citations Reports® 2022)



Contents lists available at ScienceDirect

Environmental Research

journal homepage: www.elsevier.com/locate/envres

High-resolution spatiotemporal modeling of daily near-surface air temperature in Germany over the period 2000–2020

Nikolaos Nikolaou^{a,b,*}, Marco Dallavalle^{a,b}, Massimo Stafoggia^c, Laurens M. Bouwer^d, Annette Peters^{a,b}, Kai Chen^{e,f}, Kathrin Wolf^{a,1}, Alexandra Schneider^{a,1}

^a Institute of Epidemiology, Helmholtz Zentrum München, German Research Center for Environmental Health, Neuherberg, Germany

^b Institute for Medical Information Processing, Biometry, and Epidemiology, Pettenkofer School of Public Health, LMU Munich, Munich, Germany

^c Department of Epidemiology, Lazio Regional Health Service, Rome, Italy

^d Climate Service Center Germany (GERICS), Helmholtz-Zentrum Hereon, Hamburg, Germany

^e Department of Environmental Health Sciences, Yale School of Public Health, New Haven, CT, USA

^f Yale Center on Climate Change and Health, Yale School of Public Health, New Haven, CT, USA

ARTICLE INFO

Keywords:

Near-surface air temperature
Land surface temperature
Spatiotemporal modeling
Validation
Exposure assessment
Environmental epidemiology

ABSTRACT

The commonly used weather stations cannot fully capture the spatiotemporal variability of near-surface air temperature (T_{air}), leading to exposure misclassification and biased health effect estimates. We aimed to improve the spatiotemporal coverage of T_{air} data in Germany by using multi-stage modeling to estimate daily 1×1 km minimum (T_{min}), mean (T_{mean}), maximum (T_{max}) T_{air} and diurnal T_{air} range during 2000–2020. We used weather station T_{air} observations, satellite-based land surface temperature (LST), elevation, vegetation and various land use predictors. In the first stage, we built a linear mixed model with daily random intercepts and slopes for LST adjusted for several spatial predictors to estimate T_{air} from cells with both T_{air} and LST available. In the second stage, we used this model to predict T_{air} for cells with only LST available. In the third stage, we regressed the second stage predictions against interpolated T_{air} values to obtain T_{air} countrywide. All models achieved high accuracy ($0.91 \leq R^2 \leq 0.98$) and low errors ($1.03 \text{ }^\circ\text{C} \leq \text{Root Mean Square Error (RMSE)} \leq 2.02 \text{ }^\circ\text{C}$). Validation with external data confirmed the good performance, locally, i.e., in Augsburg for all models ($0.74 \leq R^2 \leq 0.99$, $0.87 \text{ }^\circ\text{C} \leq \text{RMSE} \leq 2.05 \text{ }^\circ\text{C}$) and countrywide, for the T_{mean} model ($0.71 \leq R^2 \leq 0.99$, $0.79 \text{ }^\circ\text{C} \leq \text{RMSE} \leq 1.19 \text{ }^\circ\text{C}$). Annual T_{mean} averages ranged from $8.56 \text{ }^\circ\text{C}$ to $10.42 \text{ }^\circ\text{C}$ with the years beyond 2016 being constantly hotter than the 21-year average. The spatial variability within Germany exceeded $15 \text{ }^\circ\text{C}$ annually on average following patterns including mountains, rivers and urbanization. Using a case study, we showed that modeling leads to broader T_{air} variability representation for exposure assessment of participants in health cohorts. Our results indicate the proposed models as suitable for estimating nationwide T_{air} at high resolution. Our product is critical for temperature-based epidemiological studies and is also available for other research purposes.

1. Introduction

Climate change is one of the greatest global challenges for humans and their entire living environment in the 21st century. It has been at the center of various social and research disciplines, from economics (Hertel and Rosch, 2010) and animal welfare (Lacetera, 2019) to land management and food security (Shukla et al., 2019), with a particular attention to the human health domain (Peters and Schneider, 2021; Vicedo-Cabrera et al., 2021; Watts et al., 2019). Near surface air temperature (T_{air}) is one of the most important meteorological parameters

and a key indicator of climate change. T_{air} is observed to be steadily increasing globally since pre-industrial times, with the 10 warmest years on record to have occurred after 2000 (Lindsey and Dahlman, 2021). Further increases from $3 \text{ }^\circ\text{C}$ to $6.2 \text{ }^\circ\text{C}$ are expected by the end of 2100, if no action is taken (IPCC, 2022). In Germany, 32 of the last 34 years are characterized by annual T_{air} above the 1961–1990 average (DWD, 2022).

Many epidemiological studies have documented the adverse impact of T_{air} on mortality (Guo et al., 2016; Zanobetti and Schwartz, 2008) and morbidity (Ye et al., 2012), especially when exposure to extreme T_{air}

* Corresponding author. Ingolstädter Landstr. 1, D-85764, Neuherberg, Germany.

E-mail address: nikolaos.nikolaou@helmholtz-muenchen.de (N. Nikolaou).

¹ Shared last authorship.

<https://doi.org/10.1016/j.envres.2022.115062>

Received 3 July 2022; Received in revised form 9 December 2022; Accepted 12 December 2022

Available online 17 December 2022

0013-9351/© 2023 The Authors. Published by Elsevier Inc. This is an open access article under the CC BY license (<http://creativecommons.org/licenses/by/4.0/>).

values occurs (Gronlund et al., 2018; Kovats and Kristie, 2006). Besides heat waves and cold spells, increases or decreases in more moderate T_{air} ranges to which people are exposed most of the time during their life, also contribute to the observed temperature-related mortality burden (Gasparrini et al., 2015). Human health can be adversely affected by T_{air} either after short (Breitner et al., 2014) or long-term (Zafeiratou et al., 2021) exposure. Therefore, T_{air} extremes and variations pose a major threat for public health, especially with continuing global warming and the higher frequency and intensity of extreme events (Meehl and Tebaldi, 2004). In this regard, high spatiotemporally-resolved T_{air} exposure datasets are needed for improved exposure assessment in epidemiological studies.

The vast majority of environmental epidemiological studies that investigate health effects of T_{air} or implement T_{air} in their analyses as a confounder or an effect modifier, use observational data from meteorological stations, often provided by a national monitoring network. These datasets are generally highly accurate, quality controlled and publicly available and consist of various meteorological parameters, including T_{air} 2 m above the ground. However, the monitoring locations are irregularly scattered, often placed in rural or park-like environments, and their number is too limited to fully capture spatial temperature variations across urban and rural landscapes. Furthermore, in most cases airport stations are used, which, by definition, are located out of the cities. Therefore, the commonly used weather station observations are not capable to represent the full variability of T_{air} in space and in time, leading to exposure misclassification and bias of health effect estimates towards the null hypothesis of no association (Armstrong, 1998). Over the last years, researchers have developed methods to provide high-resolution spatiotemporally T_{air} exposure outputs on local, countrywide or even global scales. Several interpolation techniques have been suggested such as regression-kriging (Kilibarda et al., 2014; Li et al., 2020; Sekulić et al., 2020), modified inverse distance weighting (IDW) and thin plate spline (TPS) interpolation. For example, Sekulić et al. (2020) predicted daily mean T_{air} (T_{mean}) in 1×1 km across Croatia for 2008 using a regression kriging model with T_{mean} observations and geometrical temperature trend, digital elevation model (DEM) and topographic wetness index as covariates ($R^2 = 0.98$, Root Mean Square Error (RMSE) = 1.2 °C). Jobst et al. (2017) introduced a multi-layer approach, including TPS and lapse rate models, to estimate daily maximum T_{air} (T_{max}) and minimum T_{air} (T_{min}) in 1×1 km from 1990 to 2014, in the alpine Clutha catchment, New Zealand (T_{max} RMSE = 2.38 °C, T_{min} RMSE = 2.93 °C). Other studies compared multiple interpolation approaches in the same region. In middle Ebro Valley, Spain, Vicente-Serrano et al. (2003) compared the results of annual T_{air} models of global or local interpolators as well as geo-statistical and mixed methods. R^2 ranged from 0.39 (co-kriging) to 0.75 (regression-based) and RMSE from 0.80 °C (co-kriging) to 0.56 °C (IDW, $r = 2$). However, the traditional interpolation methods are subject to specific limitations. For instance, they are highly affected by the weather stations locations, without fully accounting for between-station variability. This issue is more profound in complex geo-climatic areas and landscapes characterized by high spatial heterogeneity. Interpolation also leads to neighbouring effects and cannot capture the T_{air} variations in city-level analysis and consequently the urban heat island (UHI) effects are not well represented. Finally, the weather stations are often poorly scattered across a country and fail to provide complete T_{air} time series.

To improve the interpolation between locations, several studies have used satellite data for their main predictors (Benali et al., 2012; Fluckiger et al., 2022; Vancutsem et al., 2010; Xu et al., 2014; Zhu et al., 2013). For instance, Xu et al. (2014) applied a linear regression and a random forest (RF) model to predict T_{max} across British-Columbia, Canada. The RF model achieved higher model's accuracy ($R^2 = 0.74$, mean absolute error (MAE) of 2.02 °C) in comparison with the linear regression model ($R^2 = 0.64$, MAE = 2.41 °C). Recently, Jin et al. (2022) estimated high-resolution spatiotemporal T_{mean} from land surface temperature (LST) and a variety of spatial predictors using a three-stage

ensemble model in Sweden over a long period. The ensemble model consisted of a generalized additive model, a generalized additive mixed model, a RF model and an extreme gradient boosting model ($R^2 = 0.98$, RMSE = 1.38 °C). In recent years, several studies applied a multi-stage regression-based approach introduced by Kloog et al. (2014), and making use of the moderate resolution imaging spectroradiometer (MODIS) LST products to predict daily T_{air} in 1×1 km (Kloog et al., 2017; Rosenfeld et al., 2017; Shi et al., 2016). This approach is straightforward to model, with high accuracy and small errors.

T_{mean} is the most frequently modeled T_{air} measure and the most commonly used in studies of environmental epidemiology. However, we also need to focus on T_{min} and T_{max} . Climate change strongly affects T_{min} and T_{max} (Modala et al., 2017) and there is evidence that T_{min} , which corresponds to the nighttime temperatures, has been increased more than T_{max} during the 20th century (Gil-Alana, 2018). Due to this substantial T_{min} increase, especially the urban areas face extensive heat stress nights, a phenomenon that will be strengthened in the future (Chapman et al., 2017). Modeling T_{min} and T_{max} also facilitates the estimates of the diurnal T_{air} range (DTR). There is already evidence that DTR affects, independently from T_{mean} , the human health (Cheng et al., 2014; Davis et al., 2020). These effects are critically important for future policies implementation, but lack of broad epidemiological investigation, especially at national scale due to the scarcity of fully spatially covered, high resolution, daily DTR data.

In this study, we aimed to extend and improve the spatiotemporal coverage of T_{air} data in the complex terrain of Germany, using remote sensing and regression-based modeling. More specifically, we aimed to map daily T_{min} , T_{mean} , T_{max} and DTR in 1×1 km across Germany during the period 2000–2020 to provide harmonized T_{air} data for epidemiological research like the German National Cohort (NAKO) with more than 200,000 participants spread around the country.

2. Methods

2.1. Study area

Germany is located in central Europe, covering $357,021$ km², with a population of 83.2 million people (Statistisches Bundesamt, 2022). The country consists of a diverse landscape, starting from the Alps in the south to the northern coast lines of the North and Baltic Seas, including big cities, small towns, mountains, various water bodies, forests and arable land. Elevation ranges from 3.54 m below sea level near Neuendorf-Sachsenbande to $2,962$ m in the Alpine mountain Zugspitze. Climate is temperate to continental according to the Köppen climate classification. There is a warm summer humid continental climate in south-eastern regions and a temperate oceanic climate in north-western regions (Beck et al., 2018b). The lowest T_{air} ever recorded in Germany was -37.8 °C measured on February 12th, 1929 in Wolznach-Hüll (DWD, 2017), while the highest was 41.2 °C measured on July 25th, 2019 in Duisburg and in Tönisvorst of North Rhine-Westphalia (DWD, 2020). We divided Germany's mainland into $366,536$ grid cells of 1×1 km based on the European INSPIRE (Infrastructure for Spatial Information in the European Community) standard using the Lambert Azimuthal Equal-Area projection, EPSG: 3035 (©GeoBasis-DE/BKG (2021)).

2.2. Materials

We collected a large number of publicly available earth- and satellite-based data derived from multiple sources for the period 2000–2020 across Germany, with the best fitting temporal and spatial resolution for our analysis. LST based on satellite data was the main predictor for T_{air} as they were strongly correlated. Moreover, we implemented in the modeling process various spatial predictors such as remote sensing elevation, vegetation, urban fabric, arable land, pastures, forests and inland waters to increase the percentage of explained

variance and enhance the model performance overall.

2.2.1. T_{air} data

We downloaded daily data of T_{min} , T_{mean} and T_{max} observations 2 m above the ground from 1080 sites, which are publicly available from the Deutscher Wetterdienst (DWD) - German Meteorological Service online database (DWD, 2021). All data were quality controlled by DWD and their metadata (e.g., station relocation or time zones) were provided as well. We did not find any unusual values such as temperatures lower or higher than the observed temperature extreme records in the country or any seasonal outliers. We excluded stations that stopped measuring before 2000 ($N = 358$), stations that weren't operating continuously over the entire study period ($N = 309$, $> 70\%$ NAs) and stations located outside the German mainland ($N = 7$). Thus, we included T_{air} data from 406 weather stations scattered across the country (Fig. 1), with each station located in a single grid cell of our gridded dataset. The DWD T_{air} dataset had only 1.4% of station-days with missing values during our study period.

2.2.2. Remote sensing data

2.2.2.1. TERRA MODIS data. We downloaded and preprocessed TERRA MODIS LST and normalized difference vegetation index (NDVI) data from the server (NASA, 2021) through the R package MODISStp (Busetto and Ranghetti, 2016). Since TERRA MODIS started measuring on February 24th, 2000, our analysis also starts on that date.

2.2.2.1.1. LST data. LST defines the radiative temperature of the earth's surface, as derived from infrared radiation and measured in the direction of the remote sensor. We used the product MOD11A1v006 that provides LST (using the generalized split-window algorithm) data in a

daily temporal resolution and a spatial resolution of 1×1 km, corrected for emissivity (Wan et al., 2015). We used daytime LST to model T_{max} and nighttime LST to model T_{min} and T_{mean} , as suggested by previous studies (Rosenfeld et al., 2017), regardless their quality assurance flag to avoid reducing the input sample size since for the most problematic cells affected by cloud effects, instrumental problems or other reasons, LST was not produced. For more insight into MODIS LST and its retrieval, we refer to the existing literature (Wan, 2014).

2.2.2.1.2. NDVI data. NDVI is used as a proxy for greenness and quantifies the amount of vegetation by calculating the near-infrared and the red light difference. We used the product MOD13A3v006 that provides monthly NDVI data, as greenness does not change considerably within a month, in a spatial resolution of 1×1 km (Didan, 2015). We also tested the enhanced vegetation index (EVI) as alternative. Since we observed strong positive correlations between NDVI and EVI (21-year average $r = 0.81$), negligible differences in the models' validation results (after the 3rd or 4th decimal point) and extremely correlated T_{air} predictions ($r = 0.999988$), we kept NDVI as model predictor.

2.2.2.2. DEM data. We used the DEM (GTOPO30) developed by the US Geological Survey's Earth Resources Observation Systems Data Center. Its spatial resolution was 30-arc-second and we aggregated it to 1×1 km grid cells over mainland Germany, borders and shorelines included (Fig. S1).

2.2.2.3. Land use data. From Copernicus CORINE Land Cover 2012 (CLC2012, 250 m resolution) <https://land.copernicus.eu/pan-europe/corine-land-cover/clc-2012> and 2018 (CLC2018, 100 m resolution) <https://land.copernicus.eu/pan-european/corine-land-cover/clc2018>, we extracted the variables urban fabric (classes: "continuous urban

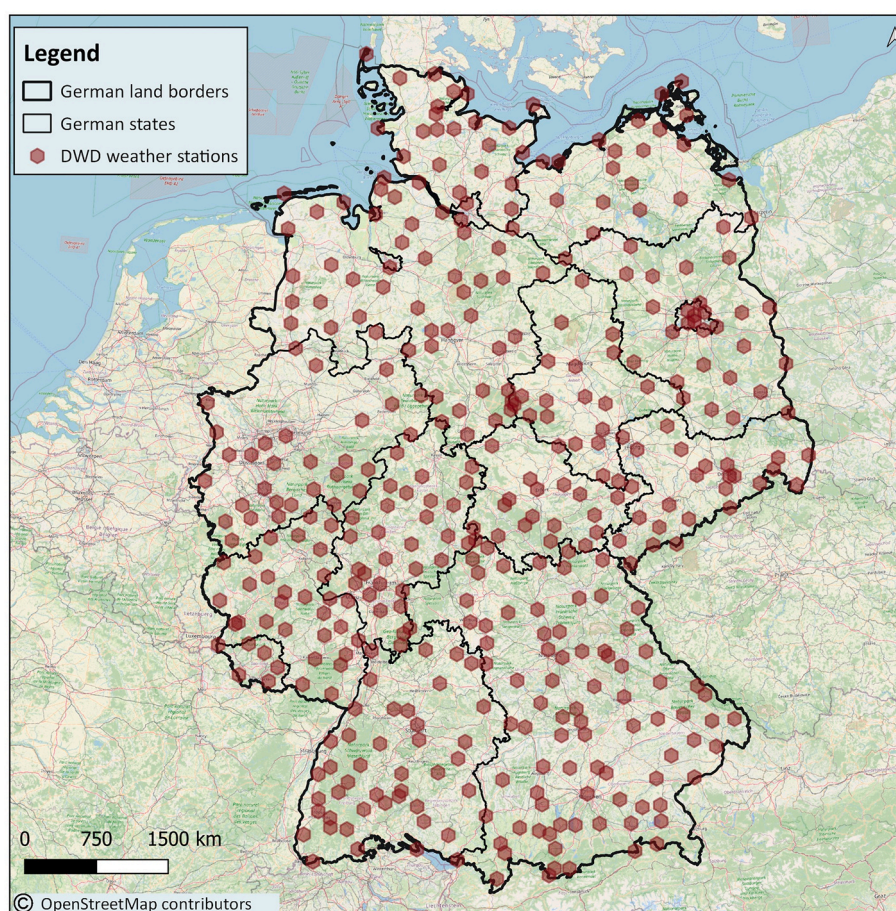


Fig. 1. Map of Germany showing the spatial distribution of the 406 T_{air} weather stations included in our analysis (2000–2020).

fabric” and “discontinuous urban fabric” from the subcategory urban fabric of the artificial surfaces category), arable land (classes: “non-irrigated arable land”, “permanently irrigated arable land” and “rice fields” from the subcategory arable land of the agricultural areas category), pastures (class: “pastures” from the subcategory arable land of the agricultural areas category), forests (classes: “broad-leaved forest”, the “coniferous forest” and the “mixed forest” from the subcategory forest of the forest and seminatural areas category) and inland waters (classes: “water courses” and the “water bodies” from the subcategory inland waters of the water bodies category). We then combined the classes of each variable and calculated each variable’s proportion of CORINE pixels to the INSPIRE 1×1 km grid cells over mainland Germany. CLC2012 was used for modeling until 2016 and CLC2018 from 2017 on.

2.3. Statistical analysis and validation

We applied a three-stage regression-based model, following the approach from Kloog et al. (2014). In previous studies following the same approach basis, the results were promising. Kloog et al. (2014) mapped T_{mean} in the northeast and mid-Atlantic USA (RMSE = 2.16 °C). Shi et al. (2016) predicted T_{mean} in southeastern USA ($R^2 = 0.97$, RMSE = 1.38 °C). Rosenfeld et al. (2017) estimated T_{min} , T_{mean} and T_{max} in Israel using LST data from both TERRA and AQUA satellites (RMSE < 1.7 °C). Finally, Kloog et al. (2017) estimated T_{mean} in France ($R^2 > 0.93$, RMSE < 1.7 °C). Given the method’s high accuracy, the small errors, its straightforward way of modeling and its successful application in different and geographically complex areas around the world, we also followed the basic concept of this approach, adjusting it to our needs with regard to Germany’s unique spatial and geo-climate features, differentiating the process where it was necessary and introducing a TPS technique implementation on the third stage of the model. More specifically, due to Germany’s unique surface and altitude fluctuation, we first adjusted our model for elevation. We also added information on water bodies, forests and arable land which corresponded to a large proportion of the country, i.e., arable land covers around 34% of Germany (and 28.32% in stage 1 - calibration stage of our analysis). Additionally, we implemented a TPS interpolation given the number and the distribution of the DWD weather stations and used grid-cell specific intercepts and slopes in the third stage to capture spatial differences in the relationship of interpolated observed T_{air} with predicted T_{air} . Our code was developed in R software, version 4.0.2 (R Core Team, 2020). The linear mixed models analyses were conducted with the R package “LM4” (Bates et al., 2014), while figures were produced either using the R package “ggplot2” (Wickham, 2009) or QGIS, version 3.10.5-A Coruña (QGIS Development Team, 2020). We applied the three-stage modeling process separately for each year and each T_{air} measure.

2.3.1. First stage: T_{air} and LST available

The first stage included grid cells where both T_{air} observations from DWD weather stations and satellite-derived LST values were available. We regressed T_{air} on LST and additional spatial information to understand and describe the T_{air} -LST relationship in the best way possible for Germany over the last two decades. A daily random slope for LST was implemented in the model to account for daily variations in the T_{air} -LST relationship.

The general mathematical formula of the first stage linear mixed effects model was the following:

$$T_{airij} = b_0 + u_j + (b_1 + v_j) * LST_{ij} + b_2 * DEM_i + b_3 * NDVI_{ij} + b_4 * UrbanFabric_i + b_5 * ArableLand_i + b_6 * Pastures_i + b_7 * Forests_i + b_8 * InlandWaters_i + \epsilon_{ij} \quad (1)$$

where,

- T_{airij} stands for the T_{air} observation at the grid cell i on day j ;
- b_0 and u_j stand for the fixed and the random intercepts, respectively;
- LST_{ij} stands for the daytime or nighttime LST measurement at the grid cell i on day j ;
- b_1 and v_j stand for the fixed and the random slopes, respectively;
- DEM_i stands for the elevation at grid cell i ;
- $NDVI_{ij}$ stands for the monthly NDVI measurement at the grid cell i on the month that day j falls in;
- $UrbanFabric_i$, $ArableLand_i$, $Pastures_i$, $Forests_i$ and $InlandWaters_i$ stand for the percentages of the urbanism, the land under temporary agricultural crops, the pastures, the forests and the water bodies at the grid cell i .
- ϵ_{ij} is the error term at grid cell i on day j .

For each T_{air} measure, we applied a separate regression.

2.3.2. Second stage: T_{air} not available and LST available

In the second stage, T_{air} was predicted for the combinations of grid cells and days without available T_{air} observations, but with available LST data by applying the regression coefficients derived from EQ. (1).

2.3.3. Third stage: neither T_{air} nor LST available

In the third stage, we predicted T_{air} for grid cells and days with neither T_{air} observations nor LST data. We regressed second stage T_{air} predictions against daily interpolated T_{air} values in 1×1 km across Germany via a linear mixed model with random grid-cell-specific intercepts and slopes. Since previous studies suggested that TPS outperformed alternative interpolation techniques such as kriging or IDW for T_{air} modeling (Wu et al., 2015), we applied it to interpolate the DWD T_{air} data. The smoothing parameter was chosen by a generalized cross validation (CV) method. We used the R package “fields” (Nychka et al., 2017) for the TPS interpolation.

The general mathematical formula of the third stage linear mixed effects model was the following:

$$\text{Second stage } T_{airij} = a_i + b_i * \text{int}T_{airij} + \epsilon_{ij} \quad (2)$$

where,

- Second stage T_{airij} stands for the T_{air} predictions given by the second stage at the grid cell i , on the day j ;
- a_i and b_i stand for the i grid-cell-specific intercepts and slopes;
- $\text{int}T_{airij}$ stands for the interpolated T_{air} values at the grid cell i on day j ;
- ϵ_{ij} is the error term at grid cell i on day j .

For each T_{air} measure, we applied a separate regression.

After predicting T_{min} , T_{mean} and T_{max} , we also calculated the DTR by taking the difference of T_{min} from T_{max} . All dates are represented in the standard time zone for Germany, i.e., UTC+1, without adjusting for daylight-saving time.

2.3.4. Internal validation

The models’ performance was evaluated through 10-fold CV separately for the first and third stage by randomly dividing the respective datasets into testing and training sets (10:90) ten times. The models were then re-fitted in each of the ten training sets and T_{air} predicted in the respective testing sets.

For the first stage, we calculated the corresponding percent of explained T_{air} variability R^2 and the RMSE between observed and predicted T_{air} for each run for the cell-days with both T_{air} and LST available. The temporal and spatial performance (R^2 and RMSE) were also computed (Shi et al., 2016). Briefly, the temporal statistics derived by regressing (a) against (b), where: (a) is the difference of the DWD observed T_{airij} of each j day with the annual DWD observed T_{airi} in weather station location i , and (b) is the difference of the predicted T_{airij}

of each j day with the annual predicted T_{air} at the same weather station location i . Spatial statistics derived by regressing (c) against (d), where: (c) is the annual DWD observed T_{air} and (d) is the annual predicted T_{air} in weather station location i .

For the third stage, R^2 and RMSE derived from linearly regressing the predicted T_{air} against DWD observed T_{air} for each run. Before the beginning of the modeling process, this specific sub-sample of DWD weather stations T_{air} observations in cell-days without LST available, was completely held-out from the modeling process. Thus, we used these cell-days to validate our third stage predictions and to quantify the respective errors also under conditions such as of cloudy days. We also compared the predicted T_{air} of the third stage against the second stage T_{air} , i.e., the dependent variable of the third stage model, for all grid cells across Germany.

We additionally quantified the bias through measuring the mean signed error between the DWD observed T_{air} and our models' T_{air} as predicted from all the modeling stages.

2.3.5. Validation with external data

We carried out two validations using external datasets and compared our predictions i) on the small scale with a monitoring network (HOBO-Logger) set up in the region of the city of Augsburg in 2012 in a cooperative work of Helmholtz Munich (Institute of Epidemiology, Environmental Risks) and the University of Augsburg (Institute of Geography, Physical Geography and Quantitative Methods) (Beck et al., 2018a) and ii) on the large scale with predictions from another German-wide model dataset developed by DWD within the "Testreferenzjahre" (TRY) project by using a completely different methodological approach (Krähenmann et al., 2018).

For the small-scale validation, we considered T_{air} measurements of 4 min resolution from 82 HOBO-Logger devices (ONSET, Type Pro v2) (2013–2018) with most of them to be located in the city of Augsburg where we did not have prior information from DWD on the first - calibration model's stage (Fig. S2). For a detailed description of the monitoring network and the measurements' quality assurance we refer to the corresponding paper (Beck et al., 2018a). To proceed with our comparison, we aggregated the 4-min data to daily T_{mean} values and we also considered the daily T_{min} and T_{max} values. We additionally investigated the intraseasonal models' performance.

For the large scale validation, we downloaded openly available daily T_{mean} predictions from the DWD TRY project on a 1×1 km spatial resolution (Krähenmann et al., 2016), generated by a 3-step interpolation method. A daily background field was constructed from a non-linear temperature gradient and it was estimated seven times a day. Then, two hourly background fields were calculated by weighting the three temporally closest background fields and they also conducted an hourly residual interpolation. For a detailed description of the modeling process, we refer to the corresponding paper (Krähenmann et al., 2018). Our comparison was restricted to mainland Germany and the overlapping time period between the two datasets from 2001 to 2012. In addition to an overall comparison of both T_{mean} models' predictions (all our model predictions against all DWD TRY model predictions across the country for every year), we also conducted several sensitivity analyses subsetting the predictions by season, without their extreme values, to their extreme values, and comparing the urban versus the rural Augsburg area.

For both 2.3.4 and 2.3.5, all stated R^2 values correspond to the fraction of variance explained by the respective models.

2.4. Case study - Augsburg

We used Augsburg as a case study to examine the spatiotemporal variability as well as the distribution of the modeled daily T_{mean} in comparison with the observed daily T_{mean} at the DWD sites. Augsburg is the third largest city in Bavaria, Germany. The overall population of its urban district and its surrounding districts (Landkreis Augsburg in the

west and Aichach-Friedberg in the east), is around 900,000 people, of which approx. 300,000 live in the city center. We chose Augsburg as it is the study region of the Cooperative Health Research in the Region of Augsburg (KORA) cohort (Holle et al., 2005) and one of the 18 study centers of the NAKO study (German National Cohort Consortium, 2014).

2.5. Spatial and temporal patterns in Germany during 2000–2020

We calculated the main descriptive statistics of the three T_{air} measures and investigated the spatiotemporal patterns of T_{air} across entire Germany, but also for the 18 study centers of the NAKO study, which are scattered across the country and represent both rural and urban areas including the biggest German cities (Fig. S3), focusing on study regions that have more than 2000 inhabitants/km² and cover a large population percentage (Mannheim, Leipzig, Kiel, Hannover, Hamburg, Essen, Düsseldorf, Berlin and Augsburg).

3. Results

3.1. Models' accuracy

T_{air} and LST were highly correlated, with an average $R^2 = 0.91$, an intercept of 4.79 °C and a slope of 0.88 over the period 2000–2020, after regressing T_{air} against LST. Table 1 shows the prediction accuracy results for the first and the third stage model of each T_{air} measure for 2000–2020 on average. The detailed results per year are in the Supplementary material (Tables S1 and S2). For the first stage, the 21-year average R^2 equalled 0.91 (yearly range: 0.86–0.93), 0.96 (yearly range: 0.95–0.97) and 0.96 (yearly range: 0.95–0.97) for the T_{min} , T_{mean} and T_{max} model in an average of 45,432, 48,925 and 42,155 cell-days, respectively. We additionally observed low values of RMSE for all the models. For the T_{min} model, the 21-year average RMSE equalled 2.02 °C (yearly range: 1.91 °C–2.13 °C), while for the T_{mean} and T_{max} equalled 1.41 °C (yearly range: 1.32 °C–1.54 °C) and 1.77 °C (yearly range: 1.67 °C–1.85 °C), respectively. The spatial and temporal R^2 remained quite high, while the corresponding errors stayed low. In the case of T_{mean} , overall spatial $R^2 = 0.88$ (yearly range: 0.84–0.93) and temporal $R^2 = 0.97$ (yearly range: 0.95–0.98), while $\text{RMSE}_{\text{spatial}} = 0.49$ °C (yearly range: 0.42 °C–0.59 °C) and $\text{RMSE}_{\text{temporal}} = 1.32$ °C (yearly range: 1.25 °C–1.45 °C).

For the third stage model (Table 1), the 21-year average $R^2 = 0.97$ (yearly range: 0.95–0.98), 0.98 (yearly range: 0.97–0.99) and 0.97 (yearly range: 0.95–0.98), while the RMSE = 1.25 °C (yearly range: 1.17 °C–1.38 °C), 1.03 °C (yearly range: 0.88 °C–1.12 °C) and 1.41 °C (yearly range: 1.22 °C–1.49 °C) for the T_{min} , T_{mean} and T_{max} model in a number of 81,166, 87,040 and 84,330 cell-days, respectively. Table S3 shows the comparison results between the third and second stage T_{air} predictions.

21-year average mean signed error was found to be 0.10 °C, 0.05 °C and -0.16 °C, for T_{min} , T_{mean} and T_{max} model, respectively. We report it in a yearly basis, together with the intercepts and slopes of the linear regressions between our predictions and the DWD observations in Table S4.

The percentage of T_{air} predictions that was provided by each stage of the modeling procedure can be found in Table S5 of the Supplementary material. On average, the first stage resulted in 0.04%, 0.04%, 0.03% of the final T_{min} , T_{mean} and T_{max} predictions, respectively, the second stage a 36.1%, 35.6% and 32.7%, while the third stage filled in the remaining approximately 62%, 62.5% and 65.4%. The missing values of our output T_{air} predictions' dataset over the period 2000–2020 were close to 1% for all the models.

3.2. Validation with external data

The small-scale validation in the Augsburg area showed that all models achieved high correspondence ($0.95 \leq R^2 \leq 0.99$) and low

Table 1Prediction accuracy for the first and the third stage predictions: 10-fold CV results for daily T_{\min} , T_{mean} and T_{\max} in Germany, averaged for 2000–2020.

First stage predictions								
Measure	R^2	R^2_{spatial}	R^2_{temporal}	RMSE (°C)	SD (°C)	RMSE _{spatial} (°C)	RMSE _{temporal} (°C)	Sample size (cell-days number)
T_{\min}	0.91	0.68	0.92	2.02	6.76	0.87	1.83	45,432
T_{mean}	0.96	0.88	0.97	1.41	7.56	0.49	1.32	48,925
T_{\max}	0.96	0.84	0.97	1.77	9.12	0.77	1.60	42,155
Third stage predictions								
Measure	R^2	RMSE (°C)	SD (°C)	Sample size (cell-days number)				
T_{\min}	0.97	1.25	6.44	81,166				
T_{mean}	0.98	1.03	7.22	87,040				
T_{\max}	0.97	1.41	8.02	84,330				

*SD: standard deviation of the DWD observed T_{air} .

errors, even below 1 °C (Table 2). By season comparison led to similar findings of high models' performance. All T_{air} models, and especially the T_{\min} model, achieved slightly better performance during the winter rather than the summer period (Table 2). Detailed results are provided in Tables S6 and S7. The linear regressions between the predicted T_{air} from our daily T_{\min} , T_{mean} and T_{\max} models and the HOBO-Logger observed daily T_{\min} , T_{mean} and T_{\max} during the comparison period, gave an intercept of 0.61, 0.28 and 0.41, and a slope of 1.04, 1.02 and 0.98, respectively (Table S8). Fig. 2 and S4 also indicates the strong correspondence of our model predictions and the HOBO-Logger network observations.

The large-scale comparison with the TRY dataset suggested a good correlation between the two models' outputs ($0.71 \leq R^2 \leq 0.99$) while most RMSE were below 1 °C (Table 3). For year by year results, please see Table S9-S13 in the Supplementary material. In Fig. 3, we visualized the model correspondence for a randomly selected example year (2010). Most of the two models' predictions met in the slope of 1.

Our model predictions captured a wider T_{air} distribution and representation of spatial T_{air} variations in small scale analysis as we observe in the example Fig. S5 for the years 2003, 2006, 2008 and 2012 (randomly chosen) in the Augsburg area.

3.3. Case study - Augsburg

We first calculated the distances between the geocoded residential addresses of the KORA study participants and the two available DWD stations across the Augsburg area (Fig. S6). Most of the participants lived 5–15 km far from a station. Additionally, we found that T_{mean} varied substantially over space (Fig. 4). The city centre was way hotter than the surrounding rural areas (variation close to 2 °C) and in these rural regions there was also substantial variation even in neighbouring tiles. The actual difference in exposure assessment from the DWD observations and our model predictions could also be seen in the long-term

assignment (Fig. 5). The DWD T_{mean} was only representative for the left-hand side distribution queue (cooler Augsburg areas). The higher temperatures are not captured by the DWD stations.

Fig. 6 is a short-term T_{mean} exposure distribution example, using an average of 7 days, which is often used for exposure assessment in epidemiological studies. Our model's predictions were close to the DWD observations at both stations. But, both stations values were below the distribution's mean and especially the T_{mean} of DWD station 1 was lower than the first quartile (Q1) of the distribution. This was mainly affected by their location, which was outside the city centre as seen in Fig. 4.

3.4. Descriptive statistics and spatiotemporal T_{air} patterns

Table 4 shows a selection of descriptive statistics (mean, standard deviation (SD), Q1, median and third quartile (Q3)) regarding the T_{\min} , T_{mean} and T_{\max} in Germany for the period 2000–2020 resulting from the DWD weather stations observations and our model predictions. The observed 21-year average T_{\min} , T_{mean} and T_{\max} from the DWD stations were 5.15 °C (SD = 6.59 °C), 9.44 °C (SD = 7.39 °C) and 13.85 °C (SD = 8.77 °C), respectively, while our models gave predicted 21-year average T_{\min} , T_{mean} and T_{\max} of 5.24 °C (SD = 5.89 °C), 9.57 °C (SD = 7.36 °C) and 14 °C (SD = 8.75 °C), respectively.

We also present the 21-year averaged predicted T_{\min} , T_{mean} and T_{\max} maps of Germany (Fig. 7, plot 1). The T_{air} spatial variability exceeded 15 °C annually on average, depending on the measure. We saw specific spatial patterns for T_{air} , including mountainous regions, rivers, lakes, forests and coastlines. For instance, the Alps and the Harz highland area were characterized by the lowest T_{air} values nationwide, while the dense urban cores (e.g., from Stuttgart to Frankfurt) or big individual cities as Munich and Berlin had much higher values of T_{air} , especially for T_{\min} and T_{mean} , than the surrounding rural areas. We also observed the high contrasts our output provided even for small areas, due to its high resolution of 1 × 1 km. We additionally present in Fig. S7, the German-wide

Table 2Accuracy results of the small-scale external validation with HOBO-Logger T_{\min} , T_{mean} and T_{\max} observations in the Augsburg area during 2013–2018, overall and by season.

Overall												
Measure	R^2	RMSE (°C)	SD (°C)	7-day average R^2	7-day average RMSE (°C)	SD (°C)						
T_{\min}	0.95	1.80	6.84	0.97	1.44	6.44						
T_{mean}	0.99	1.07	7.72	0.99	0.90	7.37						
T_{\max}	0.98	1.37	9.11	0.98	1.08	8.50						
By season												
Measure	Winter			Spring			Summer			Fall		
	R^2	RMSE (°C)	SD (°C)	R^2	RMSE (°C)	SD (°C)	R^2	RMSE (°C)	SD (°C)	R^2	RMSE (°C)	SD (°C)
T_{\min}	0.83	1.53	4.10	0.89	1.78	4.74	0.74	2.05	3.13	0.87	1.72	4.51
T_{mean}	0.93	1.00	3.94	0.97	1.06	5.15	0.92	1.24	3.49	0.97	1.02	5.10
T_{\max}	0.92	1.30	4.68	0.96	1.29	6.26	0.91	1.43	4.81	0.96	1.36	6.59

*SD: standard deviation of the dependent variable (HOBO-Logger T_{air}).

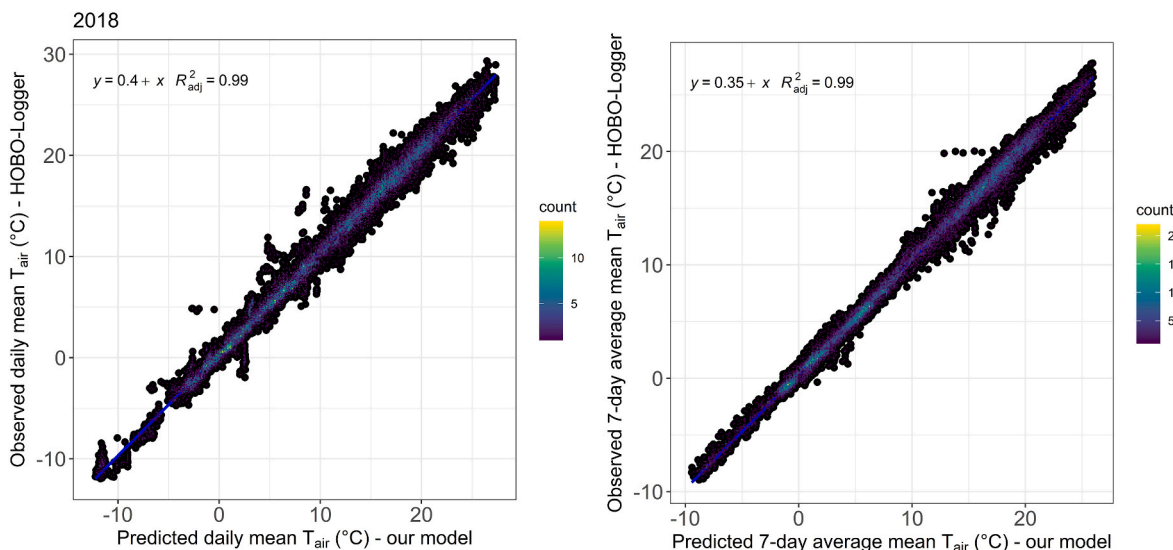


Fig. 2. Density scatterplots between the model daily T_{mean} predictions and the HOBO-Logger daily T_{mean} observations for 2018, daily average and 7-day average.

Table 3

Comparison between our model daily T_{mean} predictions and the DWD TRY model daily T_{mean} predictions in Germany during 2001–2012.

	R^2	RMSE (°C)
Overall	0.99	0.90
Season		
Winter	0.94	0.98
Spring	0.97	0.90
Summer	0.94	0.88
Fall	0.97	0.86
Without extremes		
5th pctl. < T_{mean} < 95th pctl.	0.99	0.79
To extremes		
$T_{\text{mean}} < 5\text{th pctl.}$	0.76	1.19
$T_{\text{mean}} > 95\text{th pctl.}$	0.71	0.93
District		
Augsburg Landkreis (rural)	0.99	0.84
Stadt Augsburg (urban)	0.99	0.85

DTR maps for 2016–2019, i.e., the NAKO study baseline years. Eastern Germany and more intensely the North-Eastern part of the country experienced higher DTR variations, while cities or mountains and large water bodies were characterized by smaller DTR.

Regarding the temporal T_{air} variability in Germany (and in NAKO study centers) over the first two decades of the 21st century, we report the differences between the predicted T_{mean} yearly averages and the 20-year average (Fig. 7, plot 2 and Fig. S8). The year 2000 was excluded as the model predictions started from late February. There was an obvious tendency of increased averaged T_{mean} for the last 5–7 years (continuously beyond 2016). The hottest years recorded during the studied period were 2018 ($T_{\text{mean}} = 10.45\text{ °C}$) and 2020 ($T_{\text{mean}} = 10.42\text{ °C}$). Additionally, we mapped the number of heat ($T_{\text{max}} > 30\text{ °C}$) and cold ($T_{\text{min}} < 0\text{ °C}$) days by 3-digit zip code through the years. Fig. 8 presents an example comparing the years 2001 (as a reference) and 2015, where the observed difference was pronounced. For 2015 the number of heat days increased dramatically since 2001 mainly in eastern and south-eastern Germany, whereas the cold days dropped, even if 2015 was not among the hottest years of the study period (Fig. 7, plot 2).

4. Discussion

In this paper, we developed reliable high spatiotemporally-resolved T_{min} , T_{mean} , T_{max} and DTR datasets for Germany during 2000–2020, following a regression-based method which consists of three stages. We combined meteorological and remote sensing data as well as multiple land cover predictors. All models attained very good performance, and consequently their predictive ability appears to have a strong foundation, with overall high explained variance ($0.91 \leq R^2 \leq 0.98$) and low errors ($1.03\text{ °C} \leq \text{RMSE} \leq 2.02\text{ °C}$), calculated through CV. In addition, bias was found to be close to 0 ($-0.16\text{ °C} \leq \text{mean signed error} \leq 0.10\text{ °C}$). The external small ($0.74 \leq R^2 \leq 0.99$, $0.87\text{ °C} \leq \text{RMSE} \leq 2.05\text{ °C}$) and large-scale validation ($0.71 \leq R^2 \leq 0.99$, $0.79\text{ °C} \leq \text{RMSE} \leq 1.19\text{ °C}$) confirmed the high performance of the models. We additionally showed the benefits of our spatiotemporal T_{air} modeling in terms of exposure assessment for participants of epidemiological studies, conducting a case study in the Augsburg area.

For Germany, except the datasets of a coarser resolution of 5 km or more (Brinckmann and Bissolli, 2015; Frick et al., 2014), there is the $1 \times 1\text{ km}$ hourly T_{air} dataset for 1995–2012, generated by Krähenmann et al. (2018), who applied a 3-step interpolation method (monthly RMSE $\approx 1\text{ °C}$). We used this product to externally compare our model findings with another model across the country. There was a good overall

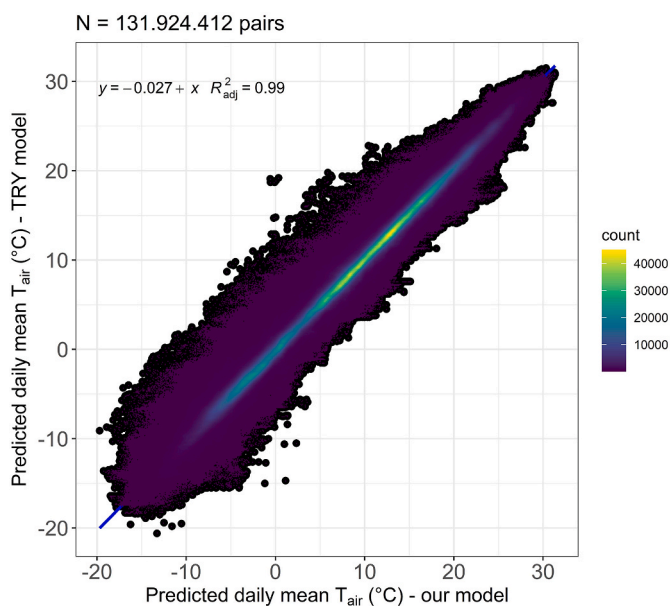


Fig. 3. Density scatterplot between our model daily T_{mean} predictions and the project TRY model daily T_{mean} predictions for 2010.

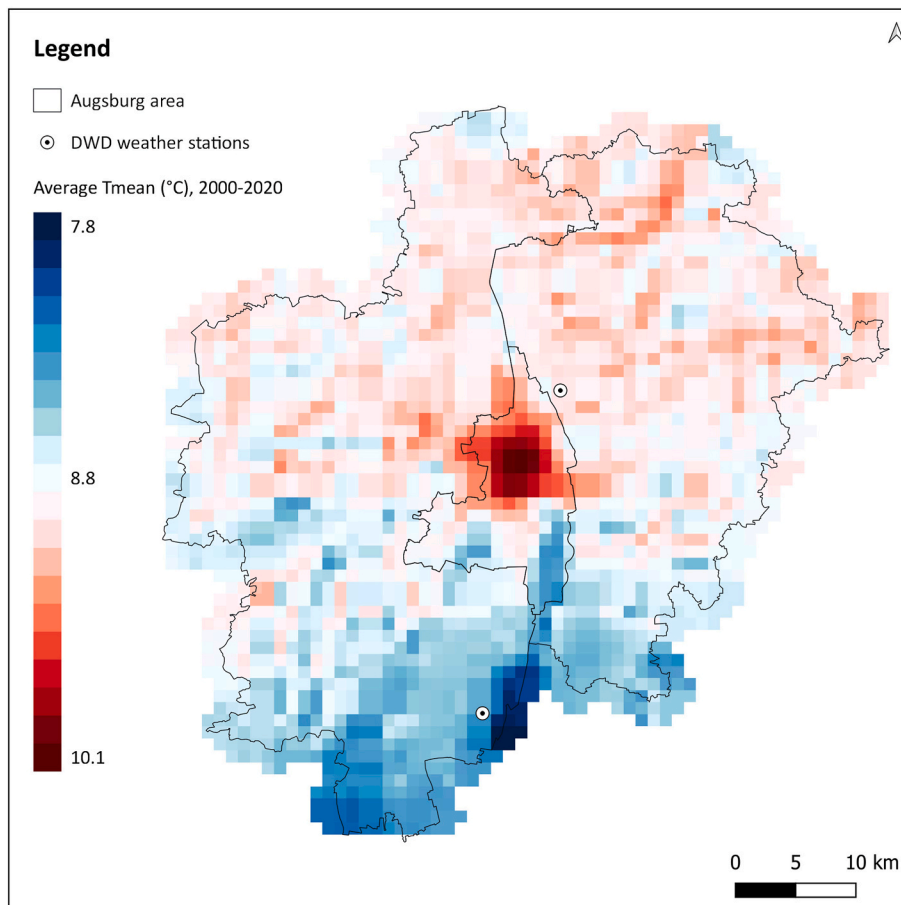


Fig. 4. Spatial pattern of the averaged predicted T_{mean} in the Augsburg area during 2000–2020.

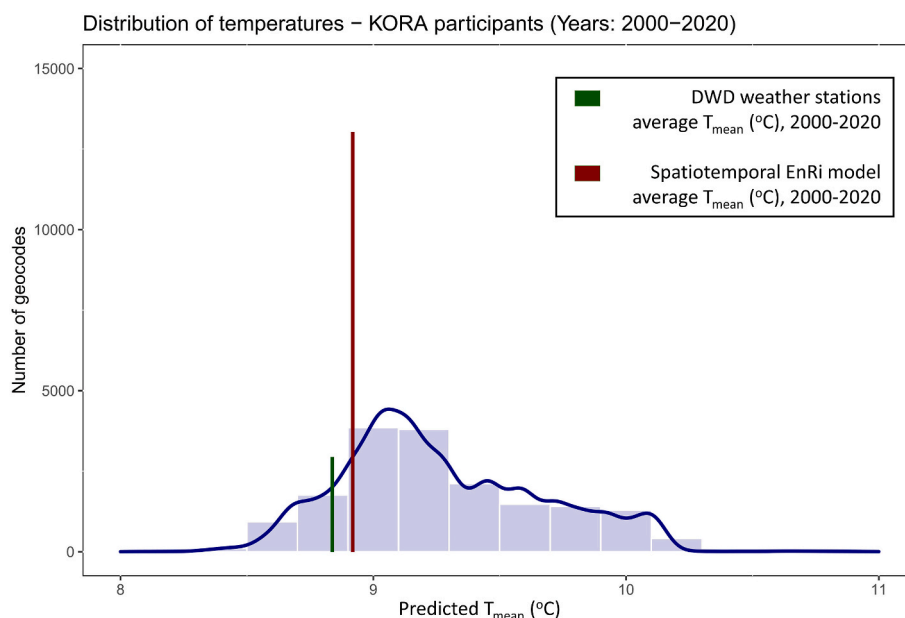


Fig. 5. Distribution of the predicted T_{mean} , assigned to KORA participants for 2000–2020 (in blue). The green and red lines show the exposure assignment based on the nearest monitoring station location. (For interpretation of the references to colour in this figure legend, the reader is referred to the Web version of this article.)

correspondence. However, our model predictions captured broader T_{air} variations, especially in city level (Fig. S5), as the interpolation methods are highly affected by the weather stations locations with limitations to fully represent between-station variability. Especially in Germany, a

complex geo-climate study domain with high spatial heterogeneity, interpolation leads to neighbouring motives, thus closer regions are assigned rather similar values, and cannot capture sufficiently either the small-scale T_{air} variability or its extreme values. Therefore, we also

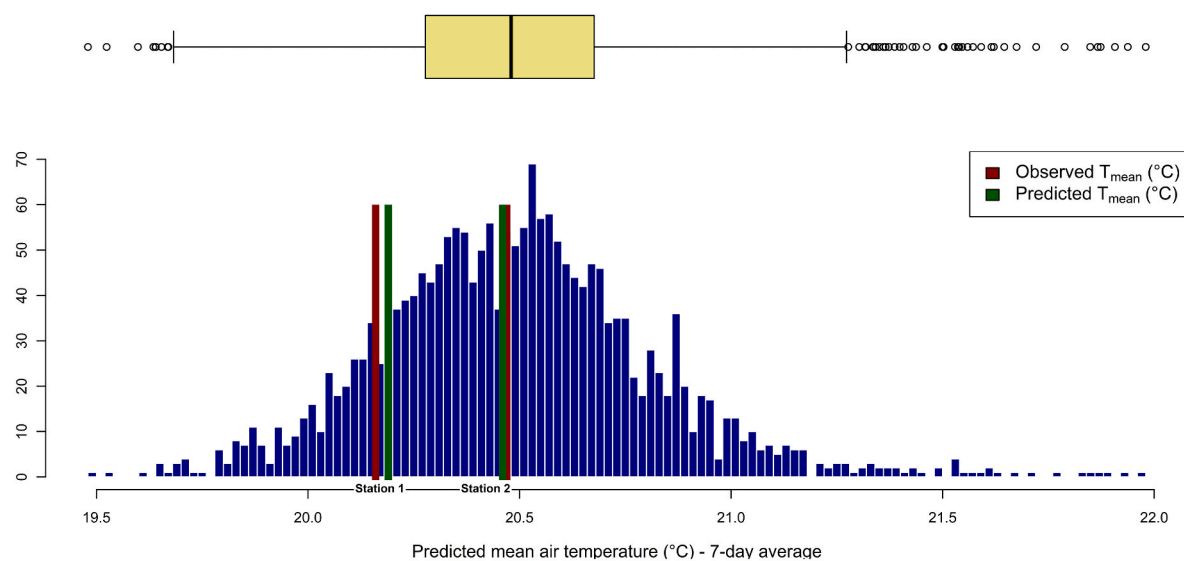


Fig. 6. Predicted 7-day average T_{mean} distribution (with blue) vs the 2 available DWD stations T_{mean} observations (with red) across the Augsburg area for 31.08.2019. The green lines represent our model's predictions at the stations locations. (For interpretation of the references to colour in this figure legend, the reader is referred to the Web version of this article.)

Table 4
Observed and predicted T_{min} , T_{mean} and T_{max} in Germany during 2000–2020.

Source	Measure	Mean (°C)	SD (°C)	Q1 (°C)	Median (°C)	Q3 (°C)
DWD observations (n = 406 stations)	T_{min}	5.15	6.59	0.34	5.33	10.33
	T_{mean}	9.44	7.39	3.71	9.59	15.27
	T_{max}	13.85	8.77	6.81	13.91	20.68
Models predictions (n = 366,536 grid cells)	T_{min}	5.24	5.89	0.24	5.24	10.29
	T_{mean}	9.57	7.36	3.76	9.71	15.19
	T_{max}	14.00	8.75	6.90	14.05	20.67

observed worse correspondence of our and TRY models to extremes, i.e., 5th and 95th percentiles (Table 3). Krähenmann et al. (2018) also lack validation with completely independent T_{air} datasets while validating the interpolation-based predictions with input data could be biased due to their strong dependence. Finally, our output had a longer and more recent temporal extent and can be used in recent German cohorts.

Aiming to produce a helpful dataset for scientists working in the field of environmental epidemiology and especially those who investigate the T_{air} health effects or implement T_{air} in their analysis as a confounder or an effect modifier, the case study example we demonstrate for Augsburg is of great importance. The prevailing way for studies exploring the T_{air} health effects is to collect their exposure data from monitoring networks consisting of a limited number of ground-based weather stations, unevenly distributed across the country and insufficient to capture the spatial T_{air} variability, especially in city centers. Taking into consideration the Augsburg area, an epidemiological study would usually assign to all participants the T_{air} observations of the station which has the shortest distance from their residential address or a weighted average of the two available stations, again depending on distances or a simple interpolation technique. Hence, the participants would not be assigned with the exposure value of their actual location, but of the station's location even 10 km away (Fig. S6), implying the need of finer resolutions. People living in the city centre, where there is no available station, would be assigned with a way lower T_{air} exposure than their representative one, as we observed in Figs. 5 and 6. All the aforementioned issues lead to exposure error and consequently the health effects are biased towards the null (Zeger et al., 2000). On the other hand, our output captured the T_{air} variability and trends and reduced the exposure misclassification. Hence, we achieved a better representation of T_{air}

variability and fulfilled one of our primary goals that was to provide more accurate T_{air} exposure assessment to German epidemiological studies.

A key finding of our analysis were the observed changes in T_{air} , which are mainly attributed to climate change that is already noticeable in Germany (Rüth et al., 2019). We showed that the four hottest years, based on an area-weighted averaging of the temperature during last two decades across the country, all occurred after 2014, while the last three consecutive years found to be the hottest overall (Fig. 7, plot 2). This finding was consistent and even more pronounced for the big constantly growing German cities (Fig. S7). Additionally, due to the high spatio-temporal resolution of the models, we detected climate change effects that cannot be captured by crude German-wide T_{air} averages. For instance, for 2015, we observed a substantial increase in hot days since 2001 even if this year's average T_{air} was lower than the 20-year average. The results of this analysis showing the impact of climate change on T_{air} locally and countrywide, are large, even over this short temporal period. With this tool, impacts on human health could be detected which then might contribute to climate change adaptation and risk reduction policies that German authorities need to enact in the following years.

4.1. Strengths

Best of our knowledge, this is the first study of T_{air} modeling which validates the models' prediction so extensively using external data. First locally, via a ground-based dense monitoring network for 6 years and then nationwide with another model based on a different approach for 12 years. The results indicated good performance and low errors in both cases, boosting our confidence in the quality of our product. An additional strength is the models' spatial resolution and spatial and temporal extent. They are German-wide and have a temporal extent of 21 years. Their national scale combined with the fine resolution of 1×1 km and the daily temporal resolution, provided us with the opportunity to study the spatiotemporal patterns of T_{air} all across Germany but also in specific places around the country, containing both urban and rural settings.

Our output product is an excellent fit for many individual-level epidemiological studies in Germany, without limitations on the study area(s). Mapping four different T_{air} measures was also important for environmental epidemiology as many recent studies report health effects of different temperature measures (Cheng et al., 2014; Guo et al., 2016; Oberheim et al., 2020; Wong et al., 2020), and there is a special

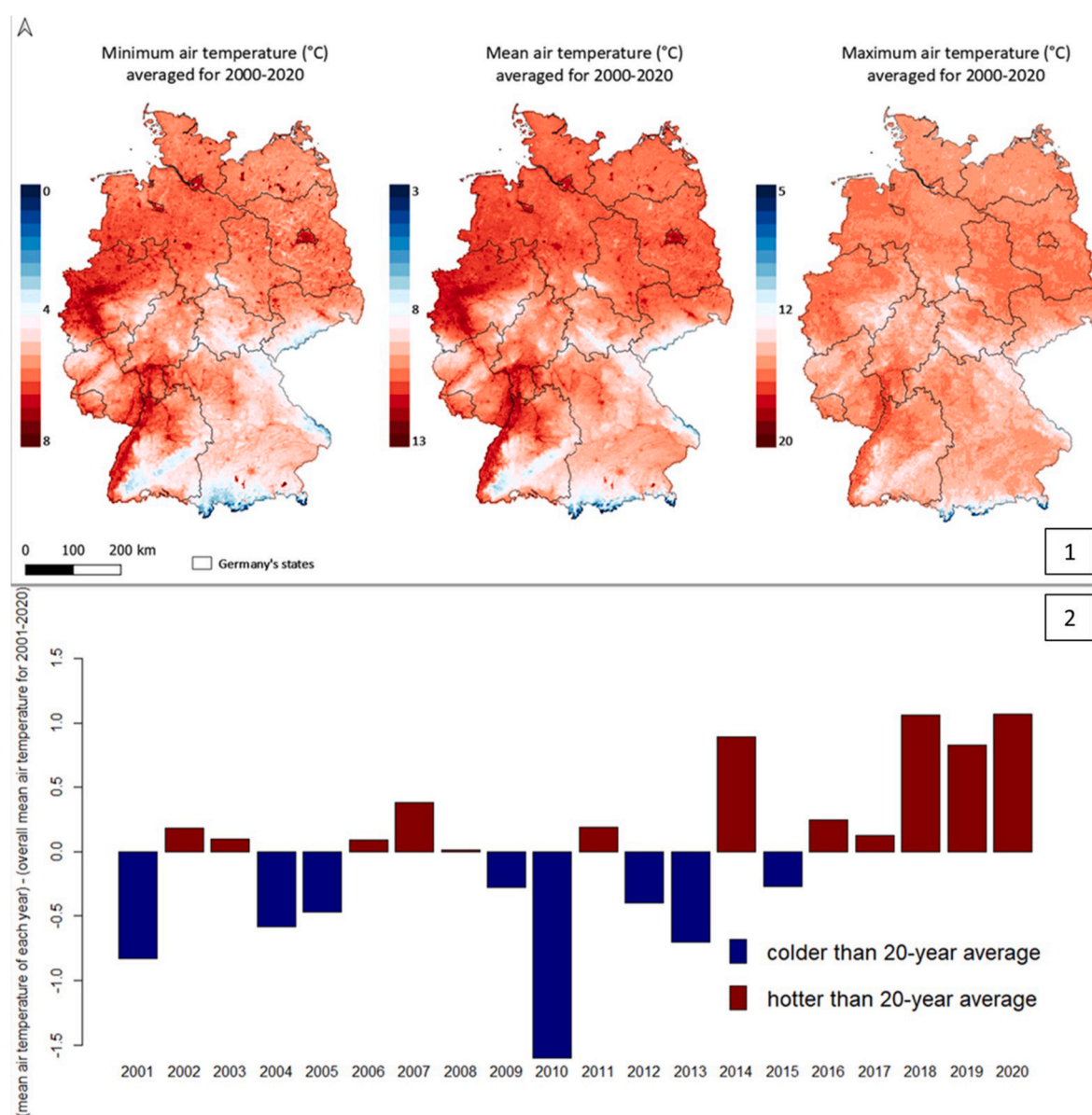


Fig. 7. Spatiotemporal T_{air} patterns in Germany for 2000–2020. Plot 1: Spatial patterns of the predicted T_{min} , T_{mean} and T_{max} in Germany, averaged for 2000-2020. Plot 2: Difference between the predicted T_{mean} yearly averages and the predicted T_{mean} 20-year average (2001-2020), German-wide.

need for further research with high spatiotemporally-resolved T_{min} , T_{mean} , T_{max} and DTR. Our final output can also be used for other research purposes outside the health field. For example, we are currently developing a high-resolution hybrid spatiotemporal RF model in order to predict daily mean relative humidity (RH) in Germany. To accomplish it, we use our daily T_{mean} predictions dataset as the main predictor in the RF model, due to its strong association (negative) with RH (Nikolaou et al., 2022).

4.2. Limitations

On the other hand, there are some limitations. First of all, the main predictor for estimating T_{air} is LST either at its daily or nightly value. It is well known that LST datasets include a high percentage of missing values because of cloud coverage, atmosphere dust, snow or sensor failure (Ghafariyan Malamiri et al., 2018). However, using the TPS interpolated T_{air} data in the third stage model, we observed high accuracy for third stage predictions with quite low errors even when we compared them with independent observations from ground-based

weather station networks. Moreover, we could not estimate the models performance, internally, in locations that have not been trained on. We tackled this issue by externally validating our T_{air} predictions with the HOBO-Logger T_{air} measurements for cells where the models were not trained on, and we observed high performance. Therefore, we are confident that even in the cell-days without available DWD T_{air} or LST data, our predictions are equally reliable. An additional factor that limits our product is its spatial resolution of 1×1 km, which is sufficient for country-wide analysis, but it might be a bit coarse for small-area/local analyses, especially for studies exploring the UHI effect. However, even in small scale analysis, our 1×1 km resolution dataset provides a better representation of T_{air} variability in comparison with the existing weather stations, as we showed in the case study of Augsburg's area. Higher spatiotemporal resolution, at least for the cities, might be a very good future upgrade in the framework of T_{air} modeling in Germany, given the example of previous studies in neighbouring countries (Hough et al., 2020). Finally, the 21-year extent we used to understand the spatiotemporal T_{air} patterns over Germany might be short to investigate climate change (usually a 30-year period). It is

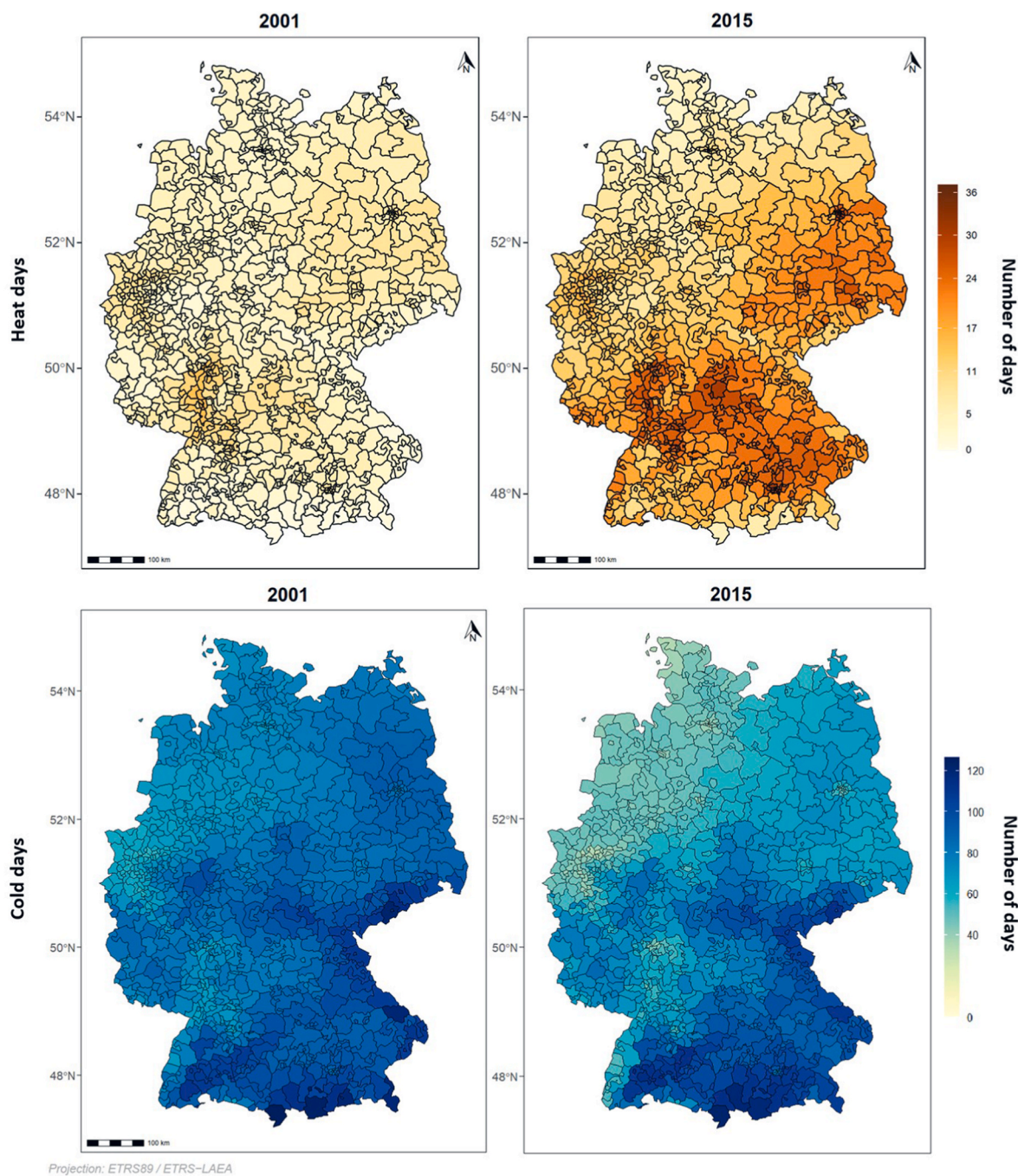


Fig. 8. Number of heat ($T_{\max} > 30\text{ }^{\circ}\text{C}$) and cold ($T_{\min} < 0\text{ }^{\circ}\text{C}$) days by 3-digit zip code in Germany, 2001) versus 2015.

nevertheless a good starting point to understand the T_{air} patterns and find useful climate change indications in Germany.

5. Conclusion

In this study, we applied a high-resolution hybrid spatiotemporal modeling approach to estimate daily T_{\min} , T_{mean} and T_{\max} as well as to calculate DTR across Germany over the period 2000–2020. We achieved excellent models' performances, validated extensively both locally and nationwide. Our product contributes substantially to exposure misclassification decrease accomplishing a better representation of T_{air} variability, and helps towards understanding the spatiotemporal T_{air} patterns and observing the impact of climate change during the last decades in Germany. Finally, our dataset is a great fit for recent German

health cohorts and environmental epidemiology studies overall, but could also be used for other research purposes.

Author contributions

Nikolaos Nikolaou: Conceptualization, Data curation, Methodology, Formal analysis, Visualization, Writing – original draft, Writing – review & editing. **Marco Dallavalle:** Data curation, Methodology, Visualization, Writing – review & editing. **Massimo Stafoggia:** Methodology, Writing – review & editing. **Laurens M. Boucher:** Data curation, Validation, Writing – review & editing. **Annette Peters:** Conceptualization, Writing – review & editing, Supervision. **Kai Chen:** Conceptualization, Data curation, Methodology, Formal analysis, Writing – review & editing. **Kathrin Wolf:** Conceptualization, Data

curation, Methodology, Writing – review & editing, Supervision. **Alexandra Schneider:** Conceptualization, Methodology, Writing – review & editing, Supervision.

Declaration of competing interest

The authors declare that they have no known competing financial interests or personal relationships that could have appeared to influence the work reported in this paper.

Data availability

Data will be made available on request.

Acknowledgements

This work was supported by the Helmholtz Climate Initiative (HI-CAM) project, which is funded by the Helmholtz Association's Initiative and Networking Fund. The authors are responsible for the content of this publication.

Appendix A. Supplementary data

Supplementary data to this article can be found online at <https://doi.org/10.1016/j.envres.2022.115062>.

References

- Armstrong, B.G., 1998. Effect of measurement error on epidemiological studies of environmental and occupational exposures. *Occup. Environ. Med.* 55 (10), 651–656. <https://doi.org/10.1136/oem.55.10.651>.
- Bates, D., Mächler, M., Bolker, B., Walker, S., 2014. Fitting linear mixed-effects models using lme4. *arXiv preprint arXiv: 1406.5823*. <https://doi.org/10.48550/arXiv.1406.5823>.
- Beck, C., Straub, A., Breitner, S., Cyrus, J., Philipp, A., Jacobeit, J., 2018a. Air temperature characteristics of local climate zones in the Augsburg urban area (Bavaria, southern Germany) under varying synoptic conditions. *Urban Clim.* 25, 152–166. <https://doi.org/10.1016/j.uclim.2018.04.007>.
- Beck, H.E., Zimmermann, N.E., McVicar, T.R., Vergopolan, N., Berg, A., Wood, E.F., 2018b. Present and future Köppen-Geiger climate classification maps at 1-km resolution. *Sci. Data* 5 (1), 1–12. <https://doi.org/10.1038/sdata.2018.214>.
- Benali, A., Carvalho, A., Nunes, J., Carvalhais, N., Santos, A., 2012. Estimating air surface temperature in Portugal using MODIS LST data. *Remote Sens. Environ.* 124, 108–121. <https://doi.org/10.1016/j.rse.2012.04.024>.
- Breitner, S., Wolf, K., Devlin, R.B., Diaz-Sanchez, D., Peters, A., Schneider, A., 2014. Short-term effects of air temperature on mortality and effect modification by air pollution in three cities of Bavaria, Germany: a time-series analysis. *Sci. Total Environ.* 485, 49–61. <https://doi.org/10.1016/j.scitotenv.2014.03.048>.
- Brinckmann, S., Bissolli, P., 2015. Gridded Daily Mean Near-Surface (2 M) Air Temperature for Europe (Project DecReg/Miklip). Version V001, 2015. DWD Climate Data Center (CDC). https://doi.org/10.5676/DWD_CDC/DECREG0110v1.
- Bundesamt, Statistisches, 2022. Current population - population by nationality and sex [Online]. Available from: <https://www.destatis.de/EN/Themes/Society-Environment/Population/Current-Population/Tables/census-sex-and-citizenship-2021.html>. (Accessed 19 January 2022). Accessed.
- Busetto, L., Ranghetti, L., 2016. MODISr: an R package for automatic preprocessing of MODIS Land Products time series. *Comput. Geosci.* 97, 40–48. <https://doi.org/10.1016/j.cageo.2016.08.020>.
- Chapman, S., Watson, J.E., Salazar, A., Thatcher, M., McAlpine, C.A., 2017. The impact of urbanization and climate change on urban temperatures: a systematic review. *Landsc. Ecol.* 32 (10), 1921–1935. <https://doi.org/10.1007/s10980-017-0561-4>.
- Cheng, J., Xu, Z., Zhu, R., Wang, X., Jin, L., Song, J., Su, H., 2014. Impact of diurnal temperature range on human health: a systematic review. *Int. J. Biometeorol.* 58 (9), 2011–2024. <https://doi.org/10.1007/s00484-014-0797-5>.
- Davis, R.E., Hondula, D.M., Sharif, H., 2020. Examining the diurnal temperature range enigma: why is human health related to the daily change in temperature? *Int. J. Biometeorol.* 64 (3), 397–407. <https://doi.org/10.1007/s00484-019-01825-8>.
- Didan, K., 2015. MOD13A3 MODIS/terra vegetation indices monthly L3 global 1km SIN grid V006 [data set]. NASA EOSDIS Land Processes DAAC. <https://doi.org/10.5067/MODIS/MOD13A3.006>.
- DWD, 2017. Wetterextreme in Deutschland und weltweit [Online]. Available from: https://www.dwd.de/DE/wetter/thema_des_tages/2017/2/16.html. (Accessed 19 January 2022). Accessed.
- DWD, 2020. DWD-Stationen Duisburg-Baerl und Tönisvorst jetzt Spitzenreiter mit 41, 2 Grad Celsius [Online]. Available from: https://www.dwd.de/DE/presse/press_emaillungen/DE/2020/20201217_annulierung_lingen_news.html. (Accessed 19 January 2022). Accessed.
- DWD, 2021. DWD Climate Data Center (CDC): Historical Daily Station Observations (Temperature, Pressure, Precipitation, Sunshine Duration, etc.) for Germany version v21.3, 2021.
- DWD, 2022. Zeitreihen und Trends [Online]. Available from: <https://www.dwd.de/DE/leistungen/zeitreihen/zeitreihen.html>. (Accessed 30 January 2022). Accessed.
- Flückiger, B., Kloog, I., Ragetti, M.S., Eeftens, M., Roosli, M., de Hoogh, K., 2022. Modelling daily air temperature at a fine spatial resolution dealing with challenging meteorological phenomena and topography in Switzerland. *Int. J. Climatol.* <https://doi.org/10.1002/joc.7597>.
- Frick, C., Steiner, H., Mazurkiewicz, A., Riediger, U., Rauthe, M., Reich, T., Gratzki, A., 2014. Central European high-resolution gridded daily data sets (HYRAS): mean temperature and relative humidity. *Meteorol. Z.* 23 (1), 15–32. <https://doi.org/10.1127/0941-2948/2014/0560>.
- Gasparrini, A., Guo, Y., Hashizume, M., Lavigne, E., Zanobetti, A., Schwartz, J., Forsberg, B., 2015. Mortality risk attributable to high and low ambient temperature: a multicountry observational study. *Lancet* 386 (9991), 369–375. [https://doi.org/10.1016/S0140-6736\(14\)62114-0](https://doi.org/10.1016/S0140-6736(14)62114-0).
- German National Cohort (GNC) Consortium, 2014. The German National Cohort: aims, study design and organization. *Eur. J. Epidemiol.* 29 (5), 371–382. <https://doi.org/10.1007/s10654-014-9890-7>.
- Ghafarian Malamiri, H.R., Roustai, I., Olafsson, H., Zare, H., Zhang, H., 2018. Gap-filling of MODIS time series land surface temperature (LST) products using singular spectrum analysis (SSA). *Atmosphere* 9 (9), 334. <https://doi.org/10.3390/atmos9090334>.
- Gil-Alana, L.A., 2018. Maximum and minimum temperatures in the United States: time trends and persistence. *Atmos. Sci. Lett.* 19 (4), e810. <https://doi.org/10.1002/asl.810>.
- Global 30 Arc-Second Elevation (GTOPO30). DOI:10.5066/F7DF6PQS.
- Gronlund, C.J., Sullivan, K.P., Kefelegn, Y., Cameron, L., O'Neill, M.S., 2018. Climate change and temperature extremes: a review of heat-and cold-related morbidity and mortality concerns of municipalities. *Maturitas* 114, 54–59. <https://doi.org/10.1016/j.maturitas.2018.06.002>.
- Guo, Y., Gasparrini, A., Armstrong, B.G., Tawatsupa, B., Tobias, A., Lavigne, E., Tong, S., 2016. Temperature variability and mortality: a multi-country study. *Environ. Health Perspect.* 124 (10), 1554–1559. <https://doi.org/10.1289/EHP149>.
- Hertel, T.W., Rosch, S.D., 2010. Climate change, agriculture, and poverty. *Appl. Econ. Perspect. Pol.* 32 (3), 355–385. <https://doi.org/10.1093/aep/pq016>.
- Holle, R., Hapich, M., Löwel, H., Wichmann, H.E., null for the MONICA/KORA Study Group, 2005. KORA-a research platform for population based health research. *Gesundheitswesen* 67 (S 01), 19–25. <https://doi.org/10.1055/s-2005-858235>.
- Hough, I., Just, A.C., Zhou, B., Dorman, M., Lepeule, J., Kloog, I., 2020. A multi-resolution air temperature model for France from MODIS and Landsat thermal data. *Environ. Res.* 183, 109244. <https://doi.org/10.1016/j.envres.2020.109244>.
- IPCC, 2022. In: Pörtner, H.-O., Roberts, D.C., Tignor, M., Poloczanska, E.S., Mintenbeck, K., Alegría, A., Craig, M., Langsdorf, S., Löschke, S., Möller, V., Okem, A., Rama, B. (Eds.), *Climate Change 2022: Impacts, Adaptation, and Vulnerability. Contribution of Working Group II to the Sixth Assessment Report of the Intergovernmental Panel on Climate Change*. Cambridge University Press. Cambridge University Press, Cambridge, UK and New York, NY, USA, p. 3056. <https://doi.org/10.1017/9781009325844>.
- Jin, Z., Ma, Y., Chu, L., Liu, Y., Dubrow, R., Chen, K., 2022. Predicting spatiotemporally-resolved mean air temperature over Sweden from satellite data using an ensemble model. *Environ. Res.* 204, 111960. <https://doi.org/10.1016/j.envres.2021.111960>.
- Jobst, A.M., Kingston, D.G., Cullen, N.J., Sirguey, P., 2017. Combining thin-plate spline interpolation with a lapse rate model to produce daily air temperature estimates in a data-sparse alpine catchment. *Int. J. Climatol.* 37 (1), 214–229. <https://doi.org/10.1002/joc.4699>.
- Kilibarda, M., Hengl, T., Heuvelink, G.B., Gräler, B., Pebesma, E., Perčec Tadić, M., Bajat, B., 2014. Spatio-temporal interpolation of daily temperatures for global land areas at 1 km resolution. *J. Geophys. Res. Atmos.* 119 (5), 2294–2313. <https://doi.org/10.1002/2013JD020803>.
- Kloog, I., Nordio, F., Coull, B.A., Schwartz, J., 2014. Predicting spatiotemporal mean air temperature using MODIS satellite surface temperature measurements across the Northeastern USA. *Remote Sens. Environ.* 150, 132–139. <https://doi.org/10.1016/j.rse.2014.04.024>.
- Kloog, I., Nordio, F., Lepeule, J., Padoan, A., Lee, M., Auffray, A., Schwartz, J., 2017. Modelling spatio-temporally resolved air temperature across the complex geo-climate area of France using satellite-derived land surface temperature data. *Int. J. Climatol.* 37 (1), 296–304. <https://doi.org/10.1002/joc.4705>.
- Kovats, R.S., Kristie, L.E., 2006. Heatwaves and public health in Europe. *Eur. J. Publ. Health* 16 (6), 592–599. <https://doi.org/10.1093/eurpub/ckl049>.
- Krähenmann, S., Walter, A., Brien, S., Imbery, F., Matzarakis, A., 2016. Daily means of hourly grids of air temperature for Germany (project TRY Advancement), Version V001, DWD Climate Data Center (CDC). https://doi.org/10.5676/DWD_CDC/TRY_Basis_v001, 2016.
- Krähenmann, S., Walter, A., Brien, S., Imbery, F., Matzarakis, A., 2018. High-resolution grids of hourly meteorological variables for Germany. *Theor. Appl. Climatol.* 131 (3), 899–926. <https://doi.org/10.1007/s00704-016-2003-7>.
- Lacetera, N., 2019. Impact of climate change on animal health and welfare. *Animal Frontiers* 9 (1), 26–31. <https://doi.org/10.1093/af/vfy030>.
- Li, S., Griffith, D.A., Shu, H., 2020. Temperature prediction based on a space-time regression-kriging model. *J. Appl. Stat.* 47 (7), 1168–1190. <https://doi.org/10.1080/02664763.2019.1671962>.
- Lindsey, R., Dahlman, L., 2021. Climate Change: Global Temperature [Online]. Available from: <https://www.climate.gov/news-features/understanding-climate/climate-change-global-temperature>. (Accessed 29 January 2022). Accessed.

- Meehl, G.A., Tebaldi, C., 2004. More intense, more frequent, and longer lasting heat waves in the 21st century. *Science* 305 (5686), 994–997. <https://doi.org/10.1126/science.1098704>.
- Modala, N.R., Ale, S., Goldberg, D.W., Olivares, M., Munster, C.L., Rajan, N., Feagin, R. A., 2017. Climate change projections for the Texas high plains and rolling plains. *Theor. Appl. Climatol.* 129 (1), 263–280. <https://doi.org/10.1007/s00704-016-1773-2>.
- NASA, 2021. LP DAAC [Online]. Available: <https://lpdaac.usgs.gov/>. (Accessed 17 October 2022). Accessed.
- Nikolaou, N., Bouwer, L., Valizadeh, M., Dallavalle, M., Wolf, K., Stafoggia, M., Peters, A., Schneider, A., 2022. High-resolution Hybrid Spatiotemporal Modeling of Daily Relative Humidity across Germany for Epidemiological Research: a Random Forest Approach. EGU General Assembly 2022, Vienna, Austria. <https://doi.org/10.5194/egusphere-egu22-6543>, 23–27 May 2022, EGU22-6543.
- Nychka, D., Furrer, R., Paige, J., Sain, S., 2017. fields: tools for spatial data. R package version 9 (10.5065), D6W957CT. <https://doi.org/10.5065/D6W957CT>.
- Oberheim, J., Höser, C., Lüchters, G., Kistemann, T., 2020. Small-scaled association between ambient temperature and campylobacteriosis incidence in Germany. *Sci. Rep.* 10 (1), 1–12. <https://doi.org/10.1038/s41598-020-73865-9>.
- Peters, A., Schneider, A., 2021. Cardiovascular risks of climate change. *Nat. Rev. Cardiol.* 18 (1), 1–2. <https://doi.org/10.1038/s41569-020-00473-5>.
- QGIS Development Team, 2020. QGIS geographic information system. Open source geospatial foundation project. Available from: <http://qgis.osgeo.org>.
- R Core Team, 2020. R: A Language and Environment for Statistical Computing. R Foundation for Statistical Computing, Vienna, Austria. Available from: <https://www.R-project.org/>.
- Rosenfeld, A., Dorman, M., Schwartz, J., Novack, V., Just, A.C., Kloog, I., 2017. Estimating daily minimum, maximum, and mean near surface air temperature using hybrid satellite models across Israel. *Environ. Res.* 159, 297–312. <https://doi.org/10.1016/j.envres.2017.08.017>.
- Rüth, P.V., Schönthaler, K., Andrian-Werburg, S.V., Buth, M., 2019. Monitoringbericht 2019 zur Deutschen Anpassungsstrategie an den Klimawandel Bericht der Interministeriellen Arbeitsgruppe Anpassungsstrategie der Bundesregierung. Umweltbundesamt (UBA), Dessau-Roßlau. Available from: <https://www.umweltbundesamt.de/publikationen/umweltbundesamt-2019-monitoringbericht-2019-zur>.
- Sekulić, A., Kilibarda, M., Protić, D., Tadić, M.P., Bajat, B., 2020. Spatio-temporal regression kriging model of mean daily temperature for Croatia. *Theor. Appl. Climatol.* 140 (1), 101–114. <https://doi.org/10.1007/s00704-019-03077-3>.
- Shi, L., Liu, P., Kloog, I., Lee, M., Kosheleva, A., Schwartz, J., 2016. Estimating daily air temperature across the Southeastern United States using high-resolution satellite data: a statistical modeling study. *Environ. Res.* 146, 51–58. <https://doi.org/10.1016/j.envres.2015.12.006>.
- Shukla, P., Skea, J., Calvo Buendia, E., Masson-Delmotte, V., Pörtner, H., et al., 2019. IPCC, 2019: Climate Change and Land: an IPCC Special Report on Climate Change, Desertification, Land Degradation, Sustainable Land Management, Food Security, and Greenhouse Gas Fluxes in Terrestrial Ecosystems.
- Vancutsem, C., Ceccato, P., Dinku, T., Connor, S.J., 2010. Evaluation of MODIS land surface temperature data to estimate air temperature in different ecosystems over Africa. *Remote Sens. Environ.* 114 (2), 449–465. <https://doi.org/10.1016/j.rse.2009.10.002>.
- Vicedo-Cabrera, A.M., Scovronick, N., Sera, F., Royé, D., Schneider, R., Tobias, A., et al., 2021. The burden of heat-related mortality attributable to recent human-induced climate change. *Nat. Clim. Change* 11 (6), 492–500. <https://doi.org/10.1038/s41558-021-01058-x>.
- Vicente-Serrano, S.M., Saz-Sánchez, M.A., Cuadrat, J.M., 2003. Comparative analysis of interpolation methods in the middle Ebro Valley (Spain): application to annual precipitation and temperature. *Clim. Past* 24 (2), 161–180. <https://doi.org/10.3354/cr024161>.
- Wan, Z., 2014. New refinements and validation of the collection-6 MODIS land-surface temperature/emissivity product. *Remote Sens. Environ.* 140, 36–45. <https://doi.org/10.1016/j.rse.2013.08.027>.
- Wan, Z., Hook, S., Hulley, G., 2015. MOD11A1 MODIS/terra land surface temperature/emissivity daily L3 global 1km SIN grid V006 [data set]. NASA EOSDIS Land Processes DAAC. <https://doi.org/10.5067/MODIS/MOD11A1.006>.
- Watts, N., Amann, M., Arnell, N., Ayeb-Karlsson, S., Belesova, K., Boykoff, M., et al., 2019. The 2019 report of the Lancet Countdown on health and climate change: ensuring that the health of a child born today is not defined by a changing climate. *Lancet* 394 (10211), 1836–1878. [https://doi.org/10.1016/S0140-6736\(19\)32596-6](https://doi.org/10.1016/S0140-6736(19)32596-6).
- Wickham, H., 2009. Ggplot2: Elegant Graphics for Data Analysis, second ed. Springer, New York, p. 35. <https://doi.org/10.1007/978-0-387-98141-3>. 10.1007.
- Wong, S., Cantoral, A., Téllez-Rojo, M.M., Pantic, I., Oken, E., Svensson, K., et al., 2020. Associations between daily ambient temperature and sedentary time among children 4–6 years old in Mexico City. *PLoS One* 15 (10), e0241446. <https://doi.org/10.1371/journal.pone.0241446>.
- Wu, W., Xu, A.-D., Liu, H.B., 2015. High-resolution spatial databases of monthly climate variables (1961–2010) over a complex terrain region in southwestern China 119 (1), 353–362. <https://doi.org/10.1007/s00704-014-1123-1>.
- Xu, Y., Knudby, A., Ho, H.C., 2014. Estimating daily maximum air temperature from MODIS in British Columbia, Canada. *Int. J. Rem. Sens.* 35 (24), 8108–8121. <https://doi.org/10.1080/01431161.2014.978957>.
- Ye, X., Wolff, R., Yu, W., Vaneckova, P., Pan, X., Tong, S., 2012. Ambient temperature and morbidity: a review of epidemiological evidence. *Environ. Health Perspect.* 120 (1), 19–28. <https://doi.org/10.1289/ehp.1003198>.
- Zafeiratou, S., Samoli, E., Dimakopoulou, K., Rodopoulou, S., Analitis, A., Gasparrini, A., et al., 2021. A systematic review on the association between total and cardiopulmonary mortality/morbidity or cardiovascular risk factors with long-term exposure to increased or decreased ambient temperature. *Sci. Total Environ.* 772, 145383 <https://doi.org/10.1016/j.scitotenv.2021.145383>.
- Zanobetti, A., Schwartz, J., 2008. Temperature and mortality in nine US cities. *Epidemiology* 19 (4), 563. <https://doi.org/10.1097/EDE.0b013e31816d652d>.
- Zeger, S.L., Thomas, D., Dominici, F., Samet, J.M., Schwartz, J., Dockery, D., Cohen, A., 2000. Exposure measurement error in time-series studies of air pollution: concepts and consequences. *Environ. Health Perspect.* 108 (5), 419–426. <https://doi.org/10.1289/ehp.00108419>.
- Zhu, W., Lü, A., Jia, S., 2013. Estimation of daily maximum and minimum air temperature using MODIS land surface temperature products. *Remote Sens. Environ.* 130, 62–73. <https://doi.org/10.1016/j.rse.2012.10.034>.

3.1 Supplementary material for Paper I

High-resolution spatiotemporal modeling of daily near-surface air temperature in Germany over the period 2000-2020

Nikolaos Nikolaou^{1,2*}, Marco Dallavalle^{1,2}, Massimo Stafoggia³, Laurens M. Bouwer⁴, Annette Peters^{1,2}, Kai Chen^{5,6}, Kathrin Wolf^{1**}, Alexandra Schneider^{1**}

¹Institute of Epidemiology, Helmholtz Zentrum München, German Research Center for Environmental Health, Neuherberg, Germany

²Institute for Medical Information Processing, Biometry, and Epidemiology, Pettenkofer School of Public Health, LMU Munich, Munich, Germany

³Department of Epidemiology, Lazio Regional Health Service, Rome, Italy

⁴Climate Service Center Germany (GERICS), Helmholtz-Zentrum Hereon, Hamburg, Germany

⁵Department of Environmental Health Sciences, Yale School of Public Health, New Haven, CT, USA

⁶Yale Center on Climate Change and Health, Yale School of Public Health, New Haven, CT, USA

*Corresponding author

Address: Ingolstädter Landstr. 1, D-85764 Neuherberg, Germany

Phone: +49 176 377 488 68

E-mail: nikolaos.nikolaou@helmholtz-munich.de

**Shared last authorship

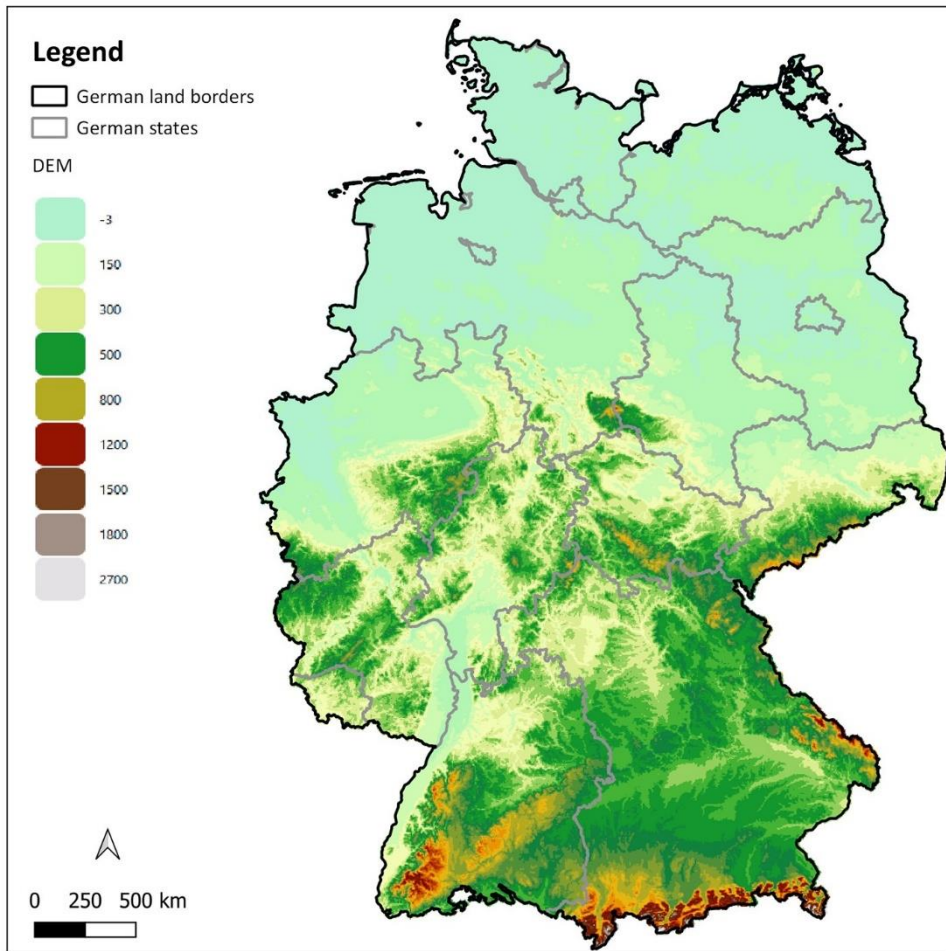


Figure S1. Map of DEM in 1×1 km spatial resolution across Germany's mainland.

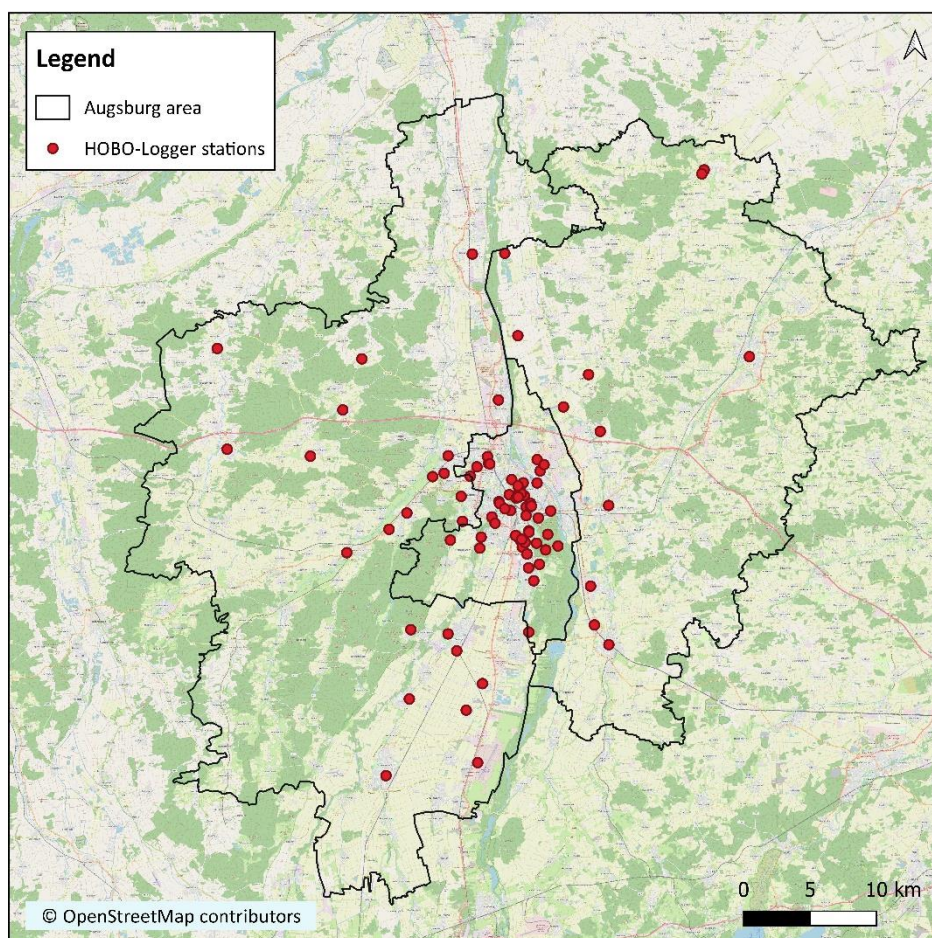


Figure S2. Map of the Augsburg study area and the sites of the HOBOLogger monitoring network during the period 2013-2018.

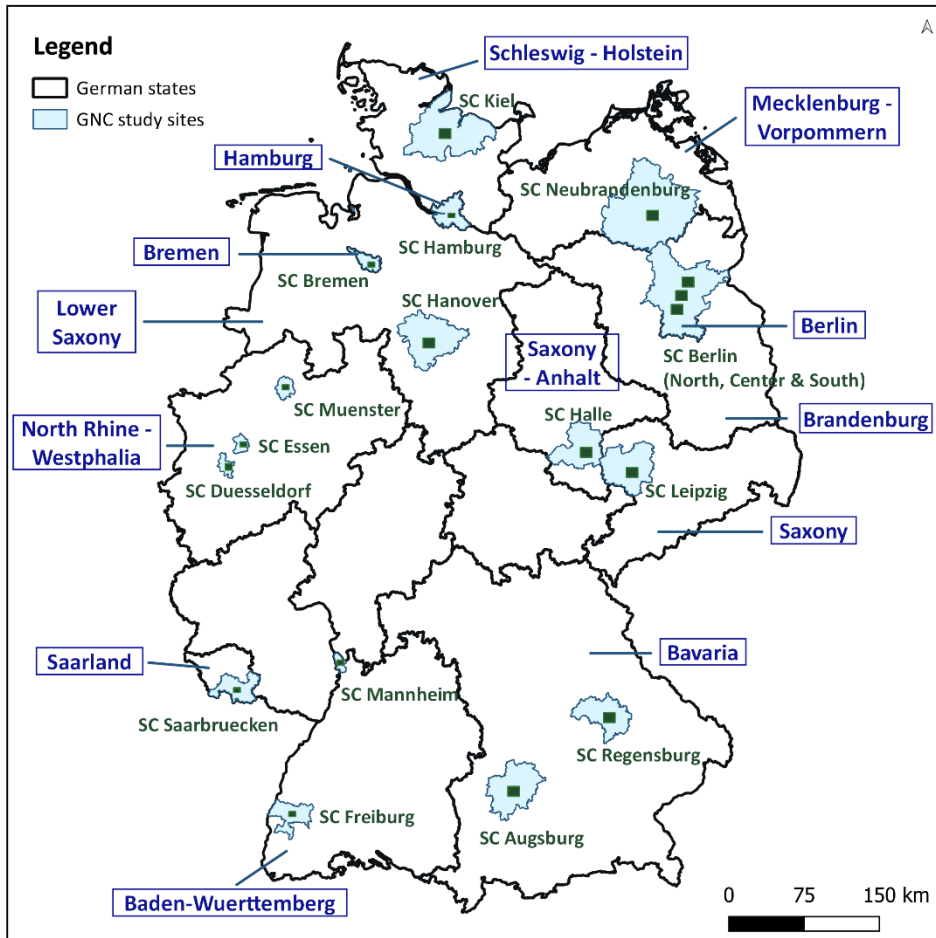


Figure S3. Map of the NAKO study sites across Germany.

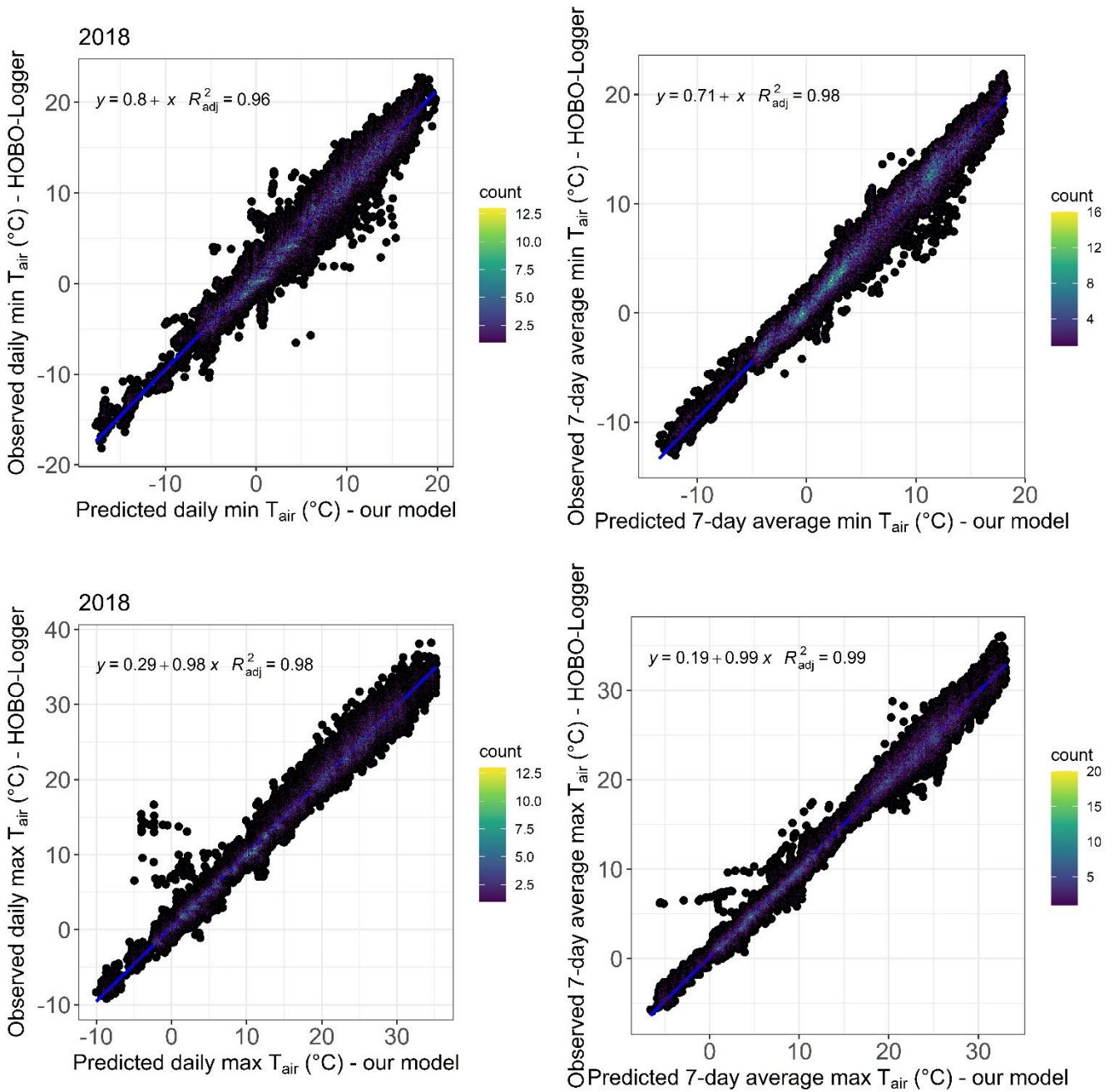


Figure S4. Density scatterplots between the model daily T_{min} and T_{max} predictions and the HOBO-Logger daily T_{min} and T_{max} observations for 2018, daily minimum and maximum and 7-day average minimum and maximum

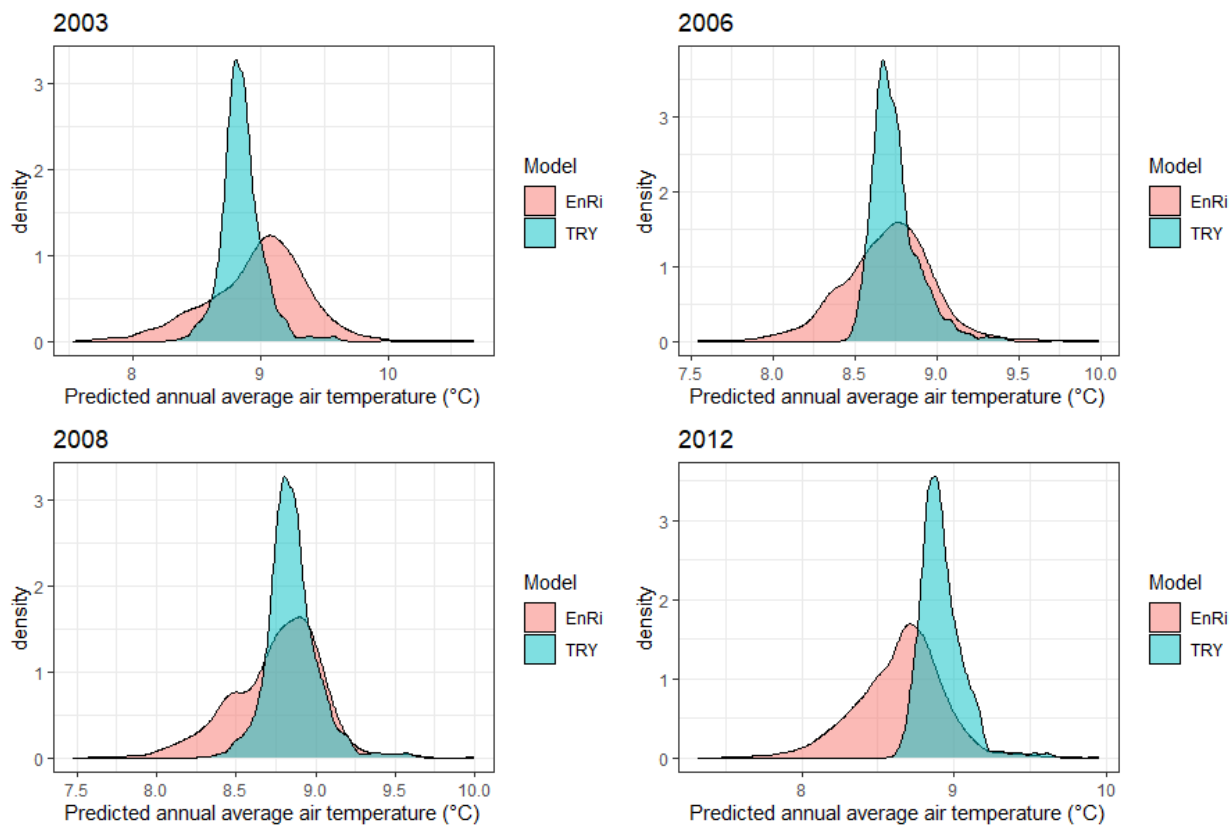


Figure S5. Distribution of our model (EnRi) T_{mean} predictions and the DWD TRY model T_{mean} predictions, averaged for the randomly selected years 2003, 2006, 2008 and 2012 in the Augsburg area.

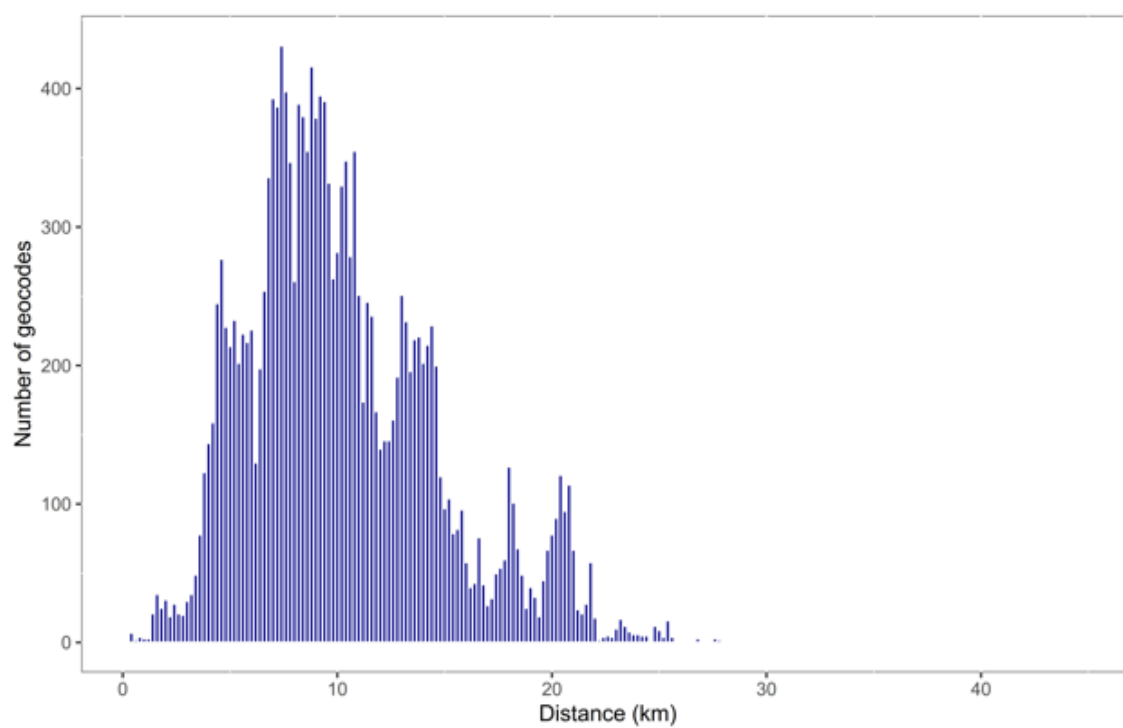


Figure S6. Distribution of distances (km) between the geocoded residential addresses of the KORA study participants and the nearest DWD weather stations.

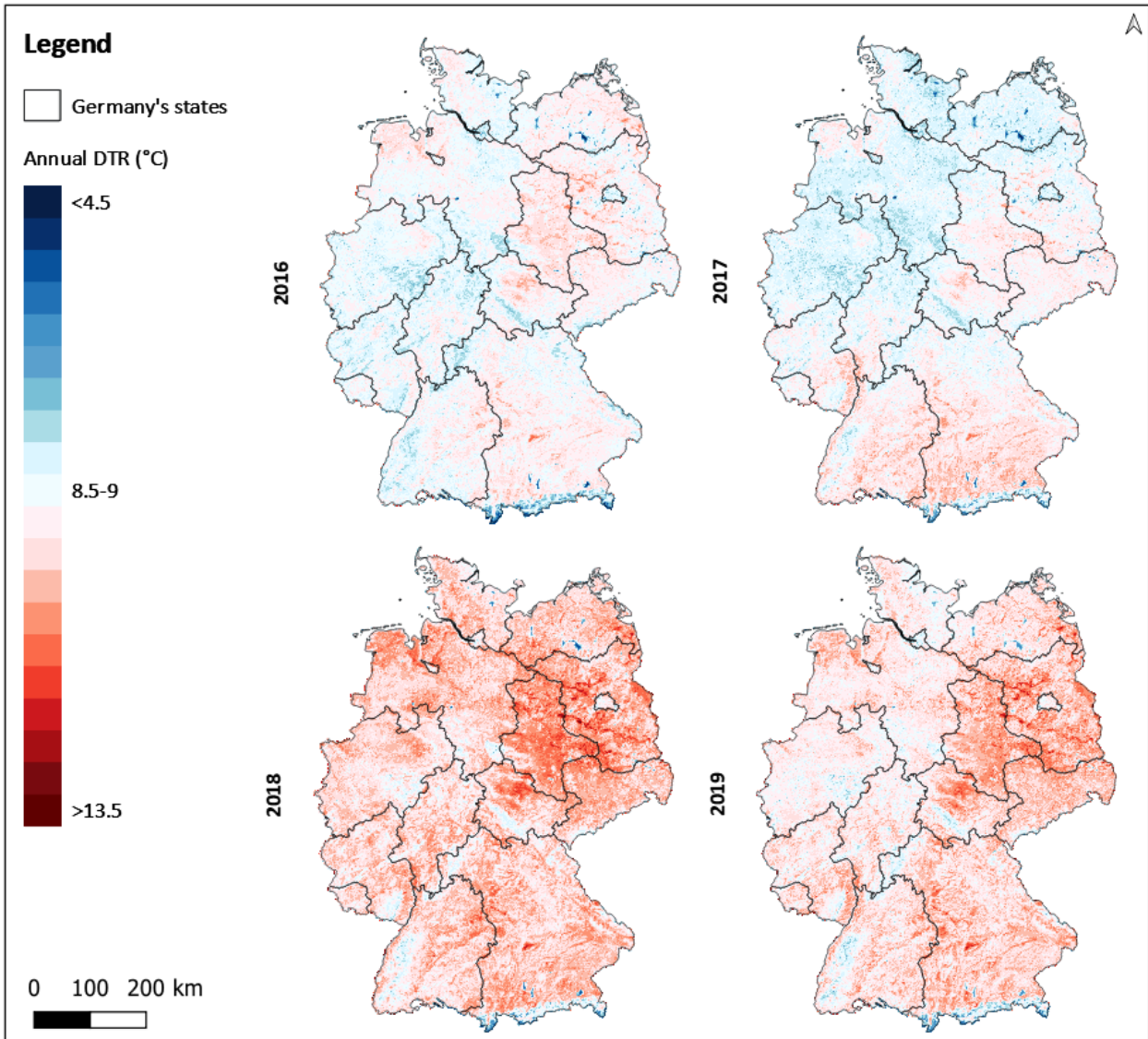


Figure S7. German-wide annual DTR maps during 2016-2019.

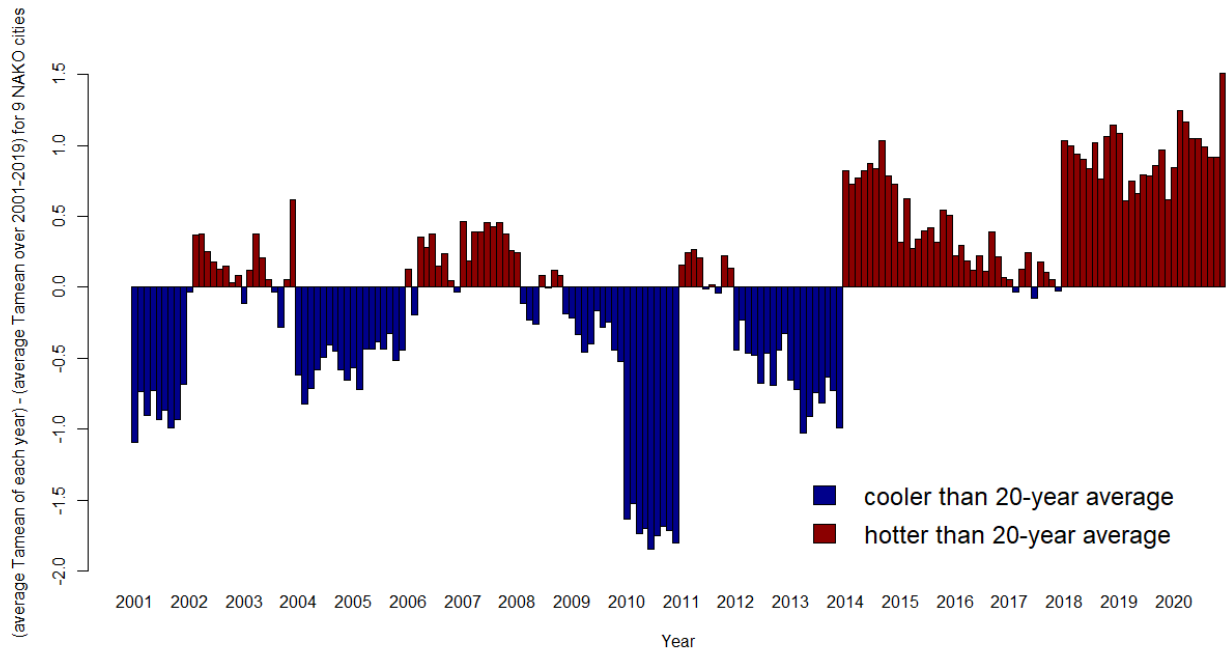


Figure S8. Difference between the predicted T_{mean} yearly averages and the predicted T_{mean} 20-year average (2001-2020) for 9 NAKO study sites.

Table S1. Prediction accuracy for the first stage predictions: 10-fold CV results for daily T_{\min} , T_{mean} and T_{\max} in Germany during 2000-2020.

Year	Measure	R^2	R^2_{spatial}	R^2_{temporal}	RMSE (°C)	SD (°C)	RMSE _{spatial} (°C)	RMSE _{temporal} (°C)	Sample size (cell-days number)
2000	T_{\min}	0.86	0.77	0.87	1.92	5.19	0.69	1.80	34,823
	T_{mean}	0.95	0.86	0.95	1.40	6.16	0.55	1.29	35,984
	T_{\max}	0.95	0.85	0.96	1.85	7.91	0.88	1.63	30,090
2001	T_{\min}	0.93	0.80	0.93	1.94	7.25	0.70	1.82	37,116
	T_{mean}	0.97	0.90	0.97	1.48	8.21	0.49	1.40	40,458
	T_{\max}	0.96	0.87	0.97	1.86	9.91	0.81	1.67	32,741
2002	T_{\min}	0.92	0.85	0.93	2.05	7.41	0.76	1.91	37,471
	T_{mean}	0.96	0.92	0.97	1.54	8.04	0.53	1.45	40,695
	T_{\max}	0.96	0.90	0.97	1.81	9.35	0.73	1.65	35,992
2003	T_{\min}	0.93	0.75	0.94	2.18	8.02	0.90	1.93	47,608
	T_{mean}	0.97	0.88	0.98	1.50	8.91	0.59	1.34	51,694
	T_{\max}	0.97	0.88	0.97	1.83	10.29	0.86	1.62	47,675
2004	T_{\min}	0.90	0.74	0.91	2.05	6.53	0.84	1.87	40,580
	T_{mean}	0.96	0.91	0.96	1.45	7.30	0.53	1.35	44,252
	T_{\max}	0.96	0.91	0.97	1.80	8.88	0.77	1.61	36,361
2005	T_{\min}	0.91	0.70	0.92	2.06	6.88	0.93	1.84	46,572
	T_{mean}	0.97	0.90	0.97	1.38	7.60	0.49	1.23	50,380
	T_{\max}	0.96	0.88	0.97	1.76	9.26	0.75	1.59	44,389
2006	T_{\min}	0.93	0.76	0.94	2.12	7.95	0.94	1.91	45,894
	T_{mean}	0.97	0.92	0.97	1.47	8.87	0.48	1.39	49,758
	T_{\max}	0.97	0.89	0.97	1.75	10.11	0.72	1.60	43,673
2007	T_{\min}	0.88	0.65	0.90	2.01	5.74	0.94	1.78	48,611
	T_{mean}	0.95	0.88	0.96	1.37	6.37	0.49	1.29	52,456
	T_{\max}	0.95	0.88	0.96	1.71	7.94	0.72	1.54	45,147
2008	T_{\min}	0.90	0.73	0.91	1.95	6.21	0.86	1.76	44,545
	T_{mean}	0.97	0.93	0.97	1.32	7.08	0.43	1.25	48,245
	T_{\max}	0.96	0.89	0.97	1.71	8.74	0.73	1.55	41,010

2009	T _{min}	0.92	0.65	0.93	2.04	7.06	0.89	1.85	48,389
	T _{mean}	0.97	0.86	0.97	1.40	7.71	0.52	1.30	52,302
	T _{max}	0.96	0.86	0.97	1.80	9.26	0.77	1.62	43,237
2010	T _{min}	0.92	0.68	0.93	2.12	7.68	0.89	1.94	41,812
	T _{mean}	0.97	0.90	0.97	1.45	8.40	0.50	1.36	45,108
	T _{max}	0.97	0.91	0.97	1.78	10.10	0.81	1.58	38,930
2011	T _{min}	0.90	0.63	0.92	2.02	6.37	0.89	1.82	53,263
	T _{mean}	0.96	0.86	0.96	1.41	6.99	0.48	1.33	57,317
	T _{max}	0.96	0.89	0.96	1.75	8.35	0.72	1.59	50,829
2012	T _{min}	0.93	0.64	0.94	1.99	7.66	0.87	1.80	48,365
	T _{mean}	0.97	0.84	0.97	1.41	8.38	0.48	1.33	52,085
	T _{max}	0.97	0.88	0.97	1.77	10.14	0.74	1.61	43,802
2013	T _{min}	0.92	0.70	0.93	2.04	7.08	0.81	1.88	42,103
	T _{mean}	0.97	0.91	0.97	1.37	8.07	0.44	1.30	45,370
	T _{max}	0.97	0.89	0.97	1.80	9.66	0.77	1.62	37,730
2014	T _{min}	0.88	0.64	0.90	1.91	5.56	0.84	1.72	44,965
	T _{mean}	0.95	0.86	0.95	1.36	6.05	0.46	1.27	48,284
	T _{max}	0.95	0.85	0.96	1.67	7.43	0.76	1.49	42,330
2015	T _{min}	0.89	0.61	0.91	1.90	6.13	0.87	1.80	49,495
	T _{mean}	0.96	0.87	0.96	1.44	7.04	0.47	1.36	53,030
	T _{max}	0.96	0.89	0.96	1.81	8.79	0.75	1.63	45,086
2016	T _{min}	0.92	0.65	0.93	1.96	6.94	0.84	1.78	46,982
	T _{mean}	0.97	0.90	0.97	1.39	7.89	0.42	1.33	50,514
	T _{max}	0.97	0.89	0.97	1.70	9.49	0.69	1.55	42,318
2017	T _{min}	0.91	0.64	0.92	2.03	6.84	0.86	1.85	46,011
	T _{mean}	0.96	0.87	0.97	1.42	7.47	0.46	1.34	49,429
	T _{max}	0.96	0.89	0.97	1.78	8.94	0.77	1.60	42,026
2018	T _{min}	0.92	0.58	0.93	2.04	7.22	0.91	1.84	53,784
	T _{mean}	0.97	0.87	0.98	1.39	8.40	0.51	1.29	57,588
	T _{max}	0.97	0.87	0.97	1.77	9.89	0.84	1.55	52,838
2019	T _{min}	0.90	0.56	0.92	2.00	6.39	0.93	1.78	51,125
	T _{mean}	0.97	0.86	0.97	1.37	7.30	0.48	1.29	54,620

	T _{max}	0.96	0.87	0.97	1.75	8.81	0.76	1.58	47,012
2020	T _{min}	0.88	0.54	0.90	2.03	5.78	1.01	1.82	44,556
	T _{mean}	0.96	0.83	0.96	1.34	6.59	0.51	1.30	47,865
	T _{max}	0.95	0.84	0.96	1.75	8.18	0.73	1.65	42,045
Overall	T_{min}	0.91	0.68	0.92	2.02	6.76	0.87	1.83	45,432
	T_{mean}	0.96	0.88	0.97	1.41	7.56	0.49	1.32	48,925
	T_{max}	0.96	0.84	0.97	1.77	9.12	0.77	1.60	42,155

*SD: standard deviation of the DWD observed T_{air}

Table S2. Prediction accuracy for the third stage predictions against held-out DWD observations (in grid cells with monitoring stations data available but without LST): 10-fold CV results for daily T_{\min} , T_{mean} and T_{\max} in Germany during 2000-2020.

Year	Measure	R^2	RMSE ($^{\circ}\text{C}$)	SD ($^{\circ}\text{C}$)	Sample size (cell-days number)
2000	T_{\min}	0.95	1.27	5.30	65,403
	T_{mean}	0.97	1.12	5.86	67,698
	T_{\max}	0.95	1.49	6.51	70,136
2001	T_{\min}	0.97	1.24	6.53	75,724
	T_{mean}	0.98	1.11	7.04	81,900
	T_{\max}	0.97	1.48	7.72	82,095
2002	T_{\min}	0.96	1.24	6.25	78,458
	T_{mean}	0.98	1.10	6.83	84,934
	T_{\max}	0.97	1.45	7.60	79,574
2003	T_{\min}	0.97	1.38	7.24	67,766
	T_{mean}	0.98	1.11	8.14	73,190
	T_{\max}	0.97	1.49	8.91	67,348
2004	T_{\min}	0.96	1.31	6.43	77,368
	T_{mean}	0.98	1.12	7.14	83,716
	T_{\max}	0.97	1.50	7.97	81,229
2005	T_{\min}	0.97	1.29	7.04	78,804
	T_{mean}	0.98	1.06	7.74	84,737
	T_{\max}	0.97	1.45	8.39	80,259
2006	T_{\min}	0.97	1.30	7.10	81,781
	T_{mean}	0.98	1.05	7.75	87,996
	T_{\max}	0.97	1.41	8.52	84,013
2007	T_{\min}	0.96	1.24	5.97	82,125
	T_{mean}	0.98	1.04	6.75	88,337
	T_{\max}	0.97	1.41	7.47	84,494
2008	T_{\min}	0.96	1.22	6.02	86,894
	T_{mean}	0.98	1.03	6.80	93,298

	T _{max}	0.97	1.39	7.61	90,431
2009	T _{min}	0.97	1.22	6.87	85,118
	T _{mean}	0.98	0.99	7.63	91,288
	T _{max}	0.98	1.38	8.48	90,270
2010	T _{min}	0.98	1.23	7.78	92,174
	T _{mean}	0.99	0.98	8.52	98,991
	T _{max}	0.98	1.36	9.20	95,056
2011	T _{min}	0.96	1.26	6.19	80,560
	T _{mean}	0.98	0.99	7.07	86,531
	T _{max}	0.97	1.38	8.07	82,994
2012	T _{min}	0.97	1.20	6.67	85,584
	T _{mean}	0.98	0.98	7.37	91,717
	T _{max}	0.97	1.33	8.12	90,147
2013	T _{min}	0.97	1.17	6.72	91,852
	T _{mean}	0.98	0.99	7.61	98,008
	T _{max}	0.98	1.38	8.47	96,226
2014	T _{min}	0.96	1.20	5.88	89,646
	T _{mean}	0.98	0.97	6.61	95,750
	T _{max}	0.97	1.40	7.53	92,651
2015	T _{min}	0.96	1.25	6.04	84,677
	T _{mean}	0.98	1.00	6.89	90,420
	T _{max}	0.97	1.39	7.68	87,262
2016	T _{min}	0.97	1.18	6.30	84,146
	T _{mean}	0.98	1.01	7.01	89,842
	T _{max}	0.97	1.41	7.84	88,811
2017	T _{min}	0.97	1.20	6.37	88,818
	T _{mean}	0.98	1.01	7.22	94,839
	T _{max}	0.97	1.40	8.04	92,803
2018	T _{min}	0.97	1.25	6.64	80,956
	T _{mean}	0.98	1.00	7.85	86,076
	T _{max}	0.98	1.38	8.81	81,902
2019	T _{min}	0.96	1.27	6.14	81,733

	T_{mean}	0.98	1.02	7.09	86,975
	T_{max}	0.97	1.41	7.89	85,853
2020	T_{min}	0.96	1.23	5.76	64,902
	T_{mean}	0.98	0.88	6.65	71,594
	T_{max}	0.98	1.22	7.65	67,373
Overall	T_{min}	0.97	1.25	6.44	81,166
	T_{mean}	0.98	1.03	7.22	87,040
	T_{max}	0.97	1.41	8.02	84,330

*SD: standard deviation of the DWD T_{air} variable

Table S3. Comparison between third and second stage predictions: Results for daily T_{\min} , T_{mean} and T_{\max} during 2000-2020 for all grid cells across Germany.					
Year	Measure	R^2	RMSE ($^{\circ}\text{C}$)	SD ($^{\circ}\text{C}$)	Sample size (cell-days number)
2000	T_{\min}	0.93	1.27	5.09	69,584,386
	T_{mean}	0.97	0.96	5.68	69,584,386
	T_{\max}	0.97	1.23	6.26	75,246,789
2001	T_{\min}	0.97	1.27	6.31	82,252,879
	T_{mean}	0.98	1.01	6.86	82,252,879
	T_{\max}	0.98	1.24	7.52	89,856,424
2002	T_{\min}	0.96	1.34	6.07	85,825,240
	T_{mean}	0.98	1.06	6.69	85,825,240
	T_{\max}	0.98	1.20	7.42	88,489,932
2003	T_{\min}	0.97	1.33	7.00	74,648,228
	T_{mean}	0.99	1.03	7.98	74,648,228
	T_{\max}	0.98	1.27	8.72	76,032,730
2004	T_{\min}	0.96	1.25	6.20	85,567,540
	T_{mean}	0.98	0.95	6.97	85,567,540
	T_{\max}	0.98	1.17	7.73	91,325,391
2005	T_{\min}	0.96	1.31	6.83	81,702,456
	T_{mean}	0.98	0.98	7.58	81,702,456
	T_{\max}	0.98	1.22	8.18	84,804,319
2006	T_{\min}	0.97	1.34	6.92	83,184,222
	T_{mean}	0.99	1.05	7.63	83,184,222
	T_{\max}	0.99	1.19	8.37	86,769,379
2007	T_{\min}	0.95	1.24	5.78	81,751,441
	T_{mean}	0.98	1.04	6.59	81,751,441
	T_{\max}	0.98	1.17	7.25	86,083,062
2008	T_{\min}	0.95	1.25	5.81	85,109,087
	T_{mean}	0.98	0.94	6.65	85,109,087
	T_{\max}	0.98	1.17	7.39	89,787,577

2009	T _{min}	0.96	1.35	6.65	82,484,112
	T _{mean}	0.98	1.01	7.49	82,484,112
	T _{max}	0.98	1.25	8.35	88,905,862
2010	T _{min}	0.97	1.37	7.68	89,742,514
	T _{mean}	0.98	1.04	8.47	89,742,514
	T _{max}	0.98	1.22	9.10	93,543,768
2011	T _{min}	0.95	1.28	6.02	78,420,415
	T _{mean}	0.98	1.02	6.96	78,420,415
	T _{max}	0.98	1.27	7.88	82,140,829
2012	T _{min}	0.97	1.30	6.49	83,147,071
	T _{mean}	0.98	1.03	7.23	83,147,071
	T _{max}	0.98	1.27	7.93	89,049,787
2013	T _{min}	0.96	1.34	6.56	88,759,293
	T _{mean}	0.98	0.97	7.50	88,759,293
	T _{max}	0.98	1.22	8.35	94,386,787
2014	T _{min}	0.95	1.16	5.74	86,292,259
	T _{mean}	0.97	0.94	6.52	86,292,259
	T _{max}	0.97	1.14	7.38	90,320,155
2015	T _{min}	0.95	1.30	5.81	81,972,324
	T _{mean}	0.98	1.03	6.71	81,972,324
	T _{max}	0.98	1.29	7.43	86,962,223
2016	T _{min}	0.96	1.27	6.16	81,491,380
	T _{mean}	0.98	1.02	6.91	81,491,380
	T _{max}	0.98	1.17	7.69	87,032,964
2017	T _{min}	0.96	1.31	6.16	85,740,094
	T _{mean}	0.98	1.01	7.06	85,740,094
	T _{max}	0.98	1.22	7.84	90,879,244
2018	T _{min}	0.96	1.32	6.41	77,371,038
	T _{mean}	0.98	1.02	7.71	77,371,038
	T _{max}	0.98	1.26	8.67	79,839,923
2019	T _{min}	0.96	1.25	5.93	79,914,991
	T _{mean}	0.98	1.00	6.96	79,914,991

	T _{max}	0.98	1.24	7.70	84,909,897
2020	T _{min}	0.94	1.28	5.54	75,815,644
	T _{mean}	0.98	1.00	6.49	75,815,644
	T _{max}	0.97	1.27	7.44	79,967,372
Overall	T_{min}	0.96	1.29	6.52	81,941,744
	T_{mean}	0.98	1.01	7.08	81,941,744
	T_{max}	0.98	1.22	7.83	86,492,115

*SD: standard deviation of the dependent variable (second stage T_{air} predictions)

Table S4. Bias calculation results for the daily T_{\min} , T_{mean} and T_{\max} predictions in Germany during 2000-2020.

Year	Measure	Intercept	Slope	Mean signed error (°C)
2000	T_{\min}	-0.35	1.06	0.05
	T_{mean}	-0.21	1.02	0.06
	T_{\max}	-0.73	1.04	-0.19
2001	T_{\min}	-0.10	1.03	0.04
	T_{mean}	-0.08	1.02	0.05
	T_{\max}	-0.44	1.02	-0.16
2002	T_{\min}	-0.09	1.03	0.08
	T_{mean}	-0.11	1.02	0.07
	T_{\max}	-0.45	1.02	-0.13
2003	T_{\min}	-0.03	1.02	0.07
	T_{mean}	-0.06	1.01	0.07
	T_{\max}	-0.37	1.02	-0.12
2004	T_{\min}	-0.09	1.04	0.08
	T_{mean}	-0.11	1.02	0.05
	T_{\max}	-0.52	1.03	-0.17
2005	T_{\min}	-0.05	1.03	0.10
	T_{mean}	-0.09	1.02	0.04
	T_{\max}	-0.47	1.02	-0.16
2006	T_{\min}	-0.01	1.03	0.12
	T_{mean}	-0.11	1.02	0.04
	T_{\max}	-0.46	1.02	-0.15
2007	T_{\min}	-0.08	1.05	0.11
	T_{mean}	-0.20	1.02	0.03
	T_{\max}	-0.65	1.03	-0.18
2008	T_{\min}	-0.14	1.04	0.12
	T_{mean}	-0.14	1.02	0.06
	T_{\max}	-0.51	1.03	-0.13
2009	T_{\min}	-0.04	1.03	0.10

	T_{mean}	-0.11	1.02	0.04
	T_{max}	-0.48	1.02	-0.14
2010	T_{min}	-0.01	1.03	0.09
	T_{mean}	-0.09	1.02	0.03
	T_{max}	-0.43	1.02	-0.17
2011	T_{min}	-0.05	1.04	0.13
	T_{mean}	-0.16	1.02	0.05
	T_{max}	-0.60	1.03	-0.16
2012	T_{min}	0.00	1.03	0.12
	T_{mean}	-0.08	1.01	0.06
	T_{max}	-0.36	1.02	-0.10
2013	T_{min}	-0.07	1.03	0.07
	T_{mean}	-0.23	1.01	0.04
	T_{max}	-0.53	1.03	-0.19
2014	T_{min}	-0.18	1.05	0.09
	T_{mean}	-0.15	1.03	0.03
	T_{max}	-0.67	1.03	-0.17
2015	T_{min}	-0.09	1.04	0.11
	T_{mean}	-0.06	1.02	0.05
	T_{max}	-0.66	1.03	-0.18
2016	T_{min}	-0.08	1.03	0.08
	T_{mean}	-0.12	1.02	0.04
	T_{max}	-0.49	1.03	-0.17
2017	T_{min}	-0.07	1.04	0.11
	T_{mean}	-0.13	1.02	0.06
	T_{max}	-0.50	1.03	-0.16
2018	T_{min}	-0.09	1.03	0.07
	T_{mean}	-0.13	1.01	0.03
	T_{max}	-0.58	1.02	-0.16
2019	T_{min}	-0.10	1.04	0.09
	T_{mean}	-0.14	1.02	0.04
	T_{max}	-0.40	1.03	-0.17

2020	T_{\min}	-0.07	1.05	0.19
	T_{mean}	-0.14	1.02	0.08
	T_{\max}	-0.52	1.03	-0.14
Overall	T_{\min}	-0.09	1.04	0.10
	T_{mean}	-0.13	1.02	0.05
	T_{\max}	-0.51	1.03	-0.16

Table S5. Contribution (%) of each stage of the modeling process for the daily T_{\min} , T_{mean} and T_{\max} predictions in Germany, averaged for 2000-2020.

Measure	Stage 1	Stage 2	Stage 3
T_{\min}	0.04	36.1	62.0
T_{mean}	0.04	35.6	62.5
T_{\max}	0.03	32.7	65.4

Table S6. Accuracy results of the small-scale external validation with HOBO-Logger T_{\min} , T_{mean} and T_{\max} observations in the Augsburg area during 2013-2018.							
Year	Measure	R^2	RMSE ($^{\circ}\text{C}$)	SD ($^{\circ}\text{C}$)	7-day average R^2	7-day average RMSE ($^{\circ}\text{C}$)	SD ($^{\circ}\text{C}$)
2013	T_{\min}	0.95	1.75	7.02	0.97	1.41	6.62
	T_{mean}	0.99	1.07	8.06	0.99	0.92	7.70
	T_{\max}	0.98	1.26	9.55	0.98	0.93	8.95
2014	T_{\min}	0.92	1.89	6.07	0.96	1.45	5.58
	T_{mean}	0.98	1.08	6.62	0.99	0.97	6.21
	T_{\max}	0.97	1.35	7.97	0.98	1.16	7.21
2015	T_{\min}	0.95	1.81	6.92	0.96	1.49	6.56
	T_{mean}	0.98	1.07	7.67	0.99	0.87	7.38
	T_{\max}	0.98	1.45	8.97	0.98	1.08	8.44
2016	T_{\min}	0.95	1.69	6.61	0.97	1.36	6.21
	T_{mean}	0.99	1.00	7.44	0.99	0.81	7.02
	T_{\max}	0.98	1.30	8.65	0.99	0.98	8.01
2017	T_{\min}	0.95	1.88	7.34	0.97	1.53	7.02
	T_{mean}	0.99	1.21	8.23	0.99	1.03	7.95
	T_{\max}	0.98	1.40	9.59	0.99	0.95	9.01
2018	T_{\min}	0.96	1.78	7.06	0.98	1.40	6.67
	T_{mean}	0.99	0.99	8.28	0.99	0.77	7.94
	T_{\max}	0.98	1.44	9.96	0.98	1.40	9.39
Overall	T_{\min}	0.95	1.80	6.84	0.97	1.44	6.44
	T_{mean}	0.99	1.07	7.72	0.99	0.90	7.37
	T_{\max}	0.98	1.37	9.11	0.98	1.08	8.50

*SD: standard deviation of the dependent variable (HOBO-Logger T_{air})

Table S7. Seasonal accuracy results of the small-scale external validation with HOBO-Logger daily T_{\min} , T_{mean} and T_{\max} observations in the Augsburg area during 2013-2018.													
Year	Measure	Winter			Spring			Summer			Fall		
		R^2	RMSE (°C)	SD (°C)									
2013	T_{\min}	0.84	1.80	5.10	0.93	1.56	5.28	0.79	2.05	3.44	0.91	1.54	4.74
	T_{mean}	0.94	1.07	4.70	0.98	0.88	5.89	0.95	1.27	4.24	0.97	1.00	5.33
	T_{\max}	0.95	0.95	5.07	0.98	1.13	7.07	0.93	1.51	5.84	0.98	1.22	6.77
2014	T_{\min}	0.60	1.39	2.23	0.79	1.81	3.41	0.71	2.11	3.02	0.84	1.80	4.19
	T_{mean}	0.83	1.06	2.36	0.93	1.21	3.60	0.90	1.26	2.81	0.96	0.99	4.74
	T_{\max}	0.90	1.28	3.85	0.92	1.42	4.82	0.90	1.26	3.95	0.96	1.32	6.24
2015	T_{\min}	0.82	1.43	3.36	0.89	1.93	5.03	0.81	2.02	3.39	0.83	1.83	4.10
	T_{mean}	0.91	0.98	3.14	0.96	1.06	4.74	0.94	1.19	4.16	0.95	1.05	4.40
	T_{\max}	0.85	1.58	4.13	0.95	1.24	5.48	0.93	1.56	5.70	0.93	1.47	5.63
2016	T_{\min}	0.87	1.56	3.92	0.91	1.63	4.38	0.72	1.80	2.69	0.92	1.71	5.41
	T_{mean}	0.96	0.91	3.88	0.98	0.93	4.94	0.91	1.07	3.09	0.98	1.04	6.09
	T_{\max}	0.94	1.21	4.52	0.96	1.33	5.99	0.90	1.35	4.25	0.98	1.16	7.28
2017	T_{\min}	0.91	1.64	5.47	0.88	1.83	4.39	0.65	2.33	3.11	0.83	1.66	3.79
	T_{mean}	0.95	1.12	5.14	0.97	1.24	5.02	0.92	1.51	3.34	0.96	1.03	4.37
	T_{\max}	0.94	1.45	5.75	0.95	1.25	6.24	0.91	1.43	4.57	0.95	1.25	6.02
2018	T_{\min}	0.93	1.34	4.49	0.94	1.90	5.92	0.78	1.98	3.13	0.90	1.77	4.84
	T_{mean}	0.97	0.88	4.39	0.99	1.01	6.73	0.92	1.12	3.30	0.97	0.98	5.69
	T_{\max}	0.94	1.31	4.78	0.97	1.36	7.97	0.90	1.47	4.55	0.95	1.73	7.59
Overall	T_{\min}	0.83	1.53	4.10	0.89	1.78	4.74	0.74	2.05	3.13	0.87	1.72	4.51
	T_{mean}	0.93	1.00	3.94	0.97	1.06	5.15	0.92	1.24	3.49	0.97	1.02	5.10
	T_{\max}	0.92	1.30	4.68	0.96	1.29	6.26	0.91	1.43	4.81	0.96	1.36	6.59

*SD: standard deviation of the dependent variable (HOBO-Logger T_{air})

Table S8. Linear regression between the models' predictions and the HOBO-Logger daily T_{\min} , T_{mean} and T_{\max} observations in the Augsburg area during 2013-2018.			
Year	Measure	Intercept	Slope
2013	T_{\min}	0.69	1.02
	T_{mean}	0.30	1.01
	T_{\max}	0.48	0.97
2014	T_{\min}	0.52	1.05
	T_{mean}	0.27	1.03
	T_{\max}	0.47	0.98
2015	T_{\min}	0.43	1.06
	T_{mean}	0.13	1.02
	T_{\max}	0.43	0.98
2016	T_{\min}	0.66	1.03
	T_{mean}	0.41	1.00
	T_{\max}	0.56	0.97
2017	T_{\min}	0.54	1.06
	T_{mean}	0.19	1.05
	T_{\max}	0.22	0.99
2018	T_{\min}	0.79	1.03
	T_{mean}	0.40	1.01
	T_{\max}	0.29	0.98
Overall	T_{\min}	0.61	1.04
	T_{mean}	0.28	1.02
	T_{\max}	0.41	0.98

Table S9. Comparison between our model daily T_{mean} predictions and the DWD TRY model daily T_{mean} predictions in Germany during 2001-2012.

Year	R ²	RMSE (°C)	Intercept	Slope
2001	0.98	0.94	-0.08	1.01
2002	0.98	0.92	-0.06	1.01
2003	0.99	1.04	-0.01	1.01
2004	0.99	0.88	-0.06	1.02
2005	0.99	0.89	-0.03	1.02
2006	0.99	0.92	-0.09	1.02
2007	0.98	0.88	-0.15	1.02
2008	0.99	0.82	-0.08	1.02
2009	0.99	0.90	-0.04	1.02
2010	0.99	0.86	-0.03	1.01
2011	0.98	0.92	-0.08	1.02
2012	0.99	0.88	-0.08	1.01
Overall	0.99	0.90	-0.07	1.02

Table S10. Comparison by season between our model daily T_{mean} predictions and the DWD TRY model daily T_{mean} predictions in Germany during 2001-2012.

Year	Winter		Spring		Summer		Fall	
	R ²	RMSE (°C)						
2001	0.93	1.04	0.97	0.94	0.95	0.90	0.97	0.85
2002	0.96	1.07	0.96	0.87	0.93	0.81	0.97	0.88
2003	0.94	1.15	0.97	1.01	0.96	1.07	0.97	0.96
2004	0.96	0.88	0.97	0.87	0.93	0.90	0.98	0.81
2005	0.96	0.89	0.98	0.91	0.94	0.88	0.98	0.89
2006	0.91	1.13	0.98	0.88	0.96	0.91	0.98	0.85
2007	0.96	0.75	0.96	0.97	0.93	0.85	0.97	0.87
2008	0.94	0.83	0.94	0.80	0.93	0.88	0.97	0.77
2009	0.92	1.08	0.97	0.88	0.94	0.86	0.97	0.82
2010	0.95	0.96	0.98	0.86	0.96	0.81	0.97	0.76
2011	0.95	1.01	0.97	0.96	0.94	0.81	0.97	0.96
2012	0.94	0.95	0.97	0.89	0.94	0.87	0.97	0.84
Overall	0.94	0.98	0.97	0.90	0.94	0.88	0.97	0.86

Table S11. Comparison without extremes between our model daily T_{mean} predictions and the DWD TRY model daily T_{mean} predictions in Germany during 2001-2012.		
Year	5 th percentile < T_{mean} < 95 th percentile	
	R^2	RMSE (°C)
2001	0.98	0.80
2002	0.98	0.78
2003	0.98	0.77
2004	0.99	0.82
2005	0.99	0.78
2006	0.99	0.77
2007	0.99	0.83
2008	0.99	0.84
2009	0.99	0.74
2010	0.98	0.78
2011	0.99	0.77
2012	0.99	0.77
Overall	0.99	0.79

Table S12. Comparison to extremes between our model daily T_{mean} predictions and the DWD TRY model daily T_{mean} predictions in Germany during 2001-2012.				
Year	$T_{\text{mean}} < 5^{\text{th}}$ percentile		$T_{\text{mean}} > 95^{\text{th}}$ percentile	
	R^2	RMSE ($^{\circ}\text{C}$)	R^2	RMSE ($^{\circ}\text{C}$)
2001	0.68	1.58	0.58	0.82
2002	0.83	1.13	0.88	0.56
2003	0.77	1.28	0.61	1.10
2004	0.75	1.06	0.54	1.08
2005	0.76	1.24	0.75	0.73
2006	0.63	1.21	0.70	0.85
2007	0.81	1.01	0.85	1.34
2008	0.74	0.91	0.52	0.95
2009	0.81	1.38	0.66	0.94
2010	0.65	1.14	0.84	0.84
2011	0.74	1.03	0.89	0.89
2012	0.90	1.34	0.73	1.00
Overall	0.76	1.19	0.71	0.93

Table S13. Comparison in rural versus urban areas (Augsburg region) between our model daily T_{mean} predictions and the DWD TRY model daily T_{mean} predictions in Germany during 2001-2012.

Year	Rural - Augsburg Landkreis		Urban - Stadt Augsburg	
	R ²	RMSE (°C)	R ²	RMSE (°C)
2001	0.99	0.89	0.99	0.89
2002	0.99	0.81	0.99	0.87
2003	0.99	1.01	0.99	0.94
2004	0.99	0.87	0.99	0.84
2005	0.99	0.81	0.99	0.82
2006	0.99	0.84	0.99	0.84
2007	0.99	0.90	0.99	0.82
2008	0.99	0.86	0.99	0.86
2009	0.99	0.81	0.99	0.85
2010	0.99	0.73	0.99	0.72
2011	0.99	0.80	0.99	0.84
2012	0.99	0.79	0.99	0.87
Overall	0.99	0.84	0.99	0.85

4. Paper II

Title: Improved daily estimates of relative humidity at high resolution across Germany: A random forest approach

Authors: Nikolaos Nikolaou, Laurens M. Bouwer, Marco Dallavalle, Mahyar Valizadeh, Massimo Stafoggia, Annette Peters, Kathrin Wolf, Alexandra Schneider

Journal: Environmental Research

Year: 2023

Volume: 238

Pages: 117173

DOI: <https://doi.org/10.1016/j.envres.2023.117173>

Supplements: <https://www.sciencedirect.com/science/article/pii/S0013935123019771?via%3Dihub#appsec1>

Impact factor: 8.3 (Journal Citations Reports® 2022)

Rank: 32/275 in category Environmental Sciences and
16/207 in category Public, Environmental & Occupational Health
(Journal Citations Reports® 2022)

Contents lists available at [ScienceDirect](https://www.sciencedirect.com)

Environmental Research

journal homepage: www.elsevier.com/locate/envres

Improved daily estimates of relative humidity at high resolution across Germany: A random forest approach

Nikolaos Nikolaou^{a,b,*}, Laurens M. Bouwer^c, Marco Dallavalle^{a,b}, Mahyar Valizadeh^a, Massimo Stafoggia^d, Annette Peters^{a,b}, Kathrin Wolf^{a,1}, Alexandra Schneider^{a,1}

^a Institute of Epidemiology, Helmholtz Zentrum München, German Research Center for Environmental Health, Neuherberg, Germany

^b Institute for Medical Information Processing, Biometry and Epidemiology (IBE), Faculty of Medicine, LMU Munich, Pettenkofer School of Public Health, Munich, Germany

^c Climate Service Center Germany (GERICS), Helmholtz-Zentrum Hereon, Hamburg, Germany

^d Department of Epidemiology, Lazio Regional Health Service – ASL Roma 1, Rome, Italy

ARTICLE INFO

Handling Editor: Jose L Domingo

Keywords:

Relative humidity
Spatiotemporal modeling
Machine learning
External validation
Exposure assessment
Environmental epidemiology

ABSTRACT

The lack of readily available methods for estimating high-resolution near-surface relative humidity (RH) and the incapability of weather stations to fully capture the spatiotemporal variability can lead to exposure misclassification in studies of environmental epidemiology. We therefore aimed to predict German-wide 1 × 1 km daily mean RH during 2000–2021. RH observations, longitude and latitude, modelled air temperature, precipitation and wind speed as well as remote sensing information on topographic elevation, vegetation, and the true color band composite were incorporated in a Random Forest (RF) model, in addition to date for capturing the temporal variations of the response-explanatory variables relationship. The model achieved high accuracy ($R^2 = 0.83$) and low errors (Root Mean Square Error (RMSE) of 5.07%, Mean Absolute Percentage Error (MAPE) of 5.19% and Mean Percentage Error (MPE) of -0.53%), calculated via ten-fold cross-validation. A comparison of our RH predictions with measurements from a dense monitoring network in the city of Augsburg, South Germany confirmed the good performance ($R^2 \geq 0.86$, $RMSE \leq 5.45\%$, $MAPE \leq 5.59\%$, $MPE \leq 3.11\%$). The model displayed high German-wide RH (22y-average of 79.00%) and high spatial variability across the country, exceeding 12% on yearly averages. Our findings indicate that the proposed RF model is suitable for estimating RH for a whole country in high-resolution and provide a reliable RH dataset for epidemiological analyses and other environmental research purposes.

1. Introduction

Relative humidity (RH) refers to the water vapor content of air and quantifies how far the atmosphere is from its saturation point. RH is a key parameter for many fields such as agriculture (Zhang et al., 2015), hydrology (Forootan, 2019) and climatology (Sherwood et al., 2010) as it contributes among others to the soil moisture, the hydrological cycle and the weather and climate conditions. Thus, RH plays an important role in plant and animal life (Xiong et al., 2017) as well as in human comfort and well-being (Davis et al., 2016; Yang et al., 2018).

RH has mostly been used as a confounder or effect modifier in studies

focusing on air temperature (T_{air}) (Armstrong, 2006; Zeng et al., 2017), or as part of an index, e.g., apparent temperature (Analitis et al., 2008). Nevertheless, there is evidence that RH is potentially an independent risk factor for mortality (Ou et al., 2014) and morbidity (Luo et al., 2020). In epidemiology, RH data are usually retrieved from weather monitors. But their locations are irregularly distributed over space, usually in rural areas, and their number is limited. Hence, weather stations are inadequate to fully represent the spatiotemporal RH variations in complex geo-climatic urban and rural landscapes, and by using their observations, error is introduced in the exposure assessment of study participants leading to estimates biased towards the null (Zeger

* Corresponding author. Address: Ingolstädter Landstr. 1, D-85764, Neuherberg, Germany.

E-mail addresses: nikolaos.nikolaou@helmholtz-munich.de (N. Nikolaou), laurens.bouwer@hereon.de (L.M. Bouwer), marco.dallavalle@helmholtz-munich.de (M. Dallavalle), mahyar.valizadeh@helmholtz-munich.de (M. Valizadeh), m.stafoggia@deplazio.it (M. Stafoggia), annette.peters@helmholtz-munich.de (A. Peters), kathrin.wolf@helmholtz-munich.de (K. Wolf), alexandra.schneider@helmholtz-munich.de (A. Schneider).

¹ Shared last authorship.

<https://doi.org/10.1016/j.envres.2023.117173>

Received 8 February 2023; Received in revised form 1 September 2023; Accepted 17 September 2023

Available online 20 September 2023

0013-9351/© 2023 The Authors. Published by Elsevier Inc. This is an open access article under the CC BY license (<http://creativecommons.org/licenses/by/4.0/>).

et al., 2000). Climate reanalysis data could be an alternative source for environmental health research (Mistry et al., 2022), but the resolution is usually coarser than 9 km and the data fail to capture the city-level exposure variability effectively. We therefore suggest to extend the methods and datasets in order to improve the predictions of RH exposure for people participating in epidemiological studies, such as prospective cohorts with data on the residential addresses of the participants.

There is a clear methodological gap in RH modeling, especially for high spatiotemporally-resolved RH predictions and for timespans up to multiple years. Li et al. (2014) mapped RH every 3 h at 1 km by using a two-step interpolation procedure of re-analysis data based on a partial thin-plate spline (TPS) and simple kriging (Root Mean Square Error (RMSE) = 11.06%). The traditional interpolation techniques have limited efficiency when mapping meteorological exposures in spatially highly heterogeneous areas, and are characterized by neighbouring effects on exposures predictions, without being capable of capturing small-scale and intra-city variations. Li and Zha (2018) used a Random Forest (RF) model and satellite data, to estimate RH during the summer of 2009 ($R^2 = 0.70$, RMSE = 7.4%). Spatiotemporal predictors which could explain a large amount of the remaining RH variance, e.g., T_{air} , were not included. Longer periods and more predictors need to be tested to capture the full annual and inter-annual RH variability. For China, the RF model had better results than TPS and kriging, but improvements are needed for better RH variability representation, higher prediction accuracy and further temporal extension to the annual level.

Remote sensing data are progressively used in environmental exposures modeling (Rosenfeld et al., 2017; Yao et al., 2022) being publicly available in high spatiotemporal resolution. There is also a growing body of machine learning (ML) methods applied in the field (Jin et al., 2022; Silibello et al., 2021; Stafoggia et al., 2019).

The specific objectives of this study were (a) to estimate highly spatiotemporal resolved RH for Germany based on T_{air} and other observation, remote sensing and modelled data by using a RF model, (b) to evaluate the model's performance and (c) to produce a reliable German-wide RH dataset for subsequent epidemiological analyses and various research purposes. Thereby, we aimed to extend the current literature and provide a generalizable method for other countries to produce highly resolved RH datasets.

2. Materials and methods

2.1. Study domain

Germany extends in an area of 357,021 km², having a strongly diverse landscape and a high elevation range (−3.54 to 2962 m). In the south-eastern regions, the climate is classified as warm summer humid continental, while in north-western regions it is characterized as temperate oceanic (Beck et al., 2018b). We divided Germany's land area into 366,536 grid cells of 1 × 1 km resolution, following the European INSPIRE (Infrastructure for Spatial Information in the European Community) standard for gridded datasets and using the Lambert Azimuthal Equal-Area (LAEA) projection, EPSG: 3035 (©GeoBasis-DE/BKG (2021)).

2.2. Input data

Large amounts of input data were incorporated in the RF modeling process. We used meteorological observations, remote sensing and spatiotemporally resolved modelled data, all retrieved from 2000 to 2021 across the study area.

2.2.1. RH data

We used daily mean RH observations (DWD, 2022a) from 406 weather stations of the German Meteorological Service (DWD) https://opendata.dwd.de/climate_environment/CDC/observations_germany/climate/daily/kl/historical/ (Figure S1). The RH data has been quality

controlled by the DWD and all the needed information such as station location as well as relocations was included in their metadata files.

2.2.2. T_{air} data

In our previous work (Nikolaou et al., 2022), we estimated daily mean T_{air} in high-resolution (1 × 1 km) across Germany using a regression-based method incorporating two linear mixed models. In brief, we predicted T_{air} by calibrating the strong relationship between the weather stations' T_{air} observations and the satellite-based land surface temperature (LST) also adjusting for various spatial predictors. We also applied a TPS interpolation in T_{air} data in order to achieve a full German-wide coverage. Extensive validation showed high performance ($R^2 \geq 0.96$) and low errors (RMSE ≤ 1.41 °C).

2.2.3. Elevation data

We downloaded elevation data at 30-arc-second spatial resolution <https://www.usgs.gov/centers/eros/science/usgs-eros-archive-digital-elevation-global-30-arc-second-elevation-gtopo30>, provided by the U.S. Geological Survey's Earth Resources Observation Systems (EROS) Data Center (Gesch et al., 1999). We aggregated these data to a 1 × 1 km grid, including the land borders and the shorelines in the North and Baltic Seas to match our intended spatial resolution (Figure S2).

2.2.4. Greenness data

The normalized difference vegetation index (NDVI) is a proxy of vegetation greenness on the Earth surface, quantifying the vegetation cover and quality over space. We retrieved NDVI data of 1 × 1 km from the TERRA MODIS product MOD13A3v006 <https://lpdaac.usgs.gov/products/mod13a3v006/> (Didan, 2015). These are monthly data - weighted temporal average values through the month, which is sufficient, as vegetation does not change considerably during a month.

2.2.5. True color band composite data

The visible red, green and blue light bands demonstrate how we see Earth's surface from space. We retrieved the daily true color band composite, i.e. the surface spectral reflectance for the red (band 1), blue (band 3) and green (band 4) bands at 500 m spatial resolution from the TERRA MODIS product MOD09Gav006 <https://lpdaac.usgs.gov/products/mod09gav006/>, corrected for atmospheric conditions (Vermote, 2015). We aggregated the data to a 1 × 1 km grid, to suit the output's spatial resolution.

2.2.6. Precipitation data

We used daily precipitation data of 1 × 1 km developed by the REGNIE (Regionalisierte Niederschlagshöhen) method which are publicly available from the DWD Climate Data Center https://opendata.dwd.de/climate_environment/CDC/grids_germany/daily/regnie/ (DWD, 2022b). REGNIE is based on the interpolated DWD weather station precipitation measurements, using a combination of multiple linear regressions and Inverse Distance Weighting (IDW), with orographic conditions considered (Rauthe et al., 2013). In a recent update, the REGNIE dataset has been substituted with HYRAS-DE-PRE (DWD, 2023), which shares the same methodology and references the identical paper by Rauthe et al. (2013).

2.2.7. Wind speed data

We retrieved daily mean wind speed (DWD, 2022a) of the same 406 weather stations as for the RH data https://opendata.dwd.de/climate_environment/CDC/observations_germany/climate/daily/kl/historical/ (Figure S1). We interpolated this dataset to 1 × 1 km spatial resolution using TPS, since studies have suggested that TPS outperformed other interpolation methods such as kriging or IDW for mapping climate variables (Wu et al., 2013, 2015). Details regarding the spatiotemporal distribution and the assessment of wind speed interpolation are available in the Supplementary material (Figure S3 and Table S1).

2.3. Modeling

RF (Breiman, 2001) is a well-known and powerful supervised ensemble ML algorithm, utilized for solving both classification and regression tasks - based on the bagging principle. For regression, random sub-samples of the given dataset (i.e., the training set in most applications) are selected (with replacement). Then, the algorithm constructs decision trees - one for every sub-sample, also including a subset of the specified features (i.e., the model predictors). Each decision tree will generate an output/prediction of the target variable. The main model's output is calculated by averaging all the outputs of the individual decision trees.

The RF algorithm copes greatly with big data, with potentially correlated predictors and their non-linearity, and with overfitting. RF is also considered as a robust method against outliers.

In our study, we trained the RF model, trying to evaluate its efficiency in reproducing the observed RH values measured by the weather stations, i.e., the ground-based truth. As RF inherent robustness alleviates the need for complex hyperparameter tuning, we did not proceed with highly sophisticated methodologies for hyperparameters tuning but rather some trial and error by deviating from the default settings. We did not observe any strong differences to the model performance by testing different sets of hyperparameters. Eventually, we used 500 trees and 8 randomly sampled variables as candidates at every split (num. trees = 500, mtry = 8), training the model for each year separately to capture annual variations. The daily observed mean RH (%) at the DWD stations was the response variable. The predictors were our previously modelled daily mean T_{air} (Celsius), the daily red, green and blue bands (dimensionless), the daily mean precipitation height (mm) and the daily mean wind speed (m/s) as well as elevation (meters) and monthly NDVI (dimensionless). We also integrated the geographical coding information [i.e., longitude (°) and latitude (°)] to account for spatial variations that might not be fully represented by other spatial features in the model, and we included the day of the year (1–365|366) in order to capture daily variations in the response-predictor variables relationship.

2.3.1. Model performance

Ten-fold cross-validation (CV) was used to assess the model performance by randomly dividing the set of the DWD weather monitors to a training and a testing set (90:10) ten times. Each time, the model was refitted using the training set and then the RH was predicted in the respective testing set. Our aim was to estimate a full time series of RH in locations without weather stations and therefore in grid cells where the RF model was not previously trained, and consequently to simulate the prediction step of the modeling procedure. Regressing the observed mean RH vs. the predicted mean RH by the RF model's testing set, we calculated the corresponding R^2 , RMSE, Mean Absolute Percentage Error (MAPE) and Mean Percentage Error (MPE) (formulations are written in the Supplementary), each of them ten times and then we took their average to represent each year's CV- R^2 , CV-RMSE, CV-MAPE and CV-MPE.

In the prediction step, we applied the RF model to all grid cells and days combinations without available RH measurements of DWD weather stations in order to obtain a complete RH dataset for entire Germany.

2.3.2. Validation with external data

An additional validation was conducted by comparing our daily mean RH predictions with measurements of an independent dense monitoring network during 2015–2019. The network included RH measurements of 4 min temporal resolution from 82 HOBO-Logger devices (ONSET, Type Pro v2), which were located in the city of Augsburg and in two adjacent counties (Augsburg county and Aichach-Friedberg) (Figure S4). Detailed information for the monitoring network and the measurements' quality assurance can be found in the corresponding paper (Beck et al., 2018a). For our comparison, we aggregated the 4-min

RH values to daily means and then 7-day averages. We generated the corresponding R^2 , RMSE, MAPE and MPE as derived from linearly regressing the predicted RH from the model against the observed RH from the HOBO-Logger monitors.

The majority of the HOBO-Logger stations were located in the city center of Augsburg or close to it, where no DWD measurements were available in the training step of the RF model (closest stations were approx. 10 and 18 km apart from the city center, see Figure S4). Thus, we investigated the performance of the model in an area without prior information but of great epidemiological interest since highly populated implicating that more people are exposed here.

2.4. Descriptive analyses and case study

Descriptive statistics [mean, standard deviation (SD), minimum (min), first quartile (Q1), median, third quartile (Q3) and maximum (max)] were calculated from our German-wide RH predictions and from the DWD observations. We also investigated the spatiotemporal RH patterns over the last 2 decades, overall and by season.

To demonstrate the improvement in our exposure assessment, we compared the spatial distributions of the daily mean RH predictions from the RF model and the daily mean RH measurements from the DWD stations in an urban location for the two last decades. The city of Regensburg covers an area of 80.76 km² with about 150,000 inhabitants, and, as one of the study sites of the German National Cohort (NAKO) (German National Cohort Consortium, 2014), has also an epidemiological research interest.

We performed our analysis in R, v. 4.2.2 (R Core Team, 2022). The RF model was developed with the R package "ranger" (Wright and Ziegler, 2017).

3. Results

Figure S5 shows the Spearman correlation coefficients for the models' variables. Briefly, RH was found to be highly and positively associated with the true color band composite ($r \approx 0.5$) while there was a strong negative correlation with T_{air} ($r \approx -0.5$). In Figure S6, we demonstrate the variable importance plot findings. Date played a very important role. We also observed that T_{air} and the blue band were the most important spatiotemporal predictors of the RF model for estimating RH. They were followed by precipitation, green band, wind speed and longitude, and then elevation, latitude, NDVI and red band. The order of the predictors was slightly different through the years, but there were main trends as described.

3.1. Model performance

The model achieved high accuracy [22-year average $R^2 = 0.83$ (range: 0.77–0.88)] and small errors [22-year average RMSE = 5.07% (range: 4.44%–6.27%), MAPE = 5.19% (range: 4.45%–6.93%) and MPE = -0.53% (range: -0.35% - -0.89%), Table 1]. We observed an increase of the model performance (increase of R^2 and decrease of errors), together with an increase of the total number of available weather station data over the years. Scatterplots depicting the example years with the lowest and highest fitting scores, specifically 2001 and 2020, have been included in the Supplementary material (Figure S7). Autumn months (September–November) had the lowest RMSE = 4.65% (range: 3.89%–5.83%) while spring months (March–May) had the highest RMSE = 5.32% (range: 4.60%–6.44%) (Fig. 1). We also observed that predictions belonging to the lower 10% of the dataset gave higher errors [RMSE = 7.85% (range: 6.86%–9.28%)] compared to the predictions of the upper 10% of the dataset [RMSE = 5.38% (range: 4.47%–6.79%)] (Fig. 1). The corresponding results for MAPE and MPE are available in the Supplementary (Figure S8 and S9).

Table 1
Prediction accuracy for the RF model: 10-fold CV results for the daily mean RH predictions over Germany during 2000–2021.

Year	R ²	RMSE (%)	MAPE (%)	MPE (%)	Sample size (number of cell-days)
2000	0.78	5.71	5.88	-0.64	100,699
2001	0.78	5.53	5.50	-0.52	121,225
2002	0.77	5.69	5.77	-0.59	123,946
2003	0.81	6.27	6.93	-0.89	123,364
2004	0.78	5.64	5.74	-0.61	126,604
2005	0.81	5.21	5.26	-0.51	134,386
2006	0.82	5.28	5.37	-0.65	135,600
2007	0.84	4.81	4.89	-0.48	139,482
2008	0.83	5.00	5.14	-0.52	140,135
2009	0.82	5.06	5.15	-0.49	142,295
2010	0.86	4.72	4.73	-0.39	142,629
2011	0.86	4.91	5.04	-0.56	141,781
2012	0.84	4.74	4.81	-0.48	141,820
2013	0.84	4.80	4.72	-0.44	140,928
2014	0.85	4.55	4.47	-0.38	142,641
2015	0.85	4.91	5.03	-0.52	142,908
2016	0.83	4.72	4.65	-0.41	139,491
2017	0.83	4.69	4.64	-0.41	143,206
2018	0.87	4.94	5.32	-0.57	143,026
2019	0.85	5.09	5.37	-0.62	140,866
2020	0.88	4.87	5.26	-0.53	116,670
2021	0.85	4.44	4.45	-0.35	116,544
Overall	0.83	5.07	5.19	-0.53	133,648

3.2. Validation with external data

We found a strong correspondence between our RH model predictions and the external HOBO-Logger network measurements with a 5-year average R² of 0.86 (range: 0.82–0.89) and a 5-year average RMSE of 5.45% (range: 5.14%–6.16%), MAPE of 5.59% (range: 5.19%–6.42%) and MPE of 2.98% (range: 1.82%–4.47%) for the daily average RH

exposure (Table 2). For the 7-day average RH exposure, as expected, the accuracy was even higher [R² = 0.87 (range: 0.84–0.92)] and the errors lower [RMSE = 4.49% (range: 4.06%–5.29%), MAPE = 4.59% (range: 4.08%–5.51%), MPE = 3.11% (range: 1.77%–4.81%)]. Density scatter-plots confirmed the good correlation (Figure S10).

3.3. Case study - Regensburg

In Fig. 2, we display the average spatial RH patterns for the region of Regensburg for the period 2000–2021. The city area showed up to 4.5% lower RH values than the surrounding rather rural county area. However, the variability of the daily values which will be also considered in subsequent epidemiological analysis is much larger than the 22-year average - e.g., up to 9% (randomly selected example day in Figure S11). Yet, the rural region was characterized by variations even in neighbouring tiles. The average RH exposure in Regensburg measured by the available DWD weather station of the region was far below the Q1 of the RH predictions of the RF model for the region (Fig. 3).

3.4. Spatiotemporal RH patterns

Table 3 shows descriptive statistics of measured and modelled RH across Germany for 2000–2021. Germany was characterized by high RH values with Q1 of both DWD stations' and model's RH distribution to be 71% and 71.91%, respectively. The observed and predicted 22-year average RH derived by the DWD stations and the RF model were 79.05% (SD = 12.38%) and 79.00% (SD = 10.46%), respectively.

Fig. 4 displays the 22-year averaged predicted RH output map of Germany (plot 1) which indicates spatial RH patterns, including urbanization, mountainous regions, rivers, forests and coastlines. Metropolitan areas such as those of Berlin, Hamburg and Munich and the extended and other dense urban cores (e.g., from Karlsruhe to Frankfurt) had much lower RH values compared to the neighbouring rural settings.

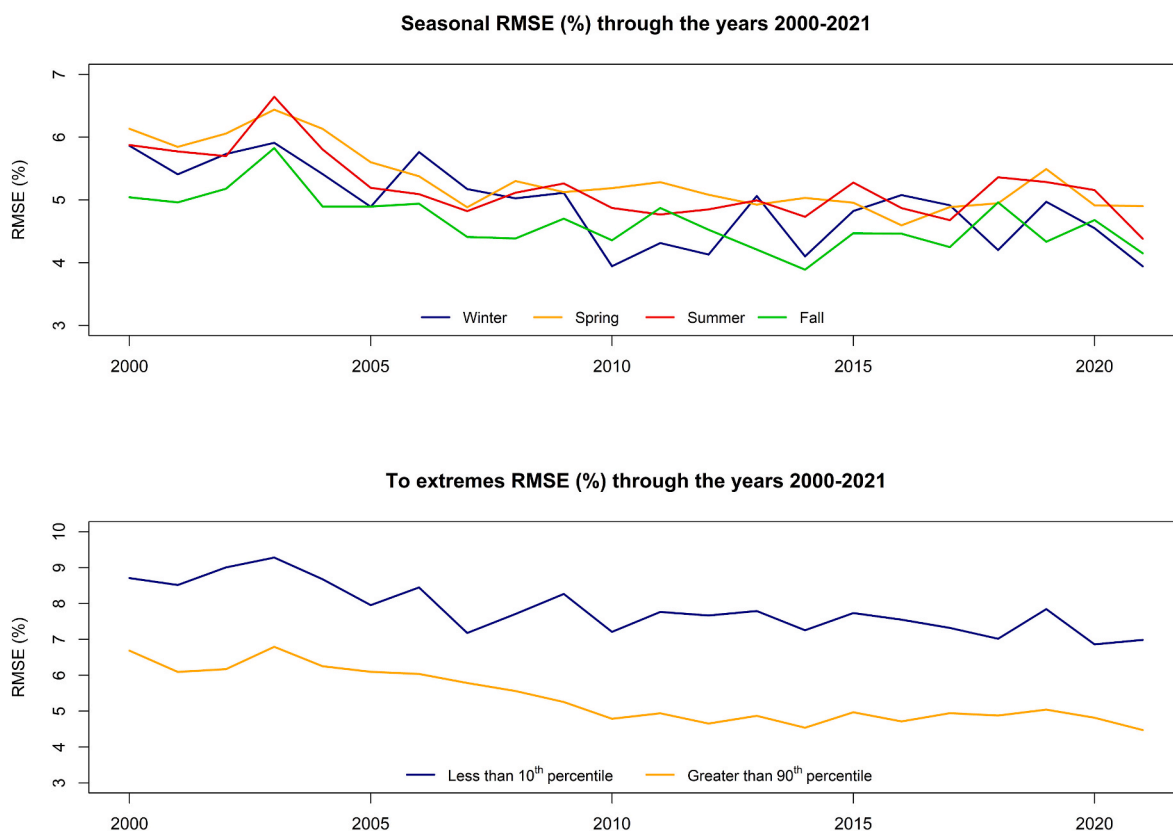


Fig. 1. Seasonal RMSE and RMSE to extremes for the model's RH predictions in Germany during 2000–2021.

Table 2

Accuracy results from the validation with external data using the HOBO-Logger daily mean RH observations and 7-day averages over the Augsburg region during 2015–2019.

Year					7-day average			
	R ²	RMSE (%)	MAPE (%)	MPE (%)	R ²	RMSE (%)	MAPE (%)	MPE (%)
2015	0.87	5.14	5.22	2.07	0.89	4.06	4.08	2.15
2016	0.82	5.23	5.19	2.48	0.84	4.14	4.10	2.58
2017	0.84	5.15	5.43	1.82	0.84	4.30	4.34	1.77
2018	0.89	5.58	5.67	4.07	0.92	4.68	4.93	4.25
2019	0.86	6.16	6.42	4.47	0.87	5.29	5.51	4.81
Overall	0.86	5.45	5.59	2.98	0.87	4.49	4.59	3.11

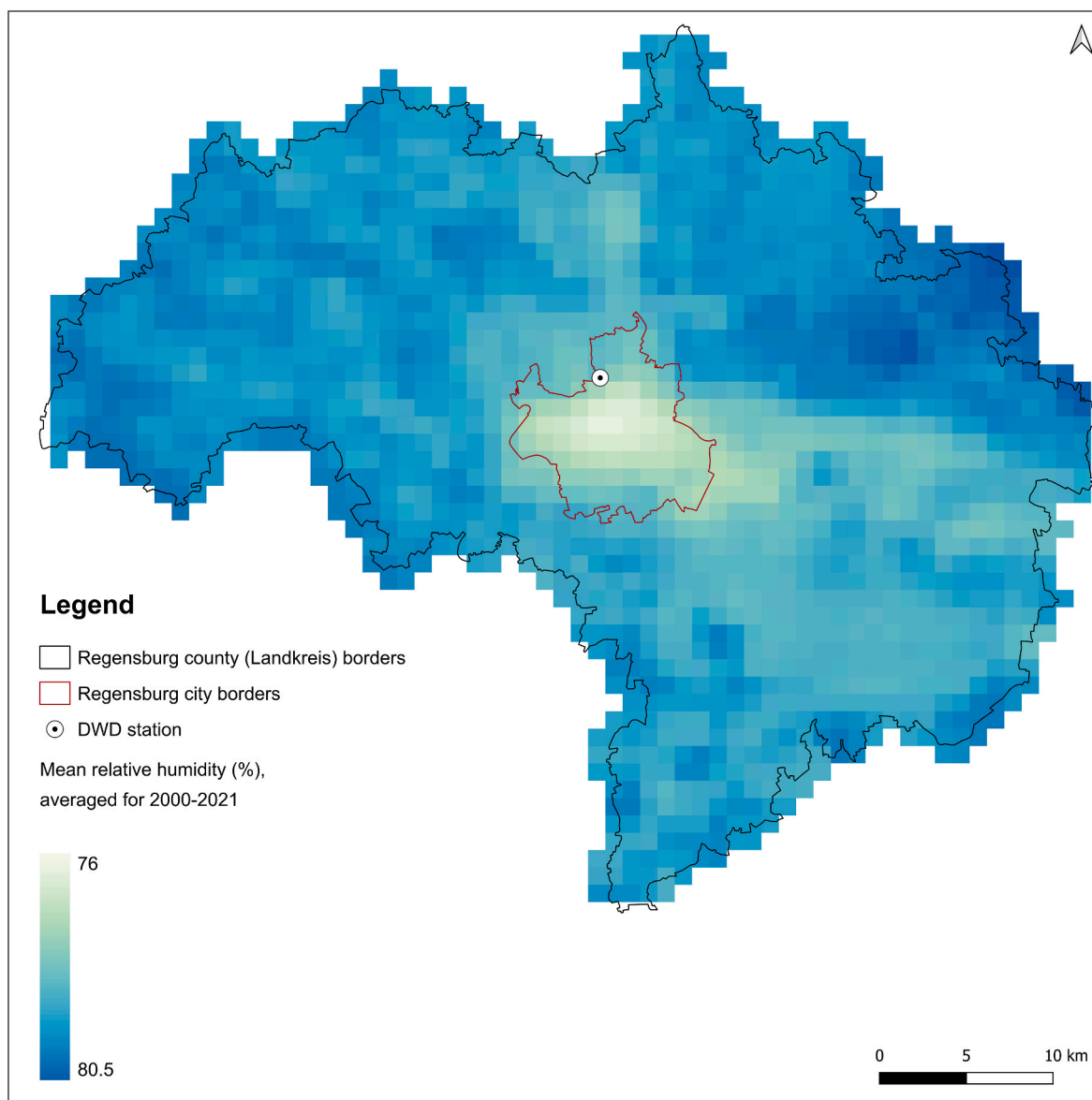


Fig. 2. Spatial pattern of the averaged predicted RH in Regensburg during 2000–2021.

In [Figure S12](#), we zoomed in the Augsburg region, which consists of the city center and two adjacent counties, to give an example of the high spatial difference between a city center and its neighbouring but less urbanized areas. Additionally, dense mountainous regions such as the Alps and Harz, coastlines as the North Sea coast and rivers as Elbe in a large part of it, had the highest RH values country-wide ([Fig. 4](#)). Furthermore, we included the spatial distribution map exhibiting the interannual change of RH ([Figure S13](#)) to ensure comprehensive

coverage. Significant interannual spatial variations were not discernible and the spatial variability which remained mostly constant through the years, aligned with the patterns observed and described in the averaged map ([Fig. 4](#), plot 1). Also, the temporal RH variability in Germany is presented for 2001–2021, by exhibiting the differences between the predicted RH yearly averages and the 21-year average ([Fig. 4](#), plot 2). We excluded the year 2000 because the model predictions are only available from late February of that year due to the missing T_{air} values

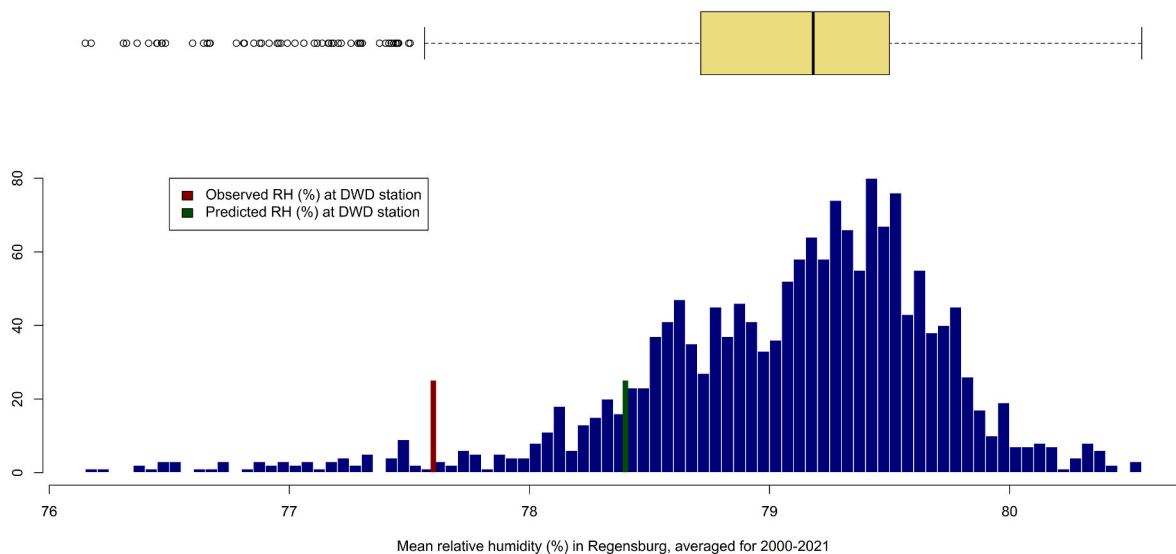


Fig. 3. Distribution of predicted RH in the Regensburg region for 2000–2021 (histogram in blue and corresponding boxplot above).

Table 3
Observed and predicted mean RH (%) over Germany during 2000–2021.

Source	Mean	SD	Min	Q1	Median	Q3	Max
DWD stations (n = 406)	79.05	12.38	3.00	71.00	81.00	88.75	100.00
RF model (n = 366,536 cells)	79.00	10.46	13.70	71.91	80.56	87.44	100.00

until then. There were some fluctuations over the years but without indication of an increasing or decreasing trend. The most humid years were 2001 (81.30%), 2014 (81.20%) and 2013 (80.94%) while the most arid were 2003 (75.31%), 2020 (75.53%) and 2018 (75.52%), which are known hot and dry years from the recent climatological record.

Mapping the 22-year average RH by season (Figure S14) identified winter and fall as the most humid seasons. High spatial RH variability was also observed within each season.

4. Discussion

In this paper, we introduced an approach for spatial and temporal modeling of RH using RF, a popular ML method for prediction tasks. The approach goes beyond the conventional interpolation of meteorological observations and uses several other data sources. We produced a reliable spatiotemporally-resolved RH dataset at 1×1 km spatial resolution across Germany for the period 2000–2021. The RF model achieved good performance with high predictive accuracy and low errors, validated with both internal data using cross-validation ($R^2 = 0.83$, $RMSE = 5.07\%$, $MAPE = 5.19\%$, $MPE = -0.53\%$), and with independent observational data ($0.86 \leq R^2 \leq 0.87$, $4.49\% \leq RMSE \leq 5.45\%$, $4.59\% \leq MAPE \leq 5.59\%$, $2.98\% \leq MPE \leq 3.11\%$). A case study for the city of Regensburg shows that our dataset is capable of capturing the full range of spatial variability of RH compared to the standard use of meteorological observations. These DWD station observations could not represent the high RH values of the peripheral areas in Regensburg, but also not the very low RH values of the city center. This clearly demonstrates the added value of our approach and how the use of additional data sources supplementing the conventional use of meteorological observations improved the RH prediction. It is especially important to capture the RH spatial variability for assessing differences in human's individual exposure in epidemiological studies. We also presented an analysis of the spatiotemporal RH patterns in Germany during 2000–2021.

The RH-health relevance has not been clarified adequately (Bind et al., 2014). RH adverse effects on human health could be partially explained by its interplay with the excessive heat stress and the body dehydration, as described in Davis et al. (2016). During extended and excessive heat events such as heatwaves, the human body struggles against heat-driven physiological responses and a key mechanism for its temperature regulation is evaporation. However, when RH is high and therefore air contains a lot of moisture, it is difficult for the sweat to be relieved and thus cooling becomes insufficient. Hence, the body core temperature increases while this increase is associated with a variety of detrimental health effects (Schneider et al., 2017). Additionally, low RH can affect the human skin sensitivity to mechanical stress (Engebretsen et al., 2016). RH is also associated with the transition of vector-borne diseases e.g., from mosquitos and ticks (Davis et al., 2016) as well as with the development and stability of microorganisms in aerosols, facilitating airborne diseases (Božič and Kanduč, 2021).

So far there is a literature gap in the investigation of the RH exposure's direct effects on human health and the accompanying underlying mechanisms. Further and more detailed research is needed. Hence, it is critically important for epidemiologists to have access to high-resolution and reliable RH datasets.

Most epidemiological studies retrieve the participants' exposure information, in this case RH, from available meteorological stations that do not capture the full variability of RH, especially at the city scale. In the Regensburg area, an epidemiological study would usually assign RH measurements from the station most closely located to each participant's residential address but fails to account for the spatial variability of RH that is actually occurring. Therefore, some measurement error would be introduced and the variability would be lost. Focusing on the city area, participants who live there would be assigned with a higher RH value than their actual one. At the same time, those living outside the city center would be assigned with RH values that are too low. This clearly demonstrates the urgent need for high spatiotemporal RH datasets for health studies for less biased exposure estimates.

Compared to other studies that use interpolation techniques such as TPS or kriging, our RF model is capable of reducing errors by half. Li et al. (2014) introduced a two-step procedure to map RH every 3 h at 1 km resolution over China during 1958–2010. They fitted a partial TPS interpolation to reanalysis data, location and elevation as predictors, to estimate a trend surface, and then a simple kriging was applied to the residuals for trend surface correction. They reported a RMSE of 11.06% whereas our model showed a RMSE of 5.07%. More recently, Li and Zha (2018) also used an RF model, combining station and satellite data, to

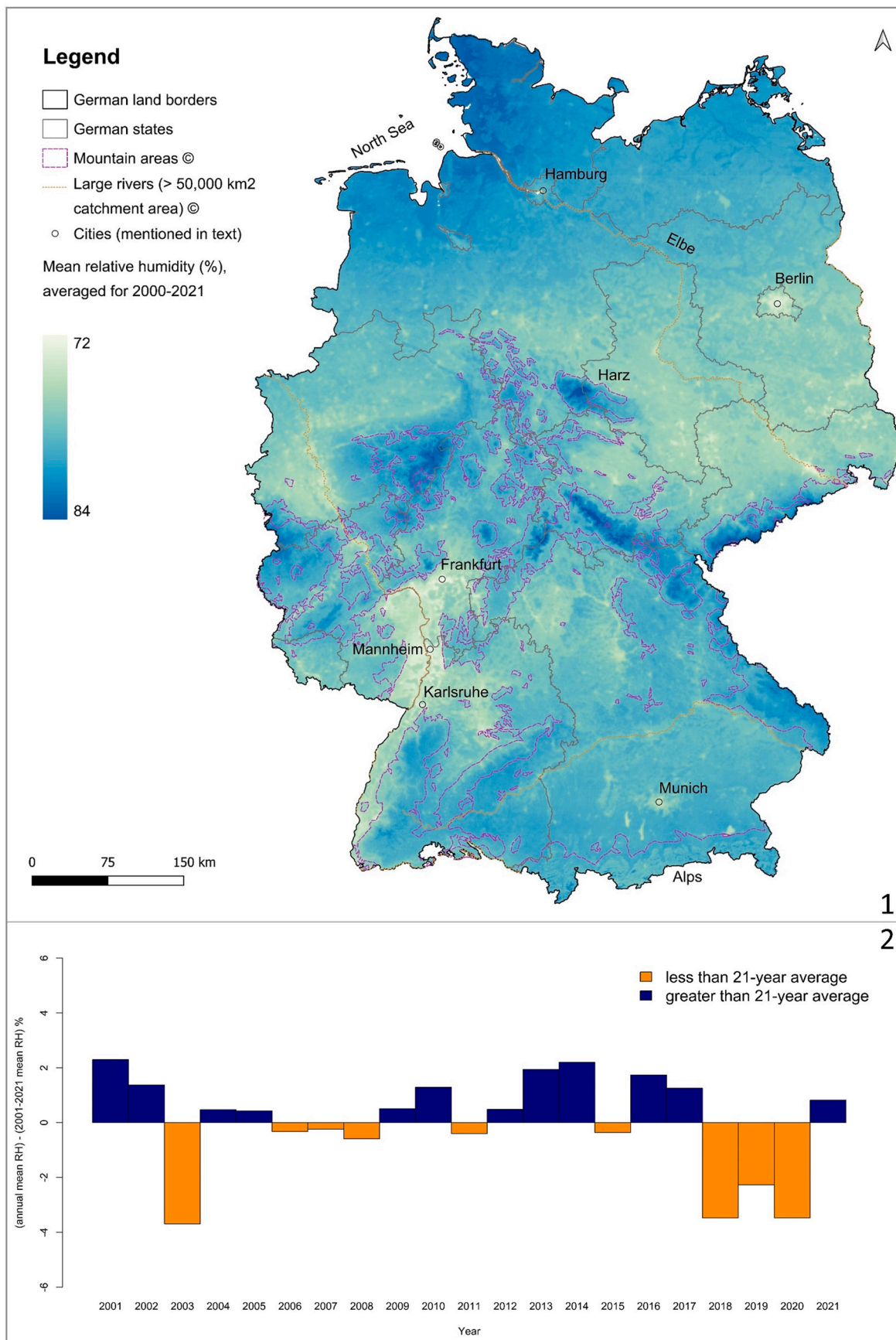


Fig. 4. Spatiotemporal RH patterns in Germany during 2000–2021. Plot 1: Spatial patterns of the predicted RH in Germany, averaged for 2000–2021. Plot 2: Difference between the predicted RH yearly averages and the predicted RH 21-year average (2001–2021), German-wide.

estimate RH during the hot summer of 2009 over China. Elevation and vegetation were found to be the most important predictors for RH. Comparing our model with their work, it seems that our additional inclusion of T_{air} , date information, precipitation and wind speed data in the modeling process, significantly improved the model's performance. Li and Zha (2018) reported a $R^2 = 0.70$ and $RMSE = 7.4\%$, whereas our model could improve the R^2 to 0.83 and lower the errors to $RMSE = 5.07\%$. In addition, our RF model allowed us to model RH for entire years and not only for one season. Lately, Kloub (2022) used an auto-encoder residual neural network, incorporating monitor, re-analysis and satellite data, to estimate various meteorological factors including RH for China in 2015. The accuracy of their RH model considerably improved from 0.77 to 0.86 upon including the monthly index, highlighting the importance of diverse temporal variables for RH models (we also incorporated the day of the year index). Kloub (2022) achieved a fairly good model performance of $R^2 = 0.86$, Mean Absolute Error (MAE) = 5.58% and $RMSE = 7.41\%$, whereas our model yielded an R^2 of 0.83, MAPE of 5.19%, and notably lower $RMSE$ of 5.07%. It is important to consider that Kloub (2022) predicted RH only for a single year, while our model covered a 22-year period. For instance, we also reported an R^2 of 0.88 for the year 2020. Significantly, the confidence for our model's performance benefited from the conducted external validation using a dense and independent monitoring network in Augsburg, a distinctive advantage not present in other studies.

This study was also subject to limitations. Satellite-derived predictors like NDVI and the true color band composite may encounter resampling errors, whereas precipitation and wind speed data involve spatial interpolation errors. Nevertheless, these datasets maintain a high standard of quality and are extensively employed in existing literature. Furthermore, the external validation set was not representative of the whole Germany. The HOBO-Logger monitoring network was placed in Augsburg, South Germany. However, we used the Augsburg's greater region which consists of a dense city center and two adjacent rural settings and therefore the validation area was characterized by high spatial RH variability. Additionally, we were already able to measure the model's predictive accuracy country-wide due to our monitor-based split in the applied CV scheme (2.3.1 Model performance). The 1×1 km spatial resolution could be too coarse for some studies, especially for local and small-scale analyses. However, as we demonstrated in the case study of the city of Regensburg, the RF model of 1×1 km provided a valid representation of the RH spatiotemporal variation at the city scale. For future analyses, we could consider downscaling methods especially for cities (Hough et al., 2020).

For future applications, there is a potential to enhance the predictive capabilities of a RH model by augmenting its array of predictors to include re-analysis data or wind direction for instance, which were absent in our study due to the lack of appropriate data for Germany. This could be advantageous if these variables achieve higher spatial resolutions in upcoming developments. However, we do not expect considerable improvements as humidity is predominantly governed by temperature and by the vertical/horizontal mixing of wind which have already been integrated into our model. Additionally, other ML methodologies, such as eXtreme Gradient Boosting (XGBoost) or Neural Networks, could be explored if they align more effectively with distinct spatial contexts and the datasets at hand. These methodologies have been examined in the literature for various exposure scenarios (Ma et al., 2020; Tian et al., 2022).

5. Conclusion

We showed how observation, remote sensing and modelled data can be combined under a RF modeling scheme to reliably estimate RH in high temporal and spatial resolution across a country. Our product contributes substantially to reduce exposure errors for subsequent epidemiological studies, by better representing the spatiotemporal RH variability. For cohort studies using geocoded participant address

information for exposure assessment, the investigation of changes over time and space is considerably improved by such a spatiotemporal model compared to relying solely on data from measurement stations. We provide a reliable RH dataset for Germany and a well-founded and generalizable approach for RH prediction for other study domains and countries.

Author contributions

Nikolaos Nikolaou: Conceptualization, Data curation, Methodology, Analysis, Visualization, Writing - original draft, Writing - review & editing. **Laurens M. Bouwer:** Conceptualization, Data curation, Methodology, Writing - review & editing. **Marco Dallavalle:** Data curation, Writing - review & editing. **Mahyar Valizadeh:** Methodology, Writing - review & editing. **Massimo Stafoggia:** Methodology, Writing - review & editing. **Annette Peters:** Conceptualization, Writing - review & editing, Supervision. **Kathrin Wolf:** Conceptualization, Data curation, Methodology, Writing - review & editing, Supervision. **Alexandra Schneider:** Conceptualization, Methodology, Writing - review & editing, Supervision.

Declaration of competing interest

The authors declare that they have no known competing financial interests or personal relationships that could have appeared to influence the work reported in this paper.

Data availability

Data will be made available on request.

Acknowledgements

This work was supported by the Helmholtz Climate Initiative (HI-CAM) project, which is funded by the Helmholtz Association's Initiative and Networking Fund, the Helmholtz Information & Data Science Academy (HIDA), financially supported by the HIDA Trainee Network program, and by the Digital Earth project, supported by the Helmholtz Association's Initiative and Networking Fund (funding code ZT-0025). The authors are responsible for the content of this publication.

Appendix A. Supplementary data

Supplementary data to this article can be found online at <https://doi.org/10.1016/j.envres.2023.117173>.

References

- Analitis, A., Katsouyanni, K., Biggeri, A., Baccini, M., Forsberg, B., Bisanti, L., Kirchmayer, U., Ballester, F., Cadum, E., Goodman, P.G., Hojs, A., Sunyer, J., Tiittanen, P., Michelozzi, P., 2008. Effects of cold weather on mortality: results from 15 European cities within the PHEWE project. *Am. J. Epidemiol.* 168 (12), 1397–1408. <https://doi.org/10.1093/aje/kwn266>.
- Armstrong, B., 2006. Models for the relationship between ambient temperature and daily mortality. *Epidemiology* 624–631. <http://www.jstor.org/stable/20486290>.
- Božić, A., Kanduć, M., 2021. Relative humidity in droplet and airborne transmission of disease. *J. Biol. Phys.* 47 (1), 1–29. <https://doi.org/10.1007/s10867-020-09562-5>.
- Beck, C., Straub, A., Breitner, S., Cyrus, J., Philipp, A., Rathmann, J., Schneider, A., Wolf, K., Jacobeit, J., 2018a. Air temperature characteristics of local climate zones in the Augsburg urban area (Bavaria, southern Germany) under varying synoptic conditions. *Urban Clim.* 25, 152–166. <https://doi.org/10.1016/j.uclim.2018.04.007>.
- Beck, H.E., Zimmermann, N.E., McVicar, T.R., Vergopolan, N., Berg, A., Wood, E.F., 2018b. Present and future Köppen-Geiger climate classification maps at 1-km resolution. *Sci. Data* 5, 1–12. <https://doi.org/10.1038/sdata.2018.214>.
- Bind, M.A., Zanobetti, A., Gasparrini, A., Peters, A., Coull, B., Baccarelli, A., Tarantini, L., Koutrakis, P., Vokonas, P., Schwartz, J., 2014. Effects of temperature and relative humidity on DNA methylation. *Epidemiology* 25 (4), 561. <https://doi.org/10.1097/EDE.0000000000000120>.
- Breiman, L., 2001. Random forests. *Mach. Learn.* 45, 5–32. <https://doi.org/10.1023/A:1010933404324>.

- Davis, R.E., McGregor, G.R., Enfield, K.B., 2016. Humidity: a review and primer on atmospheric moisture and human health. *Environ. Res.* 144, 106–116. <https://doi.org/10.1016/j.envres.2015.10.014>.
- Didan, K., 2015. MOD13A3 MODIS/Terra Vegetation Indices Monthly L3 Global 1km SIN Grid V006 [Data Set]. NASA EOSDIS Land Processes DAAC. <https://doi.org/10.5067/MODIS/MOD13A3.006>, 2022-03-21 from.
- DWD, 2022a. DWD Climate Data Center (CDC): Historical daily station observations (temperature, pressure, precipitation, sunshine duration, etc.) for Germany version v21.3, 2021.
- DWD, 2022b. DWD Climate Data Center (CDC): REGNIE Grids of Daily Precipitation. (Accessed 21 March 2022).
- DWD, 2023. DWD Climate Data Center (CDC): Raster Data Set of Daily Sums of Precipitation in Mm for Germany - HYRAS-DE-PRE. Version v5.0.
- Engelbrechtsen, K.A., Johansen, J.D., Kezic, S., Linneberg, A., Thyssen, J.P., 2016. The effect of environmental humidity and temperature on skin barrier function and dermatitis. *J. Eur. Acad. Dermatol. Venereol.* 30 (2), 223–249. <https://doi.org/10.1111/jdv.13301>.
- Forootan, E., 2019. Analysis of trends of hydrologic and climatic variables. *Soil Water Res.* 14 (3), 163–171. <https://doi.org/10.17221/154/2018-SWR>.
- German National Cohort (GNC) Consortium, 2014. The German National Cohort: aims, study design and organization. *Eur. J. Epidemiol.* 29 (5), 371–382. <https://doi.org/10.1007/s10654-014-9890-7>.
- Gesch, D.B., Verdin, K.L., Greenlee, S.K., 1999. New land surface digital elevation model covers the Earth. *EOS* 80 (6), 69–70. <https://doi.org/10.1029/99EO00050>.
- Hough, I., Just, A.C., Zhou, B., Dorman, M., Lepeule, J., Kloog, I., 2020. A multi-resolution air temperature model for France from MODIS and Landsat thermal data. *Environ. Res.* 183, 109244. <https://doi.org/10.1016/j.envres.2020.109244>.
- Jin, Z., Ma, Y., Chu, L., Liu, Y., Dubrow, R., Chen, K., 2022. Predicting spatiotemporally-resolved mean air temperature over Sweden from satellite data using an ensemble model. *Environ. Res.* 204, 111960. <https://doi.org/10.1016/j.envres.2021.111960>.
- Kloub, R.S.A.A., 2022. An optimal method for high-resolution population geo-spatial data. *Comput. Mater. Contin.* 73 (2) <https://doi.org/10.32604/cmc.2022.027847>.
- Li, T., Zheng, X., Dai, Y., Yang, C., Chen, Z., Zhang, S., Wu, G., Wang, Z., Huang, C., Shen, Y., Liao, R., 2014. Mapping near-surface air temperature, pressure, relative humidity and wind speed over Mainland China with high spatiotemporal resolution. *Adv. Atmos. Sci.* 31 (5), 1127–1135. <https://doi.org/10.1007/s00376-014-3190-8>.
- Li, L., Zha, Y., 2018. Mapping relative humidity, average and extreme temperature in hot summer over China. *Sci. Total Environ.* 615, 875–881. <https://doi.org/10.1016/j.scitotenv.2017.10.022>.
- Luo, C., Ma, Y., Liu, Y., Lv, Q., Yin, F., 2020. The burden of childhood hand-foot-mouth disease morbidity attributable to relative humidity: a multicity study in the Sichuan Basin. *China. Sci. Rep.* 10 (1), 1–10. <https://doi.org/10.1038/s41598-020-76421-7>.
- Ma, J., Yu, Z., Qu, Y., Xu, J., Cao, Y., 2020. Application of the XGBoost machine learning method in PM2.5 prediction: a case study of Shanghai. *Aerosol Air Qual. Res.* 20 (1), 128–138. <https://doi.org/10.4209/aaqr.2019.08.0408>.
- Mistry, M.N., Schneider, R., Masselot, P., Royé, D., Armstrong, B., Kysely, J., Orru, H., Sera, F., Tong, S., Lavigne, É., Urban, A., Madureira, J., García-León, D., Ibarreta, D., Ciscar, J.-C., Feyen, L., DeSchrijver, E., Coelho, M.S.Z.S., Pascal, M., Tobias, A., , Multi-Country Multi-City (MCC) Collaborative Research Network, Guo, Y., Vicedo-Cabrera, A.M., Gasparri, A., 2022. Comparison of weather station and climate reanalysis data for modelling temperature-related mortality. *Sci. Rep.* 12 (1), 1–14. <https://doi.org/10.1038/s41598-022-09049-4>.
- Nikolaou, N., Dallavalle, M., Stafoggia, M., Bouwer, L.M., Peters, A., Chen, K., Wolf, K., Schneider, A., 2022. High-resolution spatiotemporal modeling of daily near-surface air temperature in Germany over the period 2000–2020. *Environ. Res.* 115062. <https://doi.org/10.1016/j.envres.2022.115062>.
- Ou, C.Q., Yang, J., Ou, Q.Q., Liu, H.Z., Lin, G.Z., Chen, P.Y., Qian, J., Guo, Y.M., 2014. The impact of relative humidity and atmospheric pressure on mortality in Guangzhou, China. *BES (Biomed. Environ. Sci.)* 27 (12), 917–925. <https://doi.org/10.3967/bes2014.132>.
- R Core Team, 2022. R: A Language and Environment for Statistical Computing. R Foundation for Statistical Computing, Vienna, Austria. Retrieved from. <https://www.R-project.org/>.
- Rauthe, M., Steiner, H., Riediger, U., Mazurkiewicz, A., Gratzki, A., 2013. A Central European precipitation climatology - Part I: generation and validation of a high-resolution gridded daily data set (HYRAS). *Meteorol. Z.* 22 (3), 235–256. <https://doi.org/10.1127/0941-2948/2013/0436>.
- Rosenfeld, A., Dorman, M., Schwartz, J., Novack, V., Just, A.C., Kloog, I., 2017. Estimating daily minimum, maximum, and mean near surface air temperature using hybrid satellite models across Israel. *Environ. Res.* 159, 297–312. <https://doi.org/10.1016/j.envres.2017.08.017>.
- Schneider, A., Rückerl, R., Breitner, S., Wolf, K., Peters, A., 2017. Thermal control, weather, and aging. *Curr. Environ. Health Rep.* 4 (1), 21–29. <https://doi.org/10.1007/s40572-017-0129-0>.
- Sherwood, S.C., Ingram, W., Tsushima, Y., Satoh, M., Roberts, M., Vidale, P.L., O’Gorman, P.A., 2010. Relative humidity changes in a warmer climate. *J. Geophys. Res. Atmos.* 115 (D9) <https://doi.org/10.1029/2009JD012585>.
- Silibello, C., Carlino, G., Stafoggia, M., Gariazzo, C., Finardi, S., Pepe, N., Radice, P., Forastiere, F., Viegi, G., 2021. Spatial-temporal prediction of ambient nitrogen dioxide and ozone levels over Italy using a Random Forest model for population exposure assessment. *Air Qual. Atmos. Health* 14 (6), 817–829. <https://doi.org/10.1007/s11869-021-00981-4>.
- Stafoggia, M., Bellander, T., Bucci, S., Davoli, M., De Hoogh, K., De’Donato, F., Gariazzo, C., Lyapustin, A., Michelozzi, P., Renzi, M., Scortichini, M., Shtein, A., Viegi, G., Kloog, I., Schwartz, J., 2019. Estimation of daily PM10 and PM2.5 concentrations in Italy, 2013–2015, using a spatiotemporal land-use random-forest model. *Env. Int.* 124, 170–179. <https://doi.org/10.1016/j.envint.2019.01.016>.
- Tian, J., Liu, Y., Zheng, W., Yin, L., 2022. Smog prediction based on the deep belief-PP neural network model (DBN-PP). *Urban Clim.* 41, 101078. <https://doi.org/10.1016/j.urbclim.2021.101078>.
- Vermote, E.W.R., 2015. MOD09GA MODIS/Terra Surface Reflectance Daily L2G Global 1km and 500m SIN Grid V006 [Data Set]. NASA EOSDIS Land Processes DAAC. <https://doi.org/10.5067/MODIS/MOD09GA.006>, 2022-03-21 from.
- Wright, M.N., Ziegler, A., 2017. Ranger: a fast implementation of random forests for high dimensional data in C++ and R. *J. Stat. Software* 77 (1), 1–17. <https://doi.org/10.18637/jss.v077.i01>.
- Wu, W., Tang, X.-P., Yang, C., Guo, N.-J., Liu, H.-B., 2013. Spatial estimation of monthly mean daily sunshine hours and solar radiation across mainland China. *RES* 57, 546–553. <https://doi.org/10.1016/j.renene.2013.02.027>.
- Wu, W., Xu, A.-D., Liu, H.-B., 2015. High-resolution spatial databases of monthly climate variables (1961–2010) over a complex terrain region in southwestern China. *Theor. Appl. Climatol.* 119 (1), 353–362. <https://doi.org/10.1007/s00704-014-1123-1>.
- Xiong, Y., Meng, Q.-S., Jie, G., Tang, X.-F., Zhang, H.-F., 2017. Effects of relative humidity on animal health and welfare. *J. Integr. Agric.* 16 (8), 1653–1658. [https://doi.org/10.1016/S2095-3119\(16\)61532-0](https://doi.org/10.1016/S2095-3119(16)61532-0).
- Yang, Y., You, E., Wu, J., Zhang, W., Jin, J., Zhou, M., Jiang, C., Huang, F., 2018. Effects of relative humidity on childhood hand, foot, and mouth disease reinfection in Hefei, China. *Sci. Total Environ.* 630, 820–826. <https://doi.org/10.1016/j.scitotenv.2018.02.262>.
- Yao, R., Wang, L., Huang, X., Cao, Q., Peng, Y., 2022. A method for improving the estimation of extreme air temperature by satellite. *Sci. Total Environ.* 155887. <https://doi.org/10.1016/j.scitotenv.2022.155887>.
- Zeger, S.L., Thomas, D., Dominici, F., Samet, J.M., Schwartz, J., Dockery, D., Cohen, A., 2000. Exposure measurement error in time-series studies of air pollution: concepts and consequences. *EHP* 108 (5), 419–426. <https://doi.org/10.1289/ehp.00108419>.
- Zeng, J., Zhang, X., Yang, J., Bao, J., Xiang, H., Dear, K., Liu, Q., Lin, S., Lawrence, W.R., Lin, A., Huang, C., 2017. Humidity may modify the relationship between temperature and cardiovascular mortality in Zhejiang Province, China. *IJERPH* 14 (11), 1383. <https://doi.org/10.3390/ijerph14111383>.
- Zhang, P., Zhang, J., Chen, M., 2015. Available at: SSRN 2598810 Economic impacts of climate change on Chinese agriculture: the importance of relative humidity and other climatic variables. <https://doi.org/10.2139/ssrn.2598810>.

4.1 Supplementary material for Paper II

Improved daily estimates of relative humidity at high resolution across Germany: a Random Forest approach

Nikolaos Nikolaou^{1,2*}, Laurens M. Bouwer³, Marco Dallavalle^{1,2}, Mahyar Valizadeh¹, Massimo Stafoggia⁴, Annette Peters^{1,2}, Kathrin Wolf^{1§}, Alexandra Schneider^{1§}

¹Institute of Epidemiology, Helmholtz Zentrum München, German Research Center for Environmental Health, 85764 Neuherberg, Germany

²Institute for Medical Information Processing, Biometry, and Epidemiology, Pettenkofer School of Public Health, LMU Munich, 81377 Munich, Germany

³Climate Service Center Germany (GERICS), Helmholtz-Zentrum Hereon, 20095 Hamburg, Germany

⁴Department of Epidemiology, Lazio Regional Health Service – ASL Roma 1, 00147 Rome, Italy

*Corresponding author

Address: Ingolstädter Landstr. 1, D-85764 Neuherberg, Germany

Phone: +49 176 377 488 68

E-Mail: nikolaos.nikolaou@helmholtz-munich.de

§Shared last authorship

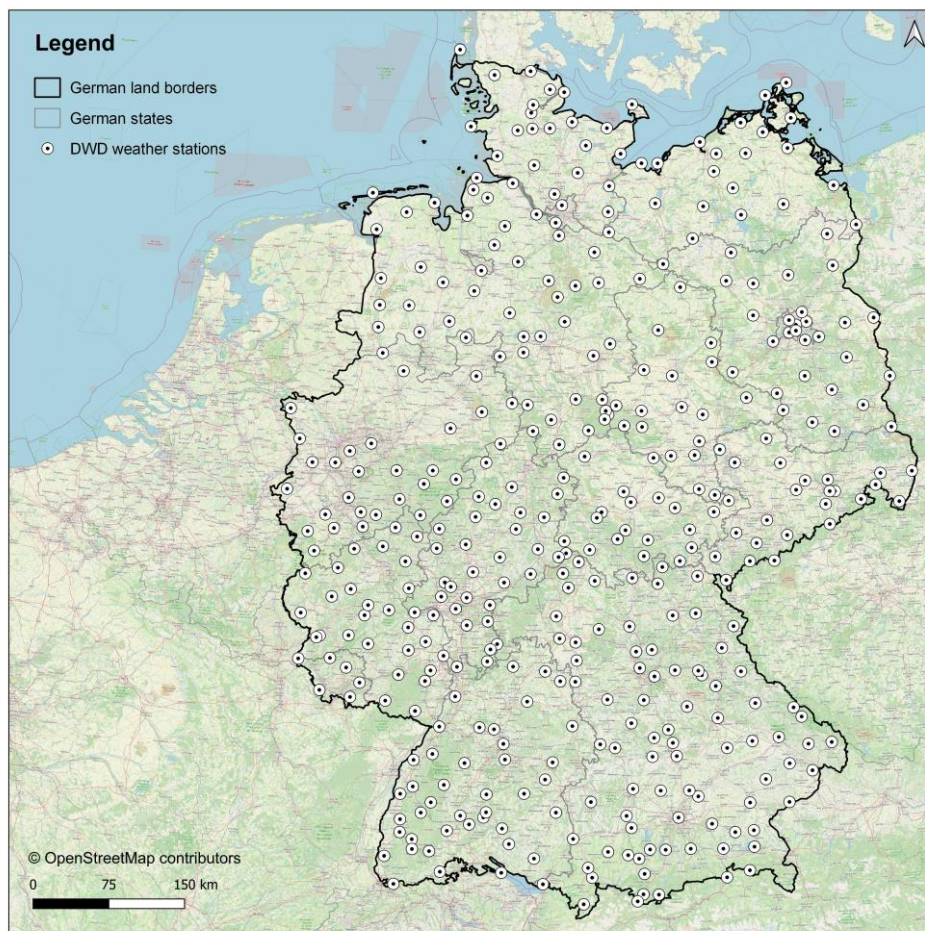


Figure S1. Spatial distribution of the 406 DWD weather stations we used for our analysis in Germany.

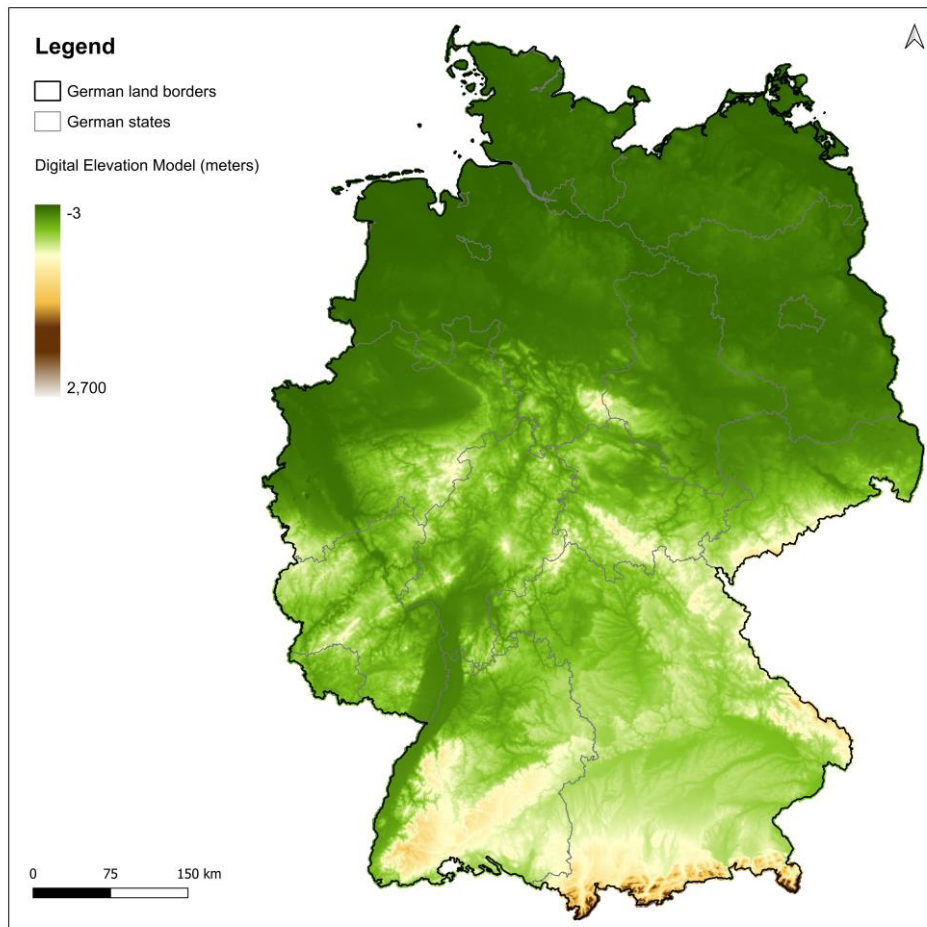


Figure S2. Elevation map of Germany in 1 × 1 km spatial resolution.

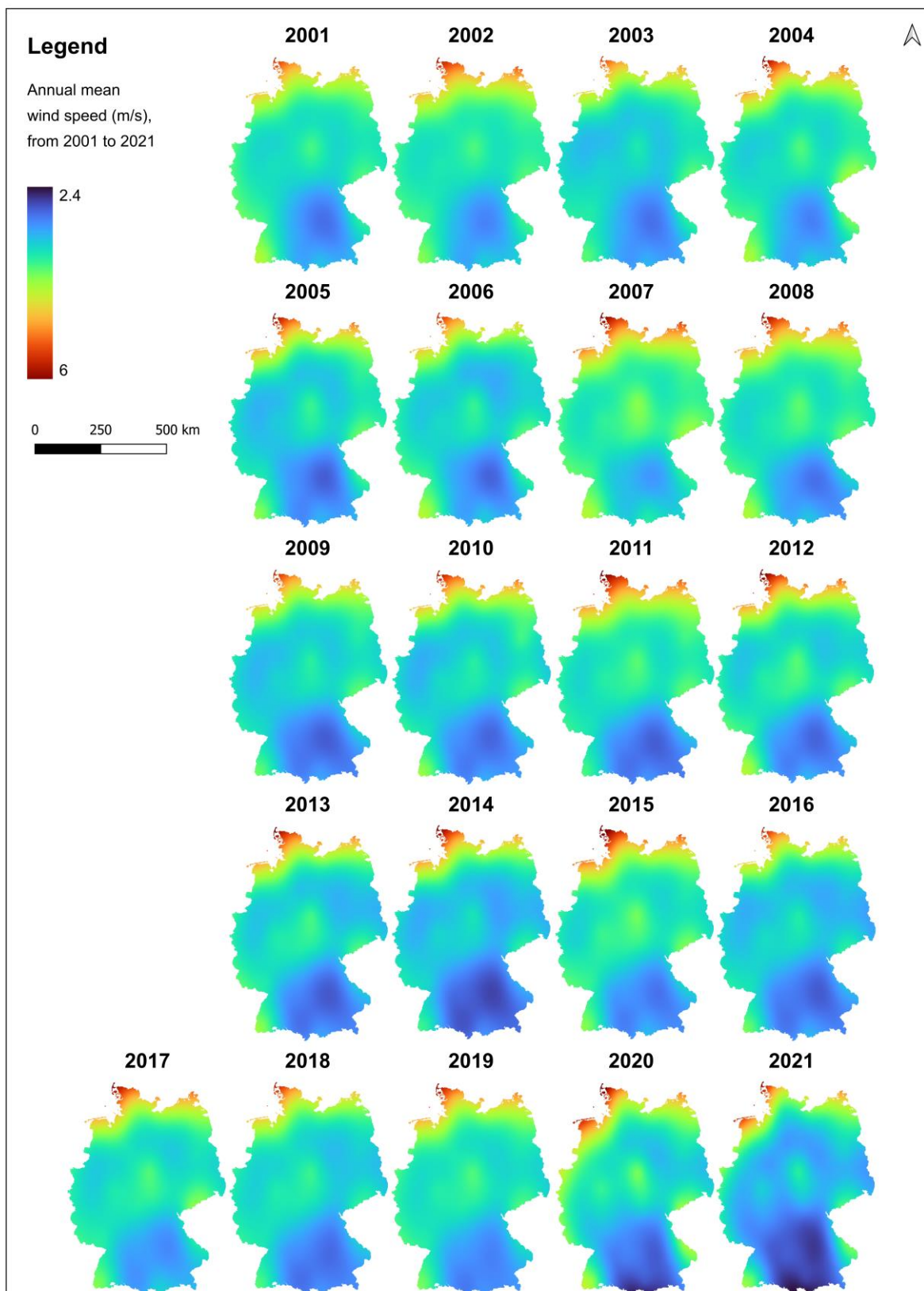


Figure S3. Spatiotemporal distribution map of wind speed interpolated data in Germany during 2001-2021.

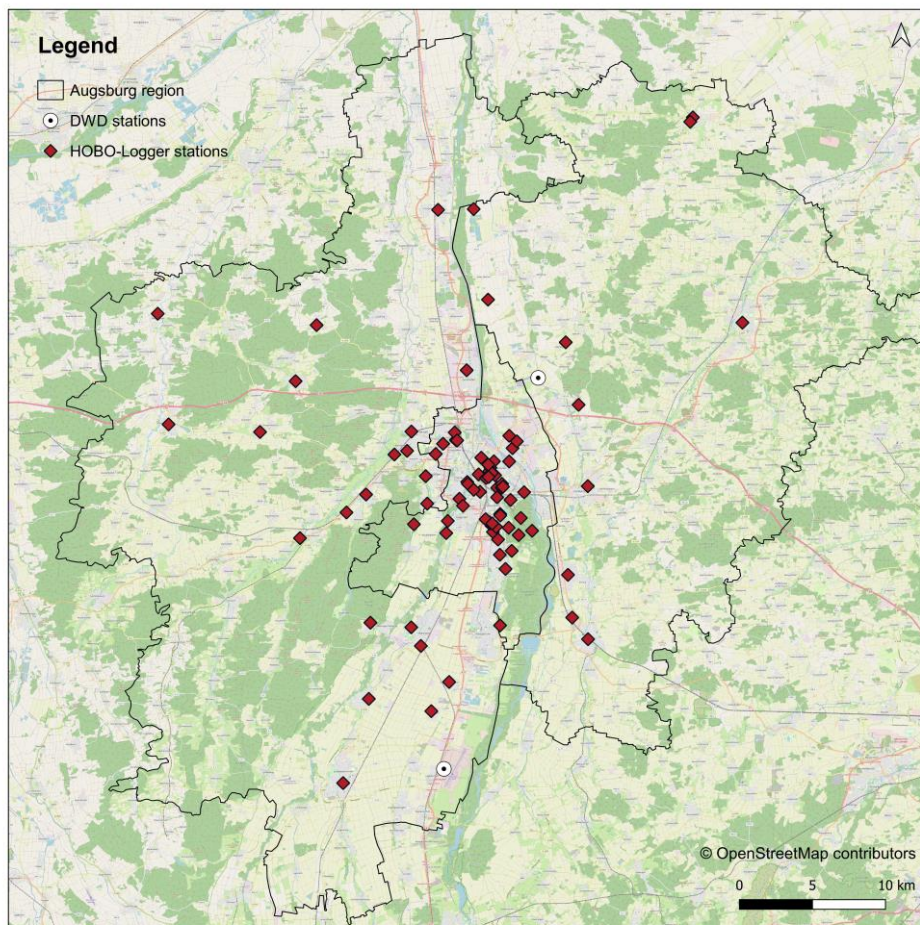


Figure S4. Map of the Augsburg region (Augsburg city and 2 adjacent counties), the sites of the HOBO-Logger monitoring network during the period 2015-2019 and the 2 available DWD weather stations.

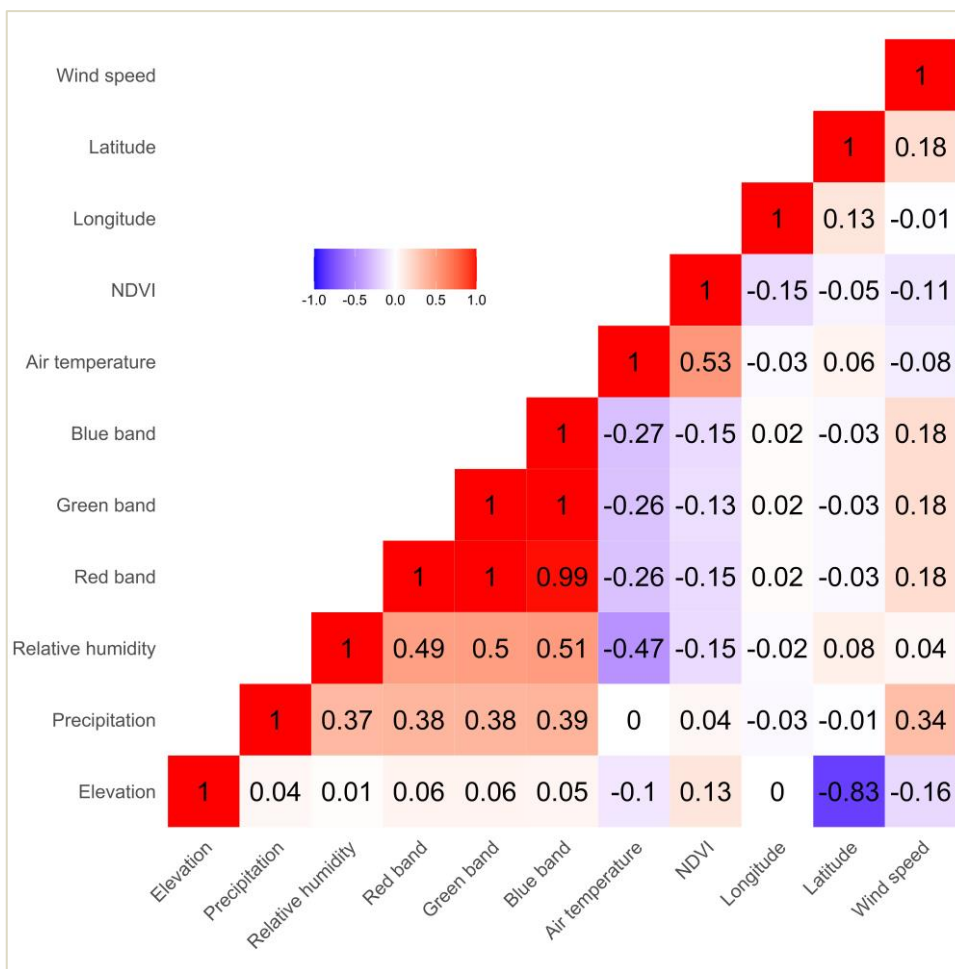


Figure S5. Correlation matrix for the RF model’s variables (spearman correlation coefficient), randomly selected year 2004

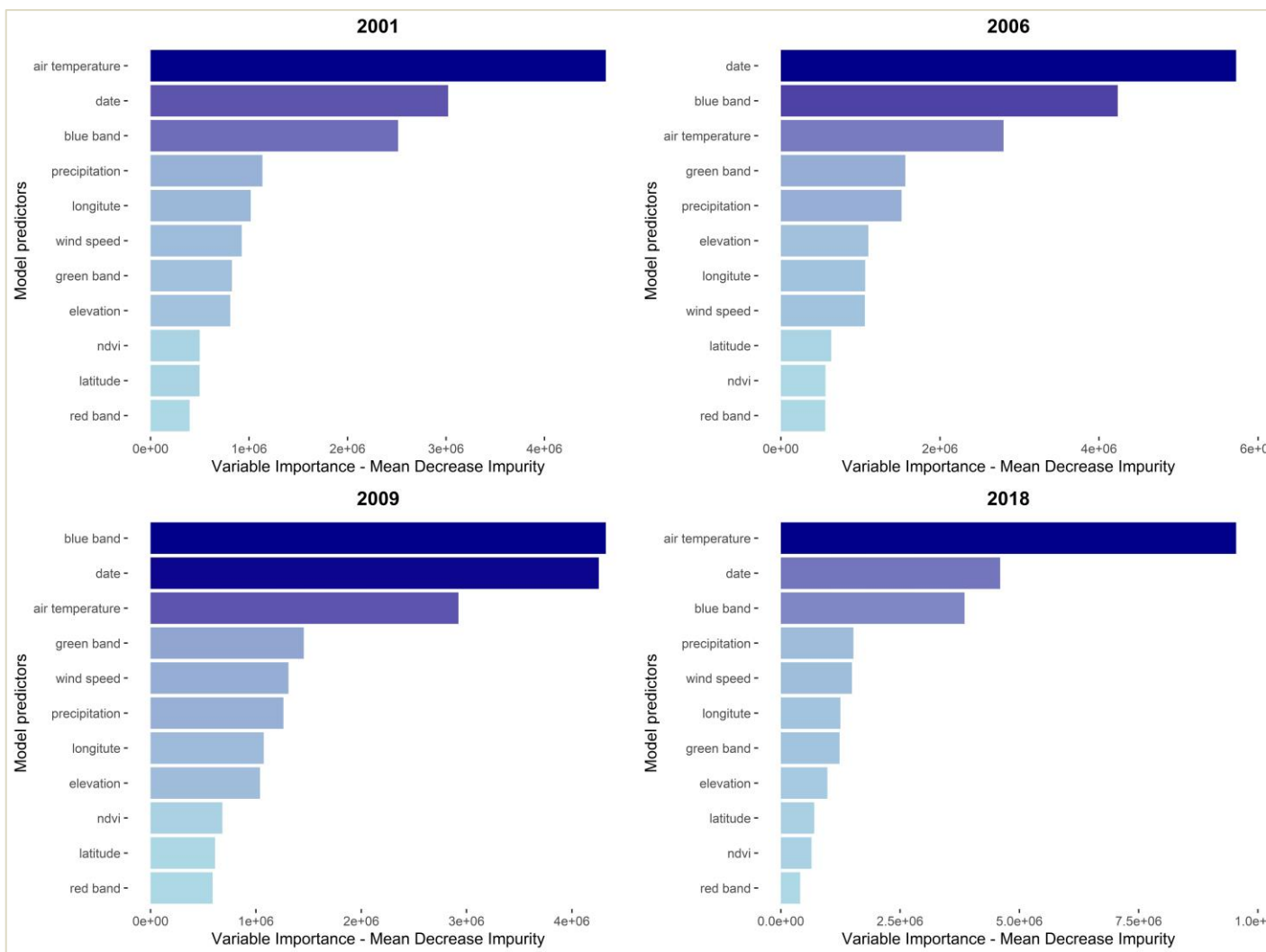


Figure S6. Variable importance of the RF model for the randomly selected years 2001, 2006, 2009 and 2018.

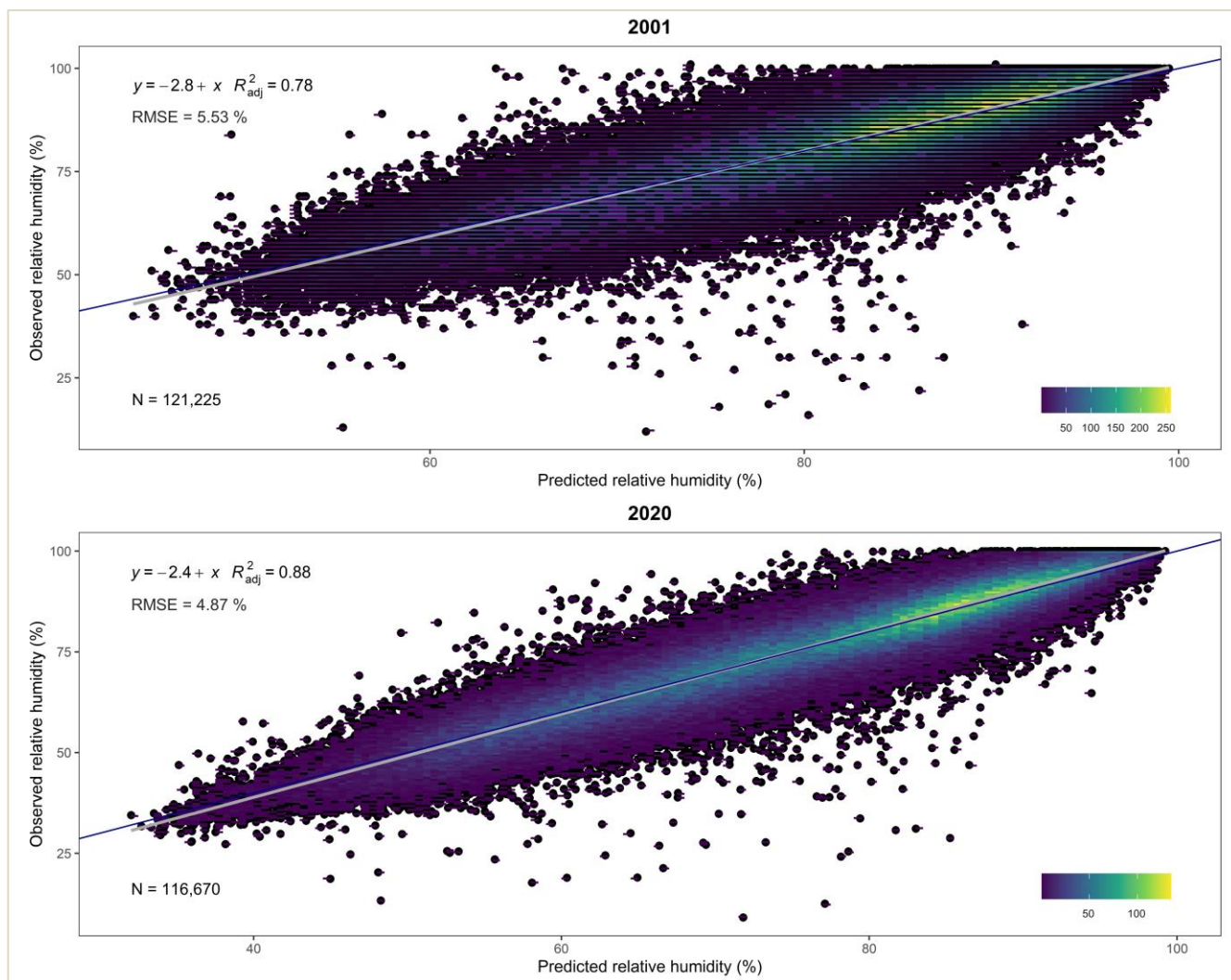


Figure S7. Density scatterplots between the model's RH predictions and the DWD RH observations for the example years with the lowest and highest fit, i.e., 2001 and 2020, respectively. Dark grey line = fitting line. Dark blue line = 1:1 diagonal line.

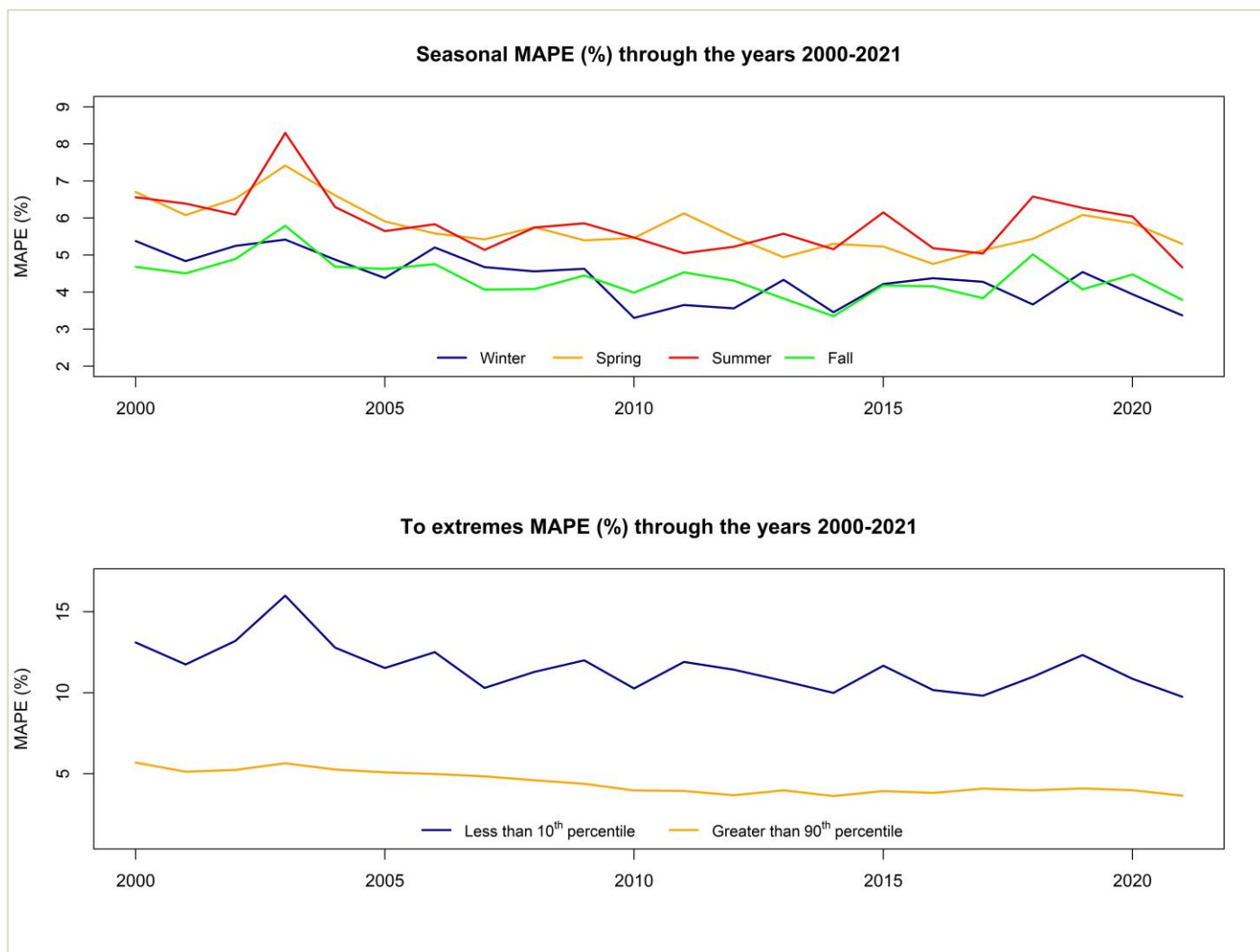


Figure S8. Seasonal MAPE and MAPE to extremes for the model's RH predictions in Germany during 2000-2021.

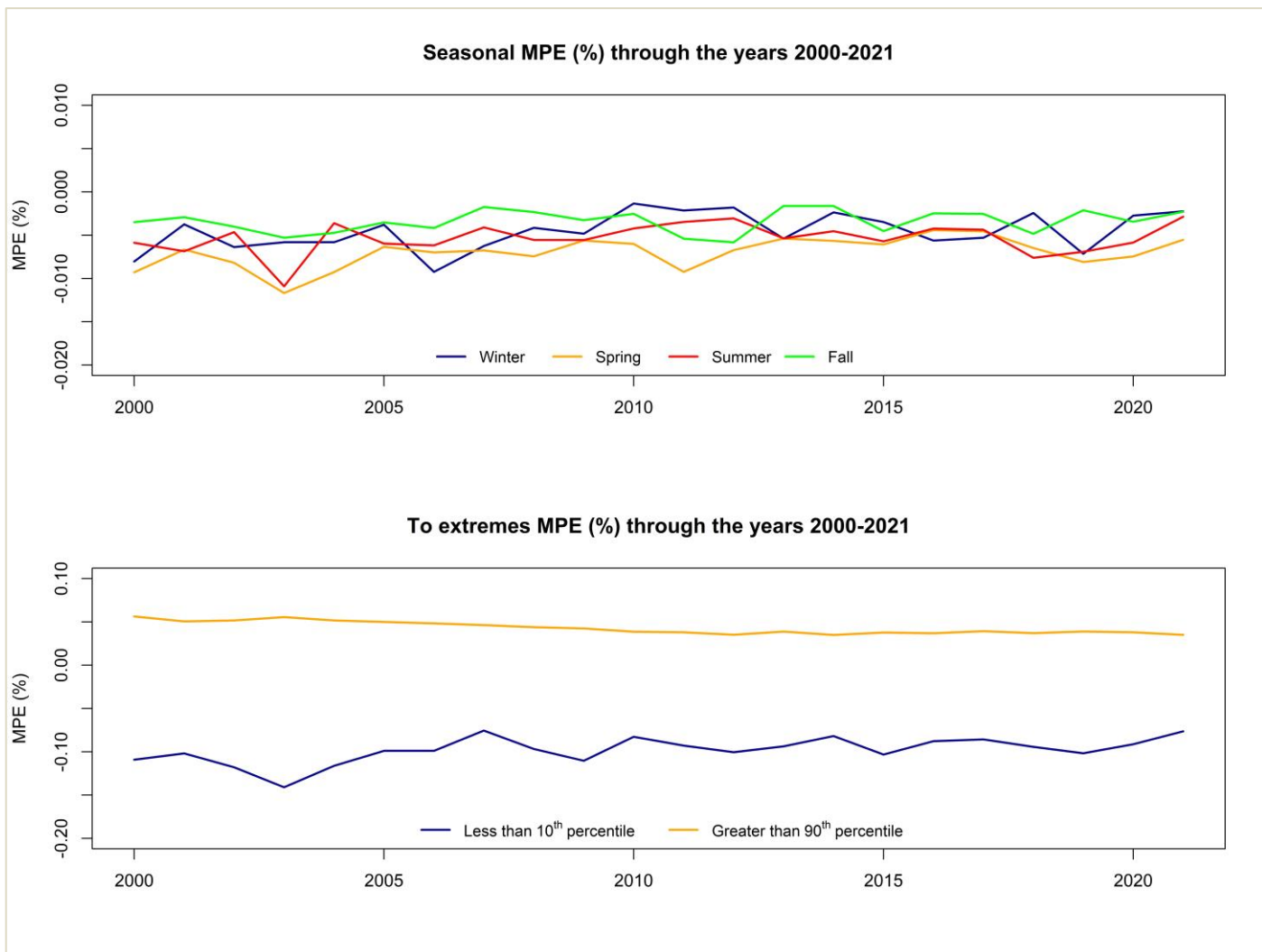


Figure S9. Seasonal MPE and MPE to extremes for the model's RH predictions in Germany during 2000-2021.

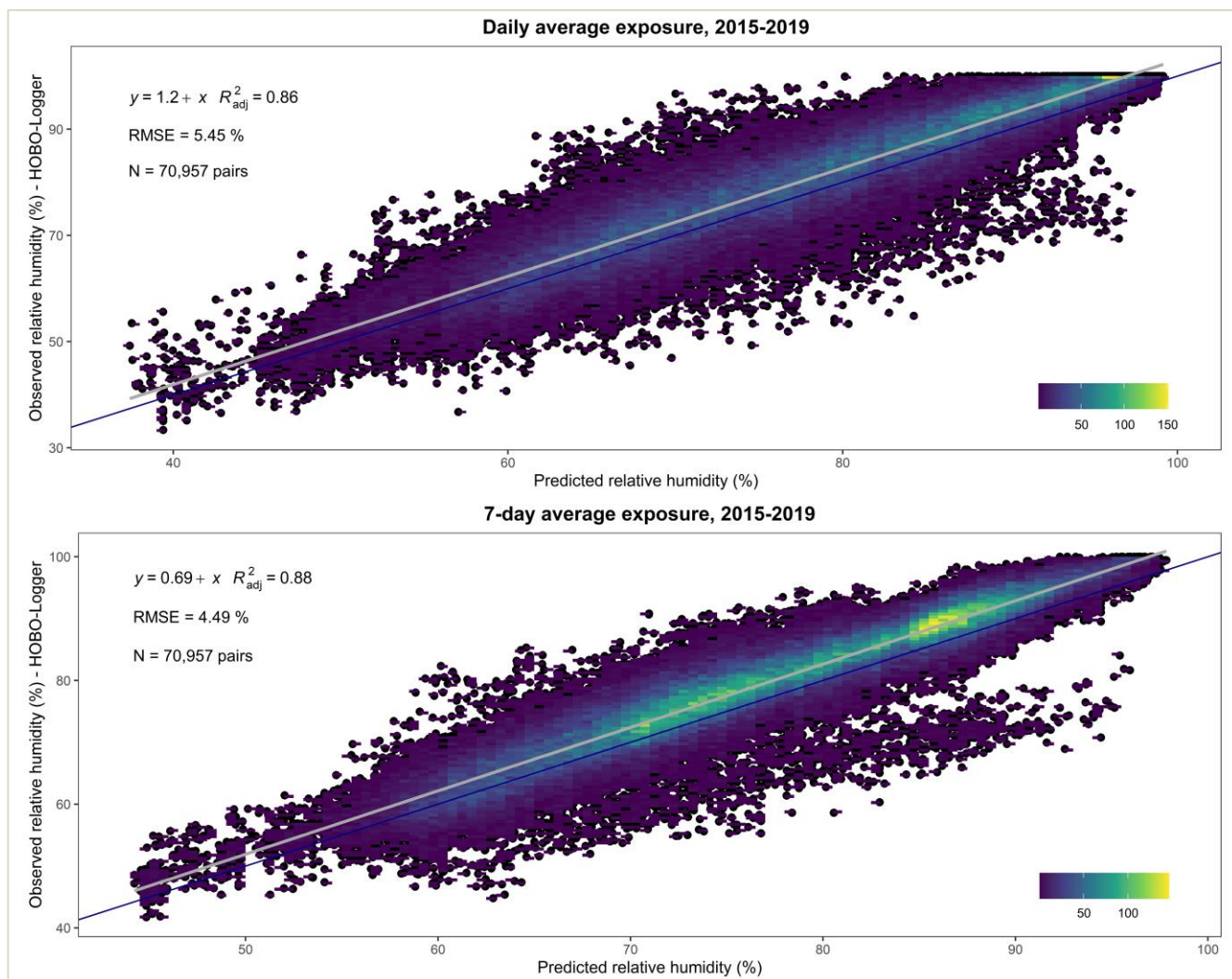


Figure S10. Density scatterplots between the model's RH predictions and the HOBO-Logger RH observations for 2015-2019, daily average and 7-day average. Dark grey line = fitting line. Dark blue line = 1:1 diagonal line.

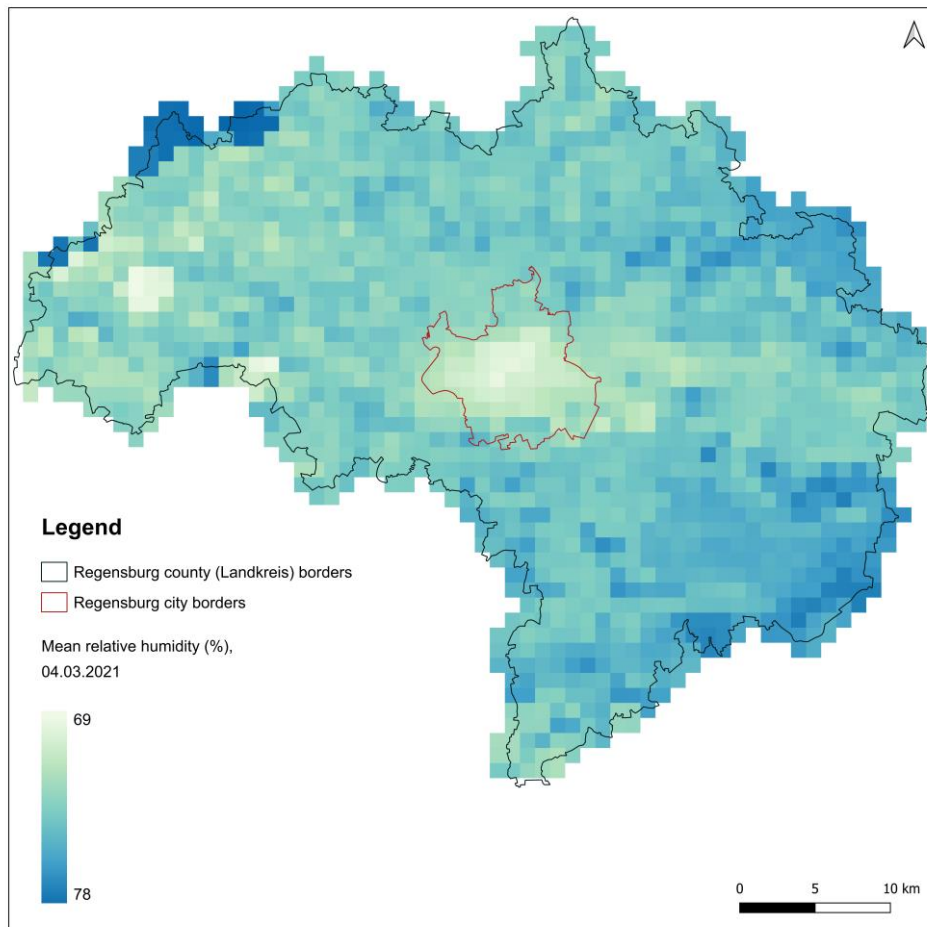


Figure S11. Spatial pattern of the predicted daily mean RH in Regensburg, 04.03.2021.

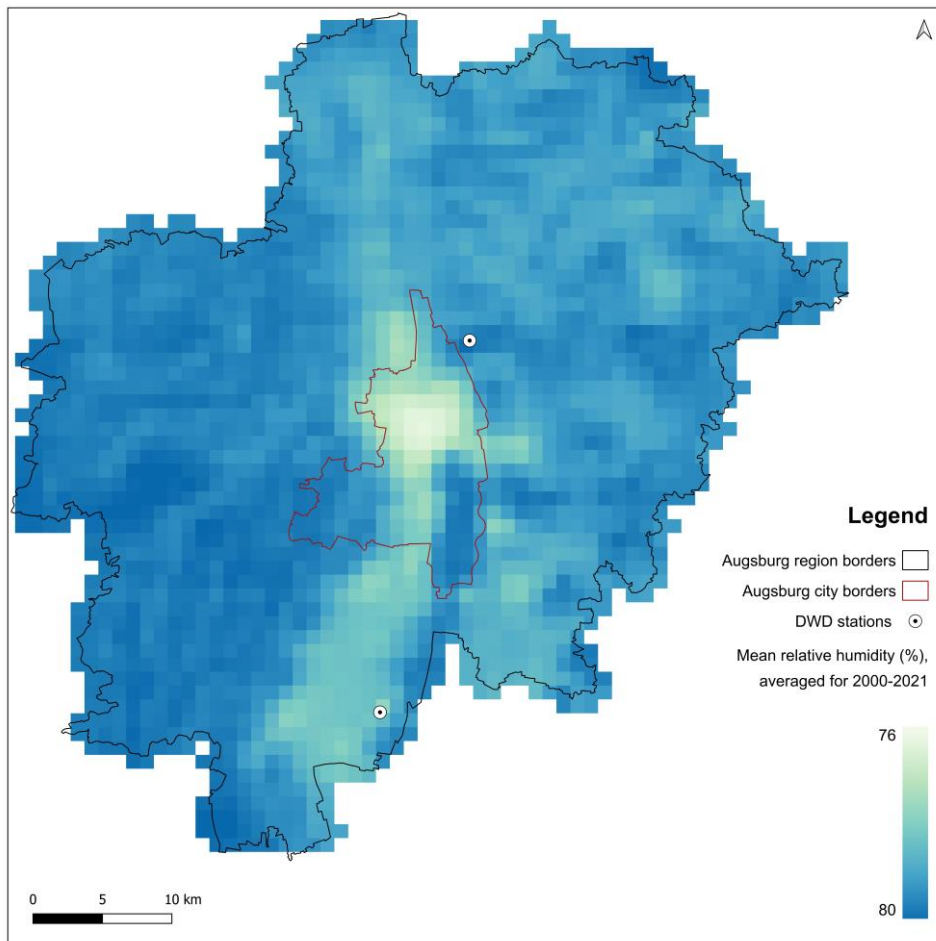


Figure S12. Spatial pattern of the averaged predicted RH in Augsburg during 2000-2021.

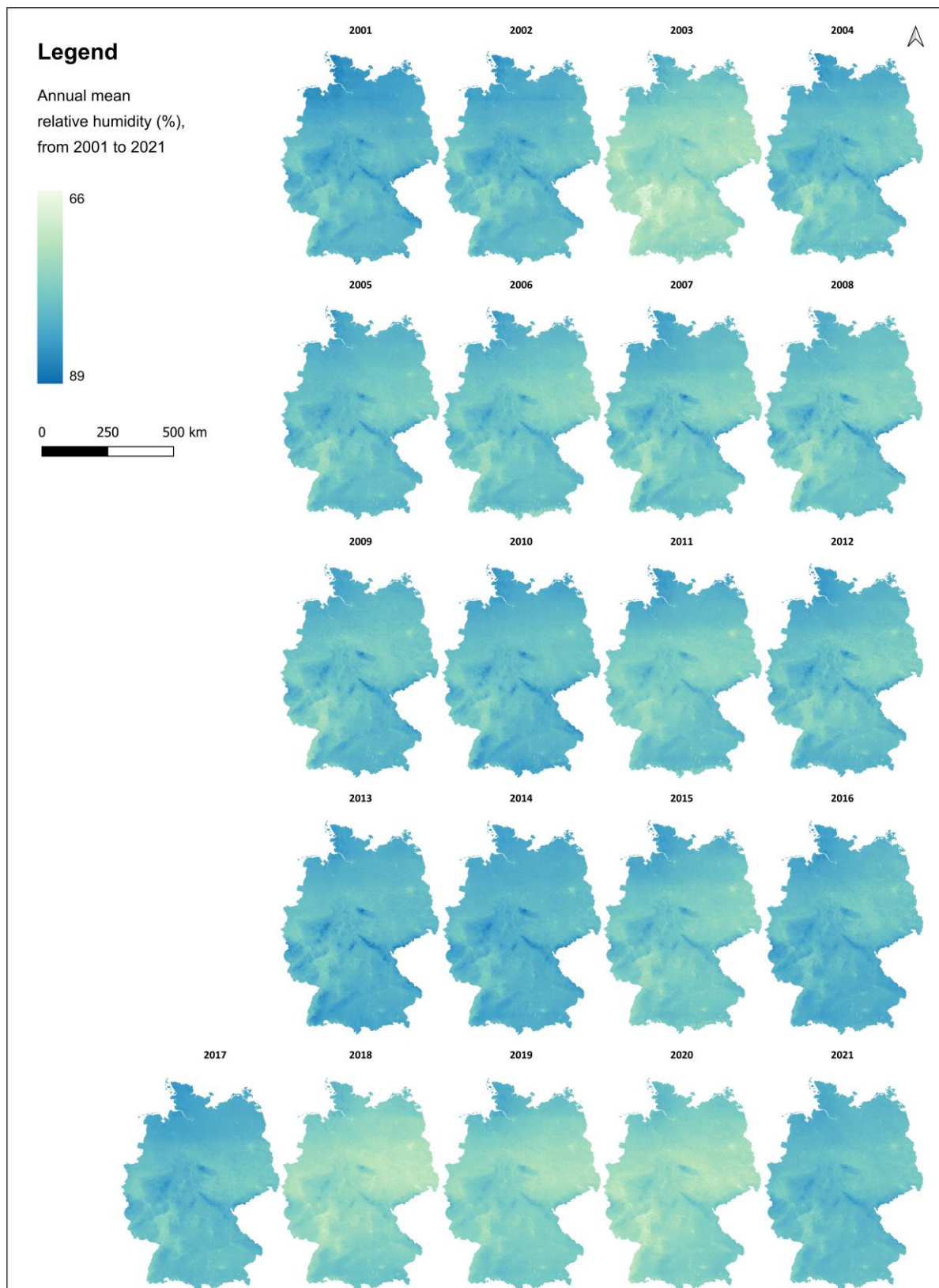


Figure S13. Spatial distribution map of interannual change of RH in Germany from 2001 to 2021.

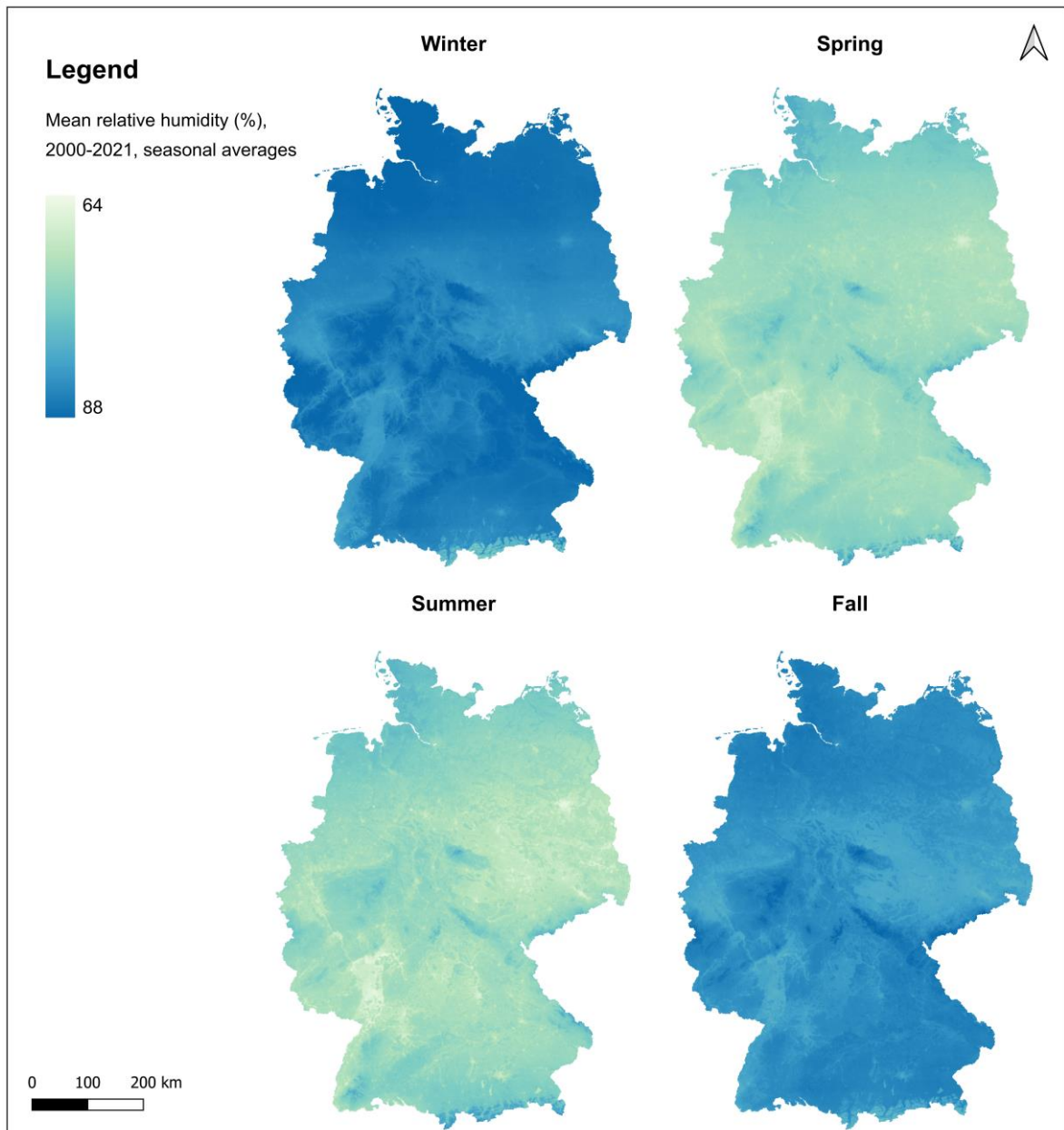


Figure S14. Maps of predicted RH by season in Germany, averaged for 2000-2021.

Table S1. Prediction accuracy for the wind speed interpolation: 10-fold cross-validation results for the daily mean wind speed interpolation over Germany during 2000-2021.

Year	R ²	RMSE (m/s)
2000	0.60	1.50
2001	0.56	1.47
2002	0.59	1.55
2003	0.54	1.47
2004	0.55	1.50
2005	0.56	1.47
2006	0.52	1.49
2007	0.59	1.52
2008	0.56	1.51
2009	0.50	1.44
2010	0.55	1.38
2011	0.58	1.40
2012	0.58	1.33
2013	0.58	1.32
2014	0.62	1.25
2015	0.62	1.36
2016	0.58	1.30
2017	0.58	1.39
2018	0.59	1.30
2019	0.58	1.36
2020	0.64	1.27
2021	0.59	1.27
Overall	0.58	1.40

Random Forest model definition

We applied the following random forest model, separately for each year:

$$\text{RelativeHumidity}_{i,j} \sim \text{AirTemperature}_{i,j} + \text{RedBand}_{i,j} + \text{GreenBand}_{i,j} + \text{BlueBand}_{i,j} + \text{Precipitation}_{i,j} + \\ + \text{WindSpeed}_{i,j} + \text{Elevation}_i + \text{NDVI}_{i,j} + \text{Longitude}_i + \text{Latitude}_i + \text{DayofYear}_j$$

where:

- $\text{RelativeHumidity}_{i,j}$ = mean relative humidity (%) at monitor location i on day j
- $\text{AirTemperature}_{i,j}$ = mean air temperature ($^{\circ}\text{C}$) at monitor location i on day j
- $\text{RedBand}_{i,j}$ = red band (dimensionless) at monitor location i on day j
- $\text{GreenBand}_{i,j}$ = green band (dimensionless) at monitor location i on day j
- $\text{BlueBand}_{i,j}$ = blue band (dimensionless) at monitor location i on day j
- $\text{Precipitation}_{i,j}$ = mean precipitation height (mm) at monitor location i on day j
- $\text{WindSpeed}_{i,j}$ = mean wind speed (m/s) at monitor location i on day j
- Elevation_i = elevation (meters) at monitor location i
- $\text{NDVI}_{i,j}$ = mean normalized difference vegetation index (dimensionless) at monitor location i on month of day j
- Longitude_i = longitude ($^{\circ}$) at monitor location i
- Latitude_i = latitude ($^{\circ}$) at monitor location i
- DayofYear_j = day j of the year

Hyperparameters: num.trees = 500 and mtry = 8

Statistical parameters - formula sheet

- $R^2 = 1 - \frac{SSR}{SST}$

where:

- SSR (Sum of Squared Residuals) = sum of the squared differences of the predicted values \hat{y} and the observed values y of the response variable (relative humidity),

i.e., $SSR = \sum_{i=1}^n (y_i - \hat{y}_i)^2$

- SST (Total Sum of Squares) = sum of the squared differences of the observed values y of the response variable (relative humidity) and its average value \bar{y} ,

i.e., $SST = \sum_{i=1}^n (y_i - \bar{y})^2$

- i = i^{th} grid cell and day combination
- n = total number of grid cell and day combinations

- $RMSE = \sqrt{\frac{\sum_{i=1}^n (y_i - \hat{y}_i)^2}{n}}$

where:

- y_i = observed value of the response variable (relative humidity) for the i^{th} grid cell and day combination
- \hat{y}_i = predicted value of the response variable (relative humidity) for the i^{th} grid cell and day combination
- n = total number of grid cell and day combinations

- $MPE = \frac{\sum_{i=1}^n \frac{y_i - \hat{y}_i}{y_i}}{n} \cdot 100$

where:

y_i = observed value of the response variable (relative humidity) for the i^{th} grid cell and day combination

\hat{y}_i = predicted value of the response variable (relative humidity) for the i^{th} grid cell and day combination

n = total number of grid cell and day combinations

- $MAPE = \frac{\sum_{i=1}^n \left| \frac{y_i - \hat{y}_i}{y_i} \right|}{n} \cdot 100$

where:

y_i = observed value of the response variable (relative humidity) for the i^{th} grid cell and day combination

\hat{y}_i = predicted value of the response variable (relative humidity) for the i^{th} grid cell and day combination

n = total number of grid cell and day combinations

References

1. <https://www.climate.gov/news-features/understanding-climate/climate-change-global-temperature>. Last Access 02/05/2024
2. Intergovernmental Panel on Climate Change (IPCC). 2023. Climate Change 2022 – Impacts, Adaptation and Vulnerability: Working Group II Contribution to the Sixth Assessment Report of the Intergovernmental Panel on Climate Change. Cambridge: Cambridge University Press., doi: <https://doi.org/10.1017/9781009325844>
3. https://www.dwd.de/EN/press/press_release/EN/2023/20231229_the_weather_in_germany_in_year_2023_news.html. Last Access 02/05/2024
4. https://www.dwd.de/DE/klimaumwelt/aktuelle_meldungen/230123/artikel_jahresueckblick-2022.html. Last Access 02/05/2024
5. Schneider A, Breitner S. 2016. Temperature effects on health-current findings and future implications. *EBioMedicine* 6 29-30. doi: <https://doi.org/10.1016/j.ebiom.2016.04.003>
6. Ye X, Wolff R, Yu W, Vaneckova P, Pan X, Tong S. 2012. Ambient temperature and morbidity: a review of epidemiological evidence. *Environmental health perspectives* 120 (1): 19-28. doi: <https://doi.org/10.1289/ehp.1003198>
7. Guo Y, Gasparrini A, Armstrong BG, Tawatsupa B, Tobias A, Lavigne E, Coelho MdSZS, Pan X, Kim H, Hashizume M. 2016. Temperature variability and mortality: a multi-country study. *Environmental health perspectives* 124 (10): 1554-9. doi: <https://doi.org/10.1289/EHP149>
8. Al-Kindi S, Motairek I, Khraishah H, Rajagopalan S. 2023. Cardiovascular disease burden attributable to non-optimal temperature: analysis of the 1990–2019 global burden of disease. *European Journal of Preventive Cardiology* 30 (15): 1623-31. doi: <https://doi.org/10.1093/eurjpc/zwad130>
9. Li X, Zhou M, Yu M, Xu Y, Li J, Xiao Y, Huang B, Hu J, Liu T, Guan W. 2021. Life loss per death of respiratory disease attributable to non-optimal temperature: results from a national study in 364 Chinese locations. *Environmental Research Letters* 16 (3): 035001. doi: <https://doi.org/10.1088/1748-9326/abe06c>

-
10. Zhang Y, Yu C, Wang L. 2017. Temperature exposure during pregnancy and birth outcomes: an updated systematic review of epidemiological evidence. *Environmental Pollution* 225 700-12. doi: <https://doi.org/10.1016/j.envpol.2017.02.066>
11. Thompson R, Hornigold R, Page L, Waite T. 2018. Associations between high ambient temperatures and heat waves with mental health outcomes: a systematic review. *Public health* 161 171-91. doi: <https://doi.org/10.1016/j.puhe.2018.06.008>
12. Ebi KL, Capon A, Berry P, Broderick C, de Dear R, Havenith G, Honda Y, Kovats RS, Ma W, Malik A. 2021. Hot weather and heat extremes: health risks. *The lancet* 398 (10301): 698-708. doi: [https://doi.org/10.1016/S0140-6736\(21\)01208-3](https://doi.org/10.1016/S0140-6736(21)01208-3)
13. Dai L, Kloog I, Coull BA, Sparrow D, Spiro III A, Vokonas PS, Schwartz JD. 2016. Cognitive function and short-term exposure to residential air temperature: A repeated measures study based on spatiotemporal estimates of temperature. *Environmental research* 150 446-51. doi: <https://doi.org/10.1016/j.envres.2016.06.036>
14. Schneider A, Ruckerl R, Breitner S, Wolf K, Peters A. 2017. Thermal control, weather, and aging. *Current environmental health reports* 4 21-9. doi: <https://doi.org/10.1007/s40572-017-0129-0>
15. Kenny GP, Yardley J, Brown C, Sigal RJ, Jay O. 2010. Heat stress in older individuals and patients with common chronic diseases. *Cmaj* 182 (10): 1053-60. doi: <https://doi.org/10.1503/cmaj.081050>
16. Xu Z, Etzel RA, Su H, Huang C, Guo Y, Tong S. 2012. Impact of ambient temperature on children's health: a systematic review. *Environmental research* 117 120-31. doi: <https://doi.org/10.1016/j.envres.2012.07.002>
17. Breitner S, Wolf K, Peters A, Schneider A. 2014. Short-term effects of air temperature on cause-specific cardiovascular mortality in Bavaria, Germany. *Heart* 100 (16): 1272-80. doi: <https://heart.bmj.com/content/100/16/1272>
18. Zafeiratou S, Samoli E, Dimakopoulou K, Rodopoulou S, Analitis A, Gasparri A, Stafoggia M, De'Donato F, Rao S, Monteiro A. 2021. A systematic review on the association between total and cardiopulmonary mortality/morbidity or cardiovascular risk factors with long-term exposure to

- increased or decreased ambient temperature. *Science of the total environment* 772 145383. doi: <https://doi.org/10.1016/j.scitotenv.2021.145383>
19. Chen K, De Schrijver E, Sivaraj S, Sera F, Scovronick N, Jiang L, Roye D, Lavigne E, Kysely J, Urban A. 2024. Impact of population aging on future temperature-related mortality at different global warming levels. *Nature communications* 15 (1): 1796. doi: <https://doi.org/10.1038/s41467-024-45901-z>
20. Gronlund CJ, Sullivan KP, Kefelegn Y, Cameron L, O'Neill MS. 2018. Climate change and temperature extremes: A review of heat-and cold-related morbidity and mortality concerns of municipalities. *Maturitas* 114 54-9. doi: <https://doi.org/10.1016/j.maturitas.2018.06.002>
21. Xu Z, Cheng J, Hu W, Tong S. 2018. Heatwave and health events: A systematic evaluation of different temperature indicators, heatwave intensities and durations. *Science of the total environment* 630 679-89. doi: <https://doi.org/10.1016/j.scitotenv.2018.02.268>
22. Gasparrini A, Guo Y, Hashizume M, Lavigne E, Zanobetti A, Schwartz J, Tobias A, Tong S, Rocklöv J, Forsberg B. 2015. Mortality risk attributable to high and low ambient temperature: a multicountry observational study. *The lancet* 386 (9991): 369-75. doi: [https://doi.org/10.1016/S0140-6736\(14\)62114-0](https://doi.org/10.1016/S0140-6736(14)62114-0)
23. Zhang P, Zhang J, Chen M. 2015. Economic impacts of climate change on Chinese agriculture: the importance of relative humidity and other climatic variables. Available at SSRN 2598810. doi: <https://dx.doi.org/10.2139/ssrn.2598810>
24. Bartková-Ščevková J. 2003. The influence of temperature, relative humidity and rainfall on the occurrence of pollen allergens (*Betula*, *Poaceae*, *Ambrosia artemisiifolia*) in the atmosphere of Bratislava (Slovakia). *International Journal of Biometeorology* 48 1-5. doi: <https://doi.org/10.1007/s00484-003-0166-2>
25. Randriamiarisoa H, Chazette P, Couvert P, Sanak J, Mégie G. 2006. Relative humidity impact on aerosol parameters in a Paris suburban area. *Atmospheric Chemistry and Physics* 6 (5): 1389-407. doi: <https://doi.org/10.5194/acp-6-1389-2006>
26. Forootan E. 2019. Analysis of trends of hydrologic and climatic variables. doi: <https://doi.org/10.17221/154/2018-SWR>

-
27. Xiong Y, Meng Q-S, Jie G, Tang X-F, Zhang H-F. 2017. Effects of relative humidity on animal health and welfare. *Journal of integrative agriculture* 16 (8): 1653-8. doi: [https://doi.org/10.1016/S2095-3119\(16\)61532-0](https://doi.org/10.1016/S2095-3119(16)61532-0)
28. Davis RE, McGregor GR, Enfield KB. 2016. Humidity: A review and primer on atmospheric moisture and human health. *Environmental research* 144 106-16. doi: <https://doi.org/10.1016/j.envres.2015.10.014>
29. Guarnieri G, Olivieri B, Senna G, Vianello A. 2023. Relative humidity and its impact on the immune system and infections. *International Journal of Molecular Sciences* 24 (11): 9456. doi: <https://doi.org/10.3390/ijms24119456>
30. Mei Y, Li A, Zhao M, Xu J, Li R, Zhao J, Zhou Q, Ge X, Xu Q. 2023. Associations and burdens of relative humidity with cause-specific mortality in three Chinese cities. *Environmental Science and Pollution Research* 30 (2): 3512-26. doi: <https://doi.org/10.1007/s11356-022-22350-z>
31. Abrignani MG, Corrao S, Biondo GB, Lombardo RM, Di Girolamo P, Braschi A, Di Girolamo A, Novo S. 2012. Effects of ambient temperature, humidity, and other meteorological variables on hospital admissions for angina pectoris. *European journal of preventive cardiology* 19 (3): 342-8. doi: <https://doi.org/10.1177/1741826711402741>
32. Tseng C-M, Chen Y-T, Ou S-M, Hsiao Y-H, Li S-Y, Wang S-J, Yang AC, Chen T-J, Perng D-W. 2013. The effect of cold temperature on increased exacerbation of chronic obstructive pulmonary disease: a nationwide study. *PloS one* 8 (3): e57066. doi: <https://doi.org/10.1371/journal.pone.0057066>
33. Rocklöv J, Forsberg B. 2010. The effect of high ambient temperature on the elderly population in three regions of Sweden. *International journal of environmental research and public health* 7 (6): 2607-19. doi: <https://doi.org/10.3390/ijerph7062607>
34. Jiang Y-F, Luo W-W, Zhang X, Ren D-D, Huang Y-B. 2023. Relative humidity affects acute otitis media visits of preschool children to the emergency department. *Ear, Nose & Throat Journal* 102 (7): 467-72. doi: <https://doi.org/10.1177/01455613211009151>
35. Onozuka D, Hashizume M. 2011. Weather variability and paediatric infectious gastroenteritis. *Epidemiology & Infection* 139 (9): 1369-78. doi: <https://doi.org/10.1017/S0950268810002451>

36. Božič A, Kanduč M. 2021. Relative humidity in droplet and airborne transmission of disease. *Journal of Biological Physics* 47 (1): 1-29. doi: <https://doi.org/10.1007/s10867-020-09562-5>
37. Santos-Vega M, Martinez P, Vaishnav K, Kohli V, Desai V, Bouma M, Pascual M. 2022. The neglected role of relative humidity in the interannual variability of urban malaria in Indian cities. *Nature communications* 13 (1): 533. doi: <https://doi.org/10.1038/s41467-022-28145-7>
38. Auler A, Cássaro F, Da Silva V, Pires L. 2020. Evidence that high temperatures and intermediate relative humidity might favor the spread of COVID-19 in tropical climate: A case study for the most affected Brazilian cities. *Science of the Total Environment* 729 139090. doi: <https://doi.org/10.1016/j.scitotenv.2020.139090>
39. Zeng J, Zhang X, Yang J, Bao J, Xiang H, Dear K, Liu Q, Lin S, Lawrence WR, Lin A. 2017. Humidity may modify the relationship between temperature and cardiovascular mortality in Zhejiang Province, China. *International journal of environmental research and public health* 14 (11): 1383. doi: <https://doi.org/10.3390/ijerph14111383>
40. D'Amato G, Holgate ST, Pawankar R, Ledford DK, Cecchi L, Al-Ahmad M, Al-Enezi F, Al-Muhsen S, Ansotegui I, Baena-Cagnani CE. 2015. Meteorological conditions, climate change, new emerging factors, and asthma and related allergic disorders. A statement of the World Allergy Organization. *World allergy organization journal* 8 1-52. doi: <https://doi.org/10.1186/s40413-015-0073-0>
41. Vanos J, Cakmak S. 2014. Changing air mass frequencies in Canada: potential links and implications for human health. *International journal of biometeorology* 58 121-35. doi: <https://doi.org/10.1007/s00484-013-0634-2>
42. Scher S, Messori G. 2019. How global warming changes the difficulty of synoptic weather forecasting. *Geophysical Research Letters* 46 (5): 2931-9. doi: <https://doi.org/10.1029/2018GL081856>
43. Zeger SL, Thomas D, Dominici F, Samet JM, Schwartz J, Dockery D, Cohen A. 2000. Exposure measurement error in time-series studies of air pollution: concepts and consequences. *Environmental health perspectives* 108 (5): 419-26. doi: <https://doi.org/10.1289/ehp.00108419>

44. Edwards JK, Keil AP. 2017. Measurement error and environmental epidemiology: a policy perspective. *Current environmental health reports* 4 79-88. doi: <https://doi.org/10.1007%2Fs40572-017-0125-4>
45. Armstrong BG. 1998. Effect of measurement error on epidemiological studies of environmental and occupational exposures. *Occupational and environmental medicine* 55 (10): 651. doi: <https://doi.org/10.1136%2Foem.55.10.651>
46. Rhomberg LR, Chandalia JK, Long CM, Goodman JE. 2011. Measurement error in environmental epidemiology and the shape of exposure-response curves. *Critical reviews in toxicology* 41 (8): 651-71. doi: <https://doi.org/10.3109/10408444.2011.563420>
47. Li S, Griffith DA, Shu H. 2020. Temperature prediction based on a space–time regression-kriging model. *Journal of Applied Statistics* 47 (7): 1168-90. doi: <https://doi.org/10.1080/02664763.2019.1671962>
48. Ozelkan E, Bagis S, Ozelkan EC, Ustundag BB, Yucel M, Ormeci C. 2015. Spatial interpolation of climatic variables using land surface temperature and modified inverse distance weighting. *International Journal of Remote Sensing* 36 (4): 1000-25. doi: <https://doi.org/10.1080/01431161.2015.1007248>
49. Jobst AM, Kingston DG, Cullen NJ, Sirguey P. 2017. Combining thin-plate spline interpolation with a lapse rate model to produce daily air temperature estimates in a data-sparse alpine catchment. *International Journal of Climatology* 37 (1): 214-29. doi: <https://doi.org/10.1002/joc.4699>
50. Li T, Zheng X, Dai Y, Yang C, Chen Z, Zhang S, Wu G, Wang Z, Huang C, Shen Y. 2014. Mapping near-surface air temperature, pressure, relative humidity and wind speed over Mainland China with high spatiotemporal resolution. *Advances in Atmospheric Sciences* 31 1127-35. doi: <https://doi.org/10.1007/s00376-014-3190-8>
51. Jin Z, Ma Y, Chu L, Liu Y, Dubrow R, Chen K. 2022. Predicting spatiotemporally-resolved mean air temperature over Sweden from satellite data using an ensemble model. *Environmental Research* 204 111960. doi: <https://doi.org/10.1016/j.envres.2021.111960>

-
52. Li L, Zha Y. 2018. Mapping relative humidity, average and extreme temperature in hot summer over China. *Science of the Total Environment* 615 875-81. doi: <https://doi.org/10.1016/j.scitotenv.2017.10.022>
53. Xu Y, Knudby A, Ho HC. 2014. Estimating daily maximum air temperature from MODIS in British Columbia, Canada. *International Journal of Remote Sensing* 35 (24): 8108-21. doi: <https://doi.org/10.1080/01431161.2014.978957>
54. Kloog I, Nordio F, Coull BA, Schwartz J. 2014. Predicting spatiotemporal mean air temperature using MODIS satellite surface temperature measurements across the Northeastern USA. *Remote sensing of environment* 150 132-9. doi: <https://doi.org/10.1016/j.rse.2014.04.024>
55. Rosenfeld A, Dorman M, Schwartz J, Novack V, Just AC, Kloog I. 2017. Estimating daily minimum, maximum, and mean near surface air temperature using hybrid satellite models across Israel. *Environmental research* 159 297-312. doi: <https://doi.org/10.1016/j.envres.2017.08.017>
56. dos Santos RS. 2020. Estimating spatio-temporal air temperature in London (UK) using machine learning and earth observation satellite data. *International Journal of Applied Earth Observation and Geoinformation* 88 102066. doi: <https://doi.org/10.1016/j.jag.2020.102066>
57. Yao R, Wang L, Huang X, Cao Q, Peng Y. 2022. A method for improving the estimation of extreme air temperature by satellite. *Science of The Total Environment* 837 155887. doi: <https://doi.org/10.1016/j.scitotenv.2022.155887>
58. Gil-Alana LA. 2018. Maximum and minimum temperatures in the United States: Time trends and persistence. *Atmospheric Science Letters* 19 (4): e810. doi: <https://doi.org/10.1002/asl.810>
59. Sarangi C, Qian Y, Li J, Leung LR, Chakraborty T, Liu Y. 2021. Urbanization amplifies nighttime heat stress on warmer days over the US. *Geophysical Research Letters* 48 (24): e2021GL095678. doi: <https://doi.org/10.1029/2021GL095678>
60. Davis RE, Hondula DM, Sharif H. 2020. Examining the diurnal temperature range enigma: why is human health related to the daily change in temperature? *International journal of biometeorology* 64 397-407. doi: <https://doi.org/10.1007/s00484-019-01825-8>
61. Armstrong B. 2006. Models for the relationship between ambient temperature and daily mortality. *Epidemiology* 624-31. doi: <http://www.jstor.org/stable/20486290>

62. Analitis A, Katsouyanni K, Biggeri A, Baccini M, Forsberg B, Bisanti L, Kirchmayer U, Ballester F, Cadum E, Goodman P. 2008. Effects of cold weather on mortality: results from 15 European cities within the PHEWE project. *American journal of epidemiology* 168 (12): 1397-408. doi: <https://doi.org/10.1093/aje/kwn266>
63. <https://www.helmholtz-munich.de/en/epi/cohort/kora>. Last Access 02/05/2024
64. <https://nako.de/>. Last Access 02/05/2024
65. https://www.destatis.de/EN/Themes/Society-Environment/Population/Current-Population/_node.html. Last Access 02/05/2024
66. Beck HE, Zimmermann NE, McVicar TR, Vergopolan N, Berg A, Wood EF. 2018. Present and future Köppen-Geiger climate classification maps at 1-km resolution. *Scientific data* 5 (1): 1-12. doi: <https://doi.org/10.1038/sdata.2018.214>
67. DWD. 2021. Historical daily station observations (temperature, pressure, precipitation, sunshine duration, etc.) for Germany, version v21.3. URL: https://opendata.dwd.de/climate_environment/CDC/observations_germany/climate/daily/kl/historical/
68. Didan K. 2015. MOD13A3 MODIS/Terra vegetation Indices Monthly L3 Global 1km SIN Grid V006 [Data set]. NASA EOSDIS Land Processes Distributed Active Archive Center. URL: <https://doi.org/10.5067/MODIS/MOD13A3.006>
69. Wan Z, Hook S, Hulley G. 2015. MOD11A1 MODIS/Terra Land Surface Temperature/Emissivity Daily L3 Global 1km SIN Grid V006 [Data set]. NASA EOSDIS Land Processes Distributed Active Archive Center. URL: <https://doi.org/10.5067/MODIS/MOD11A1.006>
70. Global 30 Arc-Second Elevation (GTOPO30). URL: <https://doi.org/10.5066/F7DF6PQS>
71. CORINE Land Cover 2012 (vector/raster 100 m), Europe, 6-yearly. URL: <https://doi.org/10.2909/a84ae124-c5c5-4577-8e10-511bfe55cc0d>
72. CORINE Land Cover 2018 (vector/raster 100 m), Europe, 6-yearly. URL: <https://doi.org/10.2909/960998c1-1870-4e82-8051-6485205ebbac>

-
73. Vermote E, Wolfe, R. 2015. MOD09GA MODIS/Terra Surface Reflectance Daily L2G Global 1km and 500m SIN Grid V006 [Data set]. NASA EOSDIS Land Processes Distributed Active Archive Center. URL: <https://doi.org/10.5067/MODIS/MOD09GA.006>
74. Nikolaou N, Dallavalle M, Stafoggia M, Bouwer LM, Peters A, Chen K, Wolf K, Schneider A. 2023. High-resolution spatiotemporal modeling of daily near-surface air temperature in Germany over the period 2000–2020. *Environmental Research* 219 115062. doi: <https://doi.org/10.1016/j.envres.2022.115062>
75. DWD. 2022. DWD Climate Data Center (CDC): REGNIE Grids of Daily Precipitation. URL: https://opendata.dwd.de/climate_environment/CDC/grids_germany/daily/regnie/
76. Beck C, Straub A, Breitner S, Cyrus J, Philipp A, Rathmann J, Schneider A, Wolf K, Jacobeit J. 2018. Air temperature characteristics of local climate zones in the Augsburg urban area (Bavaria, southern Germany) under varying synoptic conditions. *Urban Climate* 25 152-66. doi: <https://doi.org/10.1016/j.uclim.2018.04.007>
77. Krähenmann S, Walter, A., Brienen, S., Imbery, F., Matzarakis, A. 2016. Monthly means of hourly grids of air temperature for Germany (project TRY Advancement), Version V001, DWD Climate Data Center (CDC). URL: https://doi.org/10.5676/DWD_CDC/TRY_Basis_v001
78. R Core Team. 2020. R: A Language and Environment for Statistical Computing. R Foundation for Statistical Computing, Vienna, Austria. Available from: <https://www.R-project.org/>.
79. R Core Team. 2022. R: A Language and Environment for Statistical Computing. R Foundation for Statistical Computing, Vienna, Austria. Available from: <https://www.R-project.org/>.
80. Bates D, Mächler M, Bolker B, Walker S. 2014. Fitting linear mixed-effects models using lme4. arXiv preprint arXiv:14065823. doi: <https://doi.org/10.48550/arXiv.1406.5823>
81. Wright MN, Ziegler A. 2015. ranger: A fast implementation of random forests for high dimensional data in C++ and R. arXiv preprint arXiv:150804409. doi: <https://doi.org/10.18637/jss.v077.i01>
82. QGIS Development Team. 2020. Geographic Information System. Open Source Geospatial Foundation Project. doi: <http://qgis.osgeo.org>
83. <https://gadm.org/index.html>. Last Access 02/05/2024

84. Ni W, Breitner S, Nikolaou N, Wolf K, Zhang S, Peters A, Herder C, Schneider A. 2023. Effects of Short- And Medium-Term Exposures to Lower Air Temperature on 71 Novel Biomarkers of Subclinical Inflammation: Results from the KORA F4 Study. *Environ Sci Technol* 57 (33): 12210-21. doi: <https://doi.org/10.1021/acs.est.3c00302>
85. Ni W, Wolf K, Breitner S, Zhang S, Nikolaou N, Ward-Caviness CK, Waldenberger M, Gieger C, Peters A, Schneider A. 2022. Higher Daily Air Temperature Is Associated with Shorter Leukocyte Telomere Length: KORA F3 and KORA F4. *Environ Sci Technol* 56 (24): 17815-24. doi: <https://doi.org/10.1021/acs.est.2c04486>
86. Ni W, Nikolaou N, Ward-Caviness CK, Breitner S, Wolf K, Zhang S, Wilson R, Waldenberger M, Peters A, Schneider A. 2023. Associations between medium- and long-term exposure to air temperature and epigenetic age acceleration. *Environ Int* 178 108109. doi: <https://doi.org/10.1016/j.envint.2023.108109>
87. Zhang S, Breitner S, Rai M, Nikolaou N, Stafoggia M, De' Donato F, Samoli E, Zafeiratou S, Katsouyanni K, Rao S, Palomares AD, Gasparrini A, Masselot P, Aunan K, Peters A, Schneider A. 2023. Assessment of short-term heat effects on cardiovascular mortality and vulnerability factors using small area data in Europe. *Environ Int* 179 108154. doi: <https://doi.org/10.1016/j.envint.2023.108154>
88. Herder C, Zhang S, Wolf K, Maalmi H, Bonhof GJ, Rathmann W, Schwettmann L, Thorand B, Roden M, Schneider A, Ziegler D, Peters A. 2023. Environmental risk factors of incident distal sensorimotor polyneuropathy: Results from the prospective population-based KORA F4/FF4 study. *Sci Total Environ* 858 (Pt 3): 159878. doi: <https://doi.org/10.1016/j.scitotenv.2022.159878>
89. Badpa M, Schneider A, Schwettmann L, Thorand B, Wolf K, Peters A. 2024. Air pollution, traffic noise, greenness, and temperature and the risk of incident type 2 diabetes: Results from the KORA cohort study. *Environmental Epidemiology* 8 (2): e302. doi: <https://doi.org/10.1097/EE9.0000000000000302>
90. Zafeiratou S, Samoli E, Analitis A, Gasparrini A, Stafoggia M, de'Donato FK, Rao S, Zhang S, Breitner S, Masselot P. 2023. Assessing heat effects on respiratory mortality and location characteristics as modifiers of heat effects at a small area scale in Central-Northern Europe. *Environmental Epidemiology* 7 (5): e269. doi: <https://doi.org/10.1097/ee9.0000000000000269>

-
91. Niedermayer F, Wolf K, Zhang S, Dallavalle M, Nikolaou N, Schwettmann L, Selsam P, Hoffmann B, Schneider A, Peters A. 2024. Sex-specific associations of environmental exposures with prevalent diabetes and obesity—Results from the KORA Fit study. *Environmental Research* 252 118965. doi: <https://doi.org/10.1016/j.envres.2024.118965>
92. Zhang S, Breitner S, de Donato F, Stafoggia M, Nikolaou N, Aunan K, Peters A, Schneider A. Heat and Cause-Specific Cardiopulmonary Mortality in Germany: Small-Area Assessment and Vulnerability Factors. Available at SSRN 4807168. doi: <https://dx.doi.org/10.2139/ssrn.4807168>
93. Wang J, Nikolaou N, an der Heiden M, Irrgang C. 2024. Past, present, and future heat-related mortality in Germany, PREPRINT (Version 1). Research Square. doi: <https://doi.org/10.21203/rs.3.rs-3920808/v1>
94. Zhang S, Breitner S, Stafoggia M, de Donato F, Samoli E, Zafeiratou S, Katsouyanni K, Rao S, Diz-Lois Palomares A, Gasparrini A, Masselot P, Nikolaou N, Aunan K, Peters A, Schneider A. Effect Modification of Air Pollution on the Association between Heat and Mortality in Five European Countries. Available at SSRN 4854126. doi: <http://dx.doi.org/10.2139/ssrn.4854126>
95. <https://rdrr.io/cran/foreach/man/foreach-package.html>. Last Access 02/05/2024
96. Binter A-C, Alonso L, Philippat C, Mon-Williams M, Chatzi L, Vrijheid M, Nieuwenhuijsen M, Sunyer J, Guxens M. ISEE Young Virtual Conference, Basel, Switzerland, 18-19 February, 2021. doi: <https://doi.org/10.1097%2FEE9.0000000000000151>
97. Nikolaou N, Bouwer L, Valizadeh M, Dallavalle M, Wolf K, Stafoggia M, Peters A, Schneider A. 2022. High-resolution hybrid spatiotemporal modeling of daily relative humidity across Germany for epidemiological research: a Random Forest approach. EGU General Assembly Conference Abstracts. doi: <https://doi.org/10.5194/egusphere-egu22-6543>
98. Nikolaou N, Bouwer L, Dallavalle M, Wolf K, Valizadeh M, Stafoggia M, Peters A, Schneider A. 2022. Spatiotemporally resolved daily relative humidity predictions across Germany during 2000-2021: a Random Forest approach. ISEE Conference Abstracts. doi: <https://doi.org/10.1289/isee.2022.O-PK-14>
99. <https://www.helmholtz-klima.de/en>. Last Access 02/05/2024
100. <https://www.helmholtz-munich.de/en/epi/projects/noise2nako>. Last Access 02/05/2024

-
101. <https://www.exhaustion.eu/>. Last Access 02/05/2024
102. <https://ysph.yale.edu/yale-center-on-climate-change-and-health/innovative-research/the-chen-lab/air-lock/>. Last Access 02/05/2024
103. <https://www.rheinland-studie.de/en/>. Last Access 02/05/2024
104. <https://www.digimed-bayern.de/>. Last Access 02/05/2024
105. <https://innovationsfonds.g-ba.de/projekte/versorgungsforschung/klimagesvor-auswirkungen-des-klimawandels-auf-die-gesundheitsversorgung-von-patienten-mit-kardiovaskulaeren-metabolischen-und-respiratorischen-erkrankungen.590>. Last Access 02/05/2024
106. <https://www.aok.de/pk/>. Last Access 02/05/2024
107. <https://forschungsdatenzentrum.de/en>. Last Access 02/05/2024
108. Sohail H, Zhang S, Mikkonen S, Breitner S, Wolf K, Nikolaou N, Peters A, Schwettmann L, Lanki T, Schneider A. 2022. Short-term impacts of ambient temperature on self-rated health in Augsburg, Southern Germany. ISEE Conference Abstracts. doi: <https://doi.org/10.1289/isee.2022.P-0621>
109. Chen K, Ma Y, Nobile F, Marb A, Dubrow R, Stafoggia M, Breitner S, L. P, Kinney4. 2023. Effect of Air Pollution Reductions on Mortality during the COVID-19 Lockdown: A Natural Experiment Study. HEI Annual Conference. URL: <https://www.healtheffects.org/research/ongoing-research/effect-air-pollution-reductions-mortality-during-covid-19-lockdown-natural>
110. Nikolaou N, Cea D, Valizadeh M, Behzadi S, Staab J, Dallavalle M, Piraud M, Peters A, Schneider A, Taubenböck H, Wolf K. 2023. A machine learning framework for cardiovascular health prediction modeling the interplay between various environmental, neighborhood and socio-economic features: a German-wide application. Zenodo. doi: <https://doi.org/10.5281/zenodo.10222701>
111. Zhang S, Breitner S, Rai M, Stafoggia M, de'Donato F, Aunan K, Peters A, Schneider A. 2022. Short-term heat effects on cardiopulmonary morbidity using national small area data—Results of the EXHAUSTION project. ISEE Conference Abstracts. doi: <https://doi.org/10.1289/isee.2022.P-0572>

-
112. Schneider A, Zhang S, Rai M, de'Donato F, Stafoggia M, Peters A, Breitner S. 2022. Short-term effects of heat on cardiovascular mortality and morbidity in Germany—Small-area analysis in the framework of the EXHAUSTION project. ISEE Conference Abstracts. doi: <https://doi.org/10.1289/isee.2022.P-0566>
113. Breitner S, Zhang S, Rai M, De'Donato F, Stafoggia M, Aunan K, Peters A, Schneider A. 2022. Short-term effects of heat on respiratory mortality and morbidity in Germany—small-area analysis in the framework of the EXHAUSTION project. ISEE Conference Abstracts. doi: <https://doi.org/10.1289/isee.2022.P-0576>
114. Hertel D, Pößneck J, Kabisch S, Schlink U. Hitzestress in Stadtquartieren—Methodik und empirische Belege unter Nutzung des Planetary-Health-Ansatzes. Die Resiliente Stadt: Konzepte, Konflikte, Lösungen: Springer Berlin Heidelberg Berlin, Heidelberg; 2023. p. 247-66. doi: <https://doi.org/10.1007/978-3-662-66916-7>
115. <https://palm.muk.uni-hannover.de/trac>. Last Access 02/05/2024
116. <https://www.sciencedirect.com/journal/environment-international>. Last Access 02/05/2024

Appendix

Further projects

In addition to the two publications included in this PhD Thesis, my involvement extended to several projects during my PhD studies. Notably, I worked extensively for the HI-CAM⁹⁹ project, for which I generated the aforementioned T_{air} and RH datasets. Currently, our focus is on investigating the relationship between short-term exposure to T_{air} and cognitive function, along with cardio-metabolic health among NAKO⁶⁴ participants. This analysis was initially intended to be part of this PhD Thesis. However, due to significant delays in receiving the NAKO data, almost three years, we are currently pursuing this work in collaboration with our Max Delbrück Center (MDC) project partners.

In addition, I actively worked to the Noise2NAKO^{AI100} project where we developed a comprehensive ML framework capable of identifying the driving contextual factors to various health outcomes, using hypertension as a case study¹¹⁰. Our overarching aim was to provide a tool accessible to environmental epidemiologists unfamiliar with AI. Therefore, the code will be publicly available. We employed both the T_{air} and RH datasets generated in this PhD Thesis to a large input database of environmental exposures, neighborhood and SES factors as well as health and individual-level characteristics of NAKO study participants. We compared traditional regression approaches (e.g., linear regression) with various ML algorithms, including neighbor-based (e.g., k-nearest neighbor), statistical learning (e.g., support vector machine), ensemble learning (e.g., RF and XGBoost) and neural networks. In a sample with approximately 45% hypertensive participants (out of around 100,000), all models demonstrated robust performance, achieving comparable accuracies around 0.70. They highlighted key factors for hypertension, with individual characteristics (age, body mass index and sex) being the most influential, followed by environmental exposures (non-optimal temperature and air pollution) and individual SES features (income and education) factors. This work allowed me to expand my expertise in AI applications, explore various ML approaches, and network within the AI-health field.

Furthermore, during my PhD time I also started working on air pollution and T_{air} effects on odor identification in the KORA cohort, an early indicator of various neurodegenerative conditions.

Originally intended as an alternative due to prolonged delays in receiving NAKO data, this work faced setbacks of its own, including technical difficulties that resulted in further delays, preventing its inclusion in this PhD Thesis.

PhD experience - further insights

I conducted this PhD Thesis under the scope of the HI-CAM project, a Helmholtz Association's project in which 15 of the 18 Helmholtz centers across Germany were involved. The objective of the EPI-HMGU sub-project was to explore the physiological responses, particularly in cardio-metabolic and cognitive function, to better inform climate change adaptation strategies in the health sector. High resolution meteorological data were crucial for achieving this goal. Working on exposure modeling and assessment aligned perfectly with my background in mathematics and biostatistics and greatly enhanced my academic growth and career prospects.

With the guidance and support of my supervisors, I seized the invaluable opportunity to further expand my expertise in employing AI methodologies within the realm of health research, an area of significant pertinence and fascination for a biostatistician. This enriching experience has not only broadened my horizons but has also equipped me with multifaceted approaches to exposure assessment, epidemiological analysis and advanced statistical inference techniques. Such initiatives are not only indicative of contemporary trends but also underscore the dynamic evolution of our field.

I also gained substantial experience through active involvement in the T_{air} and RH data sharing. This participation provided me with valuable insights into various aspects of data management, including storage, transfer tools, and the compilation of corresponding data transfer agreements.

In addition, I engaged in paper reviews for Environment International¹¹⁶. Serving as a reviewer is a crucial and responsible role that significantly contributes to the advancement and scrutiny of scientific knowledge.

I also had the exceptional opportunity to expand my network within the Environmental Epidemiology and AI communities. This growth was nurtured through active participation in conferences, meetings, workshops, and the dissemination of research papers, fostering meaningful connections and collaborations with peers and experts in the field.

A notable highlight was my research visit in GERICS, Hamburg, financially supported by the Helmholtz Information & Data Science Academy Trainee Network. I deepened my understanding of ML techniques for meteorological exposure modeling and their applications in health research.

Two of the most memorable moments during my PhD journey was receiving two prestigious poster awards at AI events in Hamburg and Paris, for the project Noise2NAKO^{AI}, serving as a recognition of my hard work and efforts.

Last but not least, I co-wrote a project proposal with colleagues from EPI-HMGU and GERICS, focusing on AI-health research. This experience enriched my academic career, regardless of its acceptance status.

Acknowledgements

I would like to take the opportunity and thank all those who, without their unwavering assistance and support, the completion of this work would have seemed impossible.

First and foremost, I wish to express my deepest gratitude to my direct Thesis supervisor Dr. Alexandra Schneider, leader of the EnRi group and deputy director of EPI-HMGU. The trust she placed in me, her guidance, and her invaluable advice, along with her continuous and her immediate responsiveness to my queries, represent just a portion of the noteworthy aspects of our collaboration. I shall forever cherish her immeasurable support, even during personal challenges. Of course, I would like to extend my sincere appreciation to my first Thesis supervisor Prof. Dr. Annette Peters, director of EPI-HMGU. Her indispensable contributions and profound insights played a pivotal role in shaping the final version of this Thesis. Each of her remarks during my doctoral journey has been instrumental in my personal and academic growth. Prof. Dr. Annette Peters stands as a highly influential scientific role model for me, and I consider myself fortunate to have had the privilege of being under her mentorship. Additionally, I would also like to communicate my gratitude to my second and third PhD Thesis advisors, Prof. Dr. med Dennis Nowak and Prof. Dr. Helmut Küchenhoff whose invaluable guidance and insightful comments in the TAC meetings and whenever I sought their assistance have been of great significance. Last but not least, Dr. Massimo Stafoggia, who served as an external supervisor in my Thesis, for his substantial contributions and his co-authorship in my PhD Thesis papers. All in all, the knowledge I acquired from my esteemed supervisors and our interactions during my doctoral journey constitute a solid foundation and a valuable asset for my future in research.

I wish to extend my heartfelt thanks to Dr. Kathrin Wolf for her extensive collaboration and mentorship throughout our work together. Her role as co-supervisor for me in the team and project's PI has been instrumental in my professional development. I learned a lot from working closely alongside her. Also, I thank my colleagues, Dr. Marco Dallavalle for our great collaboration all these years and his vital input in my work, Dr. Susanne Breitner for her statistical expertise and Dr. Regina Pickford for her feedbacks. Of course, many thanks to all my colleagues from the EPI-HMGU family, one-by-one. Additionally, I would like to convey my gratitude to all the co-authors of my Thesis papers who contributed to this work. In particular, I would like to extend my

thanks to Laurens M. Bouwer from GERICS for the fruitful collaboration during my visit there, which was marked by excellence and constructive engagement.

Separately, I would like to thank all my exceptional fellow PhD students and friends who have made our professional journey all the more vibrant with the joyous moments, celebrations, and the camaraderie we have shared. The open space/PhD office was consistently filled with cheerful faces, always willing to assist one another with any challenges. Your support has been invaluable, and you have played a significant role in my PhD time. Special thanks to Fiona Niedermayer, Wenli Ni, Masna Rai, Mahnaz Badpa, Yueli Yao, Maximilian Schwarz, Mingming Wang, Lisa Maier, Anne Marb and Anna Kilanowski.

Furthermore, I wish to express my gratitude to the PhD-EPH community of IBE. The fellow PhD students for the scientific exchanges over the years. I would also like to offer special thanks to Dr. Annette Hartmann and Ms. Monika Darchinger from the PhD office. They have been the cornerstone of this program, and their huge support and their dedication has made a significant impact on our academic pursuits.

I would also like to thank the Helmholtz Association, the Helmholtz Associations Initiative and Networking Fund, the HELENA Graduate School, the Helmholtz Information and Data Science Academy and the German Academic Exchange Service (DAAD) for their support.

I could not overlook my parents and my wife in my expressions of gratitude. The support of my close ones in my choices constantly fills me with an abundance of strength to continue. From the very beginning, my parents, Babis and Teti, provided total support for my education and made significant sacrifices on my behalf. My wife, Dr. Eleni Tetoni, has been and continues to be my source of energy, patience, and perseverance. We started our academic journey together, as two Bachelor students, and we continue pursuing our dreams together ever since.

The acknowledgments could not conclude without a special mention of my dear late sister, Sissy. I wish to extend my heartfelt thanks to her separately and with profound sincerity. She has been a source of inspiration and a guiding influence in my life from our earliest years.

List of scientific publications to date

Nikolaou, N.; Dallavalle, M., Stafoggia, M., Bouwer, L.M., Peters, A., Chen, K., Wolf, K., Schneider, A., 2023. High-resolution spatiotemporal modeling of daily near-surface air temperature in Germany over the period 2000–2020. *Environ. Res.*, 219, p.115062.

<https://doi.org/10.1016/j.envres.2022.115062>

Nikolaou, N., Bouwer, L.M., Dallavalle, M., Valizadeh, M., Stafoggia, M., Peters, A., Wolf, K., Schneider, A., 2023. Improved daily estimates of relative humidity at high resolution across Germany: A random forest approach. *Environ. Res.*, 238, p.117173.

<https://doi.org/10.1016/j.envres.2023.117173>

Ni, W., **Nikolaou, N.**, Ward-Caviness, C.K., Breitner, S., Wolf, K., Zhang, S., Wilson, R., Waldenberger, M., Peters, A., Schneider, A., 2023. Associations between medium-and long-term exposure to air temperature and epigenetic age acceleration. *Environ. Int.*, 178, p.108109.

<https://doi.org/10.1016/j.envint.2023.108109>

Wang, J., **Nikolaou, N.**, an der Heiden, M., & Irrgang, C., 2024. Past, present, and future heat-related mortality in Germany. PREPRINT (Version 1) available at Research Square

<https://doi.org/10.21203/rs.3.rs-3920808/v1>

Ni, W., Breitner, S., **Nikolaou, N.**, Wolf, K., Zhang, S., Peters, A., Herder, C., Schneider, A., 2023. Effects of Short-And Medium-Term Exposures to Lower Air Temperature on 71 Novel Biomarkers of Subclinical Inflammation: Results from the KORA F4 Study. *Environ. Sci. Technol.*, 57 (33), pp.12210-12221. <https://doi.org/10.1021/acs.est.3c00302>

Zhang, S., Breitner, S., Rai, M., **Nikolaou, N.**, Stafoggia, M., De'Donato, F., Samoli, E., Zafeiratou, S., Katsouyanni, K., Rao, S., Palomares, A.D.L., 2023. Assessment of short-term heat effects on cardiovascular mortality and vulnerability factors using small area data in Europe. *Environ. Int.*, 179, p.108154. <https://doi.org/10.1016/j.envint.2023.108154>

Ni, W., Wolf, K., Breitner, S., Zhang, S., **Nikolaou, N.**, Ward-Caviness, C.K., Waldenberger, M., Gieger, C., Peters, A., Schneider, A., 2022. Higher Daily Air Temperature Is Associated with Shorter Leukocyte Telomere Length: KORA F3 and KORA F4. *Environ. Sci. Technol.*, 56 (24), pp.17815-17824. <https://doi.org/10.1021/acs.est.2c04486>

Niedermayer, F., Wolf, K., Zhang, S., Dallavalle, M., **Nikolaou, N.**, Schwettmann, L., Selsam, P., Hoffmann, B., Schneider, A., Peters, A., 2024. Sex-specific associations of environmental exposures with prevalent diabetes and obesity—results from the KORA Fit study. *Environ. Res.*, 252, p.118965. <https://doi.org/10.1016/j.envres.2024.118965>

Zhang, S., Breitner, S., de Donato, F., Stafoggia, M., **Nikolaou, N.**, and Aunan, K., Peters, A., Schneider, A., 2024. Heat and Cause-Specific Cardiopulmonary Mortality in Germany: Small-Area Assessment and Vulnerability Factors. Available at SSRN: <https://ssrn.com/abstract=4807168> or <http://dx.doi.org/10.2139/ssrn.4807168>

Zhang, S., Breitner, S., Stafoggia, M., de Donato, F., Samoli, E., Zafeiratou, S., Katsouyanni, K., Rao, S., Diz-Lois Palomares, A., Gasparrini, A., Masselot, P., **Nikolaou, N.**, Aunan, K., Peters, A., Schneider, A., 2024. Effect Modification of Air Pollution on the Association between Heat and Mortality in Five European Countries. Available at SSRN: <https://ssrn.com/abstract=4854126> or <http://dx.doi.org/10.2139/ssrn.4854126>

